Sheffield Hallam University

A Sheffield Hallam University thesis

ProQuest Number: 10694116

ProQuest 10694116

OPTICAL WIRELESS COMMUNICATION SYSTEMS EMPLOYING DUAL HEADER PULSE INTERVAL MODULATION (DH-PIM)

NAWRAS MOHAMED ALDIBBIAT

A thesis submitted in partial fulfilment of the requirements of Sheffield Hallam University for the degree of Doctor of Philosophy

Optical Communications Research Group

School of Engineering, Sheffield Hallam University

Sheffield, United Kingdom

December 2001
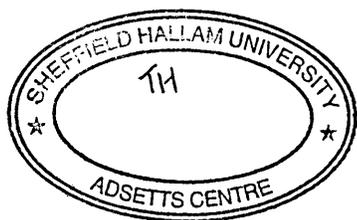
This thesis is dedicated to my beloved father, mother, Nairoz, Ali, Ola and Nibras.

ACKNOWLEDGEMENTS

DECLARATION

No portion of the work referred to in this thesis has been submitted in support of an

application for another degree or qualification to this or any other university, institute

of learning or industrial organisation.

Nawras Mohamed Aldibbiat

December 2001

ABSTRACT

Indoor optical wireless communication systems have been shown to be viable alternatives to radio systems for indoor networks because optical wireless systems offer a huge unlicensed bandwidth, high data rates, secure connectivity, immunity to electromagnetic interference and prevention from multipath fading. However, optical wireless systems are subject to multipath distortion and are governed by eye safety standards. Therefore, a modulation scheme is required that is capable of providing high speed and good immunity to multipath dispersion on indoor optical channels.

In this thesis, a critical review of optical wireless systems and suitable modulation schemes has been presented. A new modulation scheme called dual header pulse interval modulation (DH-PIM) is presented. A comprehensive theoretical analysis supported by computer simulations has been carried out to study characteristics of DH-PIM. Novel expressions for the DH-PIM pulse train, symbol length, bandwidth requirement, packet transmission rate, transmission capacity, Fourier transform, power spectral density, slot and packet error rates and power requirement and penalty due to multipath propagation have been presented.

Results from the analyses have been compared with OOK, PPM and DPIM modulation schemes. It has been shown that DH-PIM is a viable alternative scheme for indoor

optical wireless communications, due to its built-in symbol synchronisation and relatively easy slot synchronisation. Compared with PPM and DPIM, DH-PIM offers shorter symbol lengths, improved transmission rates, increased transmission capacity, improved bandwidth requirement and better immunity to multipath dispersion when the dispersion is high. However these features are at the expense of a slightly higher optical power requirement and increased probability of error. The proposed scheme is suitable for applications where there is a need for high throughput.

GLOSSARY OF ABBRIVIATIONS

3-D	Three dimensional
APD	Avalanche photodiode
AWGN	Additive white Gaussian noise
BJT	Bipolar-junction transistor
Bluetooth SIG	Bluetooth special interest group
BS	British Standards
BT	British Telecommunications
DC	Direct current
DD	Direct detection
DFE	Decision-feedback equaliser
DH-PIM	Dual header pulse interval modulation
DH-PIM$_1$	DH-PIM for $\alpha = 1$
DH-PIM$_2$	DH-PIM for $\alpha = 2$
DH-PIM$_\alpha$	DH-PIM for a given α
DPIM	Digital pulse interval modulation
DPTM	Digital pulse time modulation
FET	Field-effect transistor

EN	European Standards
FOV	Field of view
IEC	International Electrotechnical Commission
IEEE	Institute of Electrical and Electronics Engineers
i.i.d.	Independent, identically distributed
IM	Intensity modulation
IM/DD	Intensity modulation and direct detection
IR	Infrared
IrDA	Infrared Data Association
IrLAP	Infrared link access protocol
IrLMP	Infrared link management protocol
ISI	Intersymbol interference
LAN	Local area network
LD	Laser diode
LED	Light-emitting diode
LOS	Line-of-sight
MAN	Metropolitan area network
MAP detector	Maximum-a-posterior detector
MLSD	Maximum-likelihood sequence detection
MSB	Most significant bit
NRZ	Non-return-to-zero
OOK	On-off-keying
PC	Personal computer

PDA	Personal digital assistant
PER	Packet error rate
PIN	Positive-intrinsic-negative (p-intrinsic-n) photodiode
PLL	Phase locked loop
PPM	Pulse position modulation
PSD	Power spectral density
RMS	Root-mean-square
RF	Radio frequency
RZ	Return-to-zero
RZI	Return-to-zero-inverted
SIR	Serial infrared
SNR	Signal-to-noise ratio
WLAN	Wireless local area network
WPAN	Wireless personal-area networks
VCSEL	Vertical cavity surface emitting laser
ZF-DFE	Zero-forcing DEF

GLOSSARY OF Symbols

Symbol	Definition
B_{req}	Bandwidth requirement of DH-PIM
$B_{req-DPIM}$	Bandwidth requirement of DPIM
$B_{req-PPM}$	Bandwidth requirement of PPM
c_0	Zero tap
c_{cont}	Continuous impulse response of the cascaded system
c_k	Discrete-time impulse response of the cascaded system
C_T	Transmission capacity of DH-PIM
C_{Tp}	Transmission capacity
$C_{T,DPIM}$	Transmission capacity of DPIM
$C_{T,PPM}$	Transmission capacity of PPM
d	Decimal value of the input word
d_k	Number of data slots in the kth symbol
D_{mean}	Mean delay spread
d_n	Number of data slots in the nth symbol

D_{rms}	RMS delay spread
D_T	Normalised delay spread
E_p	Energy of a DH-PIM pulse
E_{p-DPIM}	Energy of a DPIM pulse
E_{p-PPM}	Energy of a PPM pulse
$E_{p,i}$	Energy of the penultimate slot
$E[x]$	Expected value of x
f_s	Slot frequency
G	A function defined in (4.17)
$H(0)$	Optical gain
H_1	Header one (h_n when $MSB = 0$)
H_2	Header 2 (h_n when $MSB = 1$)
$H(f)$	Frequency transfer function
h_n	Header sequence in the e n^{th} symbol
$h(t)$	Channel impulse response
I_B	Background photocurrent
I_p	Peak photocurrent of DH-PIM
I_{th-op}	Optimum threshold level
k	Threshold factor ($0 < k < 1$)

K	Positive integer
L	Number of slots within a PPM symbol
$\bar{L}$	The average symbol lengths of DH-PIM
$\bar{L}_{DPIM}$	The average symbol lengths of DPIM
L_{max}	The maximum symbol lengths of DH-PIM
L_{min}	The minimum symbol lengths of DH-PIM
L_{pkt}	Packet length in slots of DH-PIM
m	Number of taps in c_k
M	Bit resolution (number of bits within an OOK symbol)
$n(t)$	Shot noise
n	Instantaneous symbol number
N_{pkt}	Packet length in bits
$\bar{P}$	Average transmitted optical power
p_0	Probabilities of receiving empty slot (zero) for DH-PIM
p_1	Probabilities of receiving a pulse (one) for DH-PIM
$p_0(y)$	Probability density function for the detected DH-PIM signal in the absence of a pulse.
$p_1(y)$	Probability density function for the detected DH-PIM signal in the presence of a pulse.
P_{be-OOK}	OOK-NRZ bit error rate
P_{DC}	DC component of the DH-PIM PSD
$P_{DC,4-DH-PIM_1}$	P_{DC} for 4-DH-PIM$_1$

P_{DC-nor} P_{DC} normalised to $P_{DC,4-DH-PIM_1}$

p_{e0} Probability of false alarm.

p_{e1} Probability of erasure error.

P_{max} Maximum limit of the average value of $x(t)$

$P_{occ,i}$ Probability of occurrence of the sequence S_i

P_{pe} Packet-error-rate

$P_{pe-DPIM}$ DPIM packet error rate

P_{pe-OOK} OOK-NRZ packet error rate

P_{pe-PPM} PPM packet error rate

$P_{penalty}$ Optical power penalty in dispersive channels

P_{req} Optical power requirement in dispersive channels

$\overline{P}_{req}$ DH-PIM average optical power requirement

$\overline{P}_{req-DPIM}$ DPIM average optical power requirement

$P_{req,ideal}$ Optical power requirement in dispersive-free channels

$\overline{P}_{req-OOK}$ OOK average optical power requirement

$\overline{P}_{req-PPM}$ PPM average optical power requirement

P_{se} DH-PIM slot error rate (probability of slot error)

$P_{se-DPIM}$ DPIM slot error rate

$P_{se,i}$ Probability of slot error for the penultimate slot

P_{se-PPM} PPM slot error rate

$P_{slot,4-DH-PIM_1}(\omega)$	$P_{slot}(\omega)$ for 4-DH-PIM$_1$
$P_{slot-nor}$	$P_{slot}(\omega)$ normalised to $P_{slot,4-DH-PIM_1}(\omega)$
$P_{slot}(\omega)$	Amplitude of the slot component of the DH-PIM PSD
P_{sy_n}	probability that the nth DH-PIM symbol is in error
$p(t)$	Transmitter filter impulse response
$P(\omega)$	Power spectral density of DH-PIM
q	Number of the instantaneous symbol
q_e	Electron charge
$Q(X)$	Q-function
R	Photodiode responsivity
R_b	Bit rate
Re(x)	Real value of x
R_{pkt}	Packet transmission rate of DH-PI
$R_{pkt-DPIM}$	Packet transmission rate of DPIM
$R_{pkt-PPM}$	Packet transmission rate of PPM.
R_s	Slot transmission rate of DH-PIM
$r(t)$	Matched filter impulse response
S_i	DH-PIM i^{th} sequence of m-slots
$s_{i,m-1}$	The value of the $(m-1)^{th}$ slot in the sequence S_i
S_n	n^{th} symbol
$S_N(\omega)$	A function defined in (4.8)

$S_{N1}(\omega)$	$S_N(\omega)$ for $q < n$
$S_{N2}(\omega)$	$S_N(\omega)$ for $q = n$
$S_{N3}(\omega)$	$S_N(\omega)$ for $q > n$
SNR_{OOK}	Electrical signal-to-noise ratio for OOK-NRZ
t	Time variable
T_0	Start time of the first pulse at $n = 0$
T_h	Duration of the header
T_g	Header guard band
T_n	Start time of the nth symbol
T_s	Slot duration
T_t	Truncated time
V	Pulse amplitude
u	Variable in the $\mathrm{rect}(u)$ function
$u(t)$	Unit step function
$x_N(t)$	Truncated transmitted DH-PIM signal
$X_N(\omega)$	Fourier transform of the truncated DH-PIM signal
$X_N^*(\omega)$	Complex conjugate of $X_N(\omega)$
$x(t)$	Instantaneous transmitted optical power
Y	Number of symbols within a packet
y_i	Input of the threshold detector in the absence of noise
$y(t)$	DH-PIM signal at the matched filter input

α	Number of pulses in H_2
η	One-sided power spectral density of the noise
λ	Wavelength
μ	A function defined in (5.21)
υ	Non-zero integer
ζ	A function defined in (5.31)
ρ	Threshold level in dispersive channels
ρ_{opt}	Optimum threshold level in dispersive channels
σ	Standard deviation of the noise
σ^2	Variance of the noise
τ_{min}	Minimum pulse duration
τ_n	Duration of the pulse in the instantaneous DH-PIM symbol
φ	A function defined in (5.28)
ω	Angular frequency

LIST OF FIGURES

LIST OF TABLES

CONTENTS

Chapter 1

INTRODUCTION

1.1   Background

Both optical and radio wireless systems offer a low cost, reliable, high speed and low power point-to-point and network connectivity in indoor environments. However, the combination of the need for effective short range indoor wireless connectivity, relative security, and the promise of higher unregulated bandwidth and high data rate at a low cost makes the optical wireless link an attractive alternative to radio links [1-6]. Future multimedia application will demand high data rate and low optical power. Since the average optical power emitted by an infrared transceiver is limited, then the choice of modulation technique that can offer bandwidth and power efficiencies at a low cost is important. On-off-keying (OOK) is the simplest scheme but is unable to provide power efficiency [7-8]. Digital pulse time modulation (DPTM) schemes have received a considerable attention for use on optical wireless links [9-11]. DPTM schemes represent an alternative approach to analogue and digital modulation techniques due to their ability to improve signal-to-noise performance at the expense of bandwidth [10-

11]. Among the DPTM schemes proposed for use in optical wireless links are pulse position modulation (PPM) and digital pulse interval modulation (DPIM). PPM offers an improvement in power efficiency at the cost of relatively poor bandwidth efficiency but it requires symbol and slot synchronisation [6-7]. DPIM requires no symbol synchronisation, and offers an improvement in bandwidth efficiency compared with PPM and power efficiency compared with OOK and PPM [7,9,11].

In this work, a novel modulation scheme referred to as dual header pulse interval modulation (DH-PIM) is proposed for use over optical wireless links. DH-PIM, which has built-in symbol and slot synchronisation capabilities, offers even higher transmission capacity and requires less transmission bandwidth compared with PPM and DPIM [12-13]. Because of these characteristics, this scheme is suitable for optical wireless / optical fibre multimedia applications where the need for high transmission capacity is desirable.

1.2 Objectives of the Research

1. Comprehensive literature survey of indoor optical wireless systems and the most adopted modulation schemes such as OOK, PPM and DPIM.

2. To investigate a new modulation scheme based on digital pulse modulation for indoor wireless systems.

3. To investigate the code properties, symbol structure, transmission bandwidth, transmission rate, transmission capacity, transmitter/receiver block diagrams, spectral characteristics, probability of errors and multipath propagation of the proposed scheme, and compare the results with existing schemes.

2

4. Presentation of the findings at relevant conferences and University seminars.

5. Writing papers for publication in relevant journals and conferences.

6. Writing up of the PhD thesis.

1.3 Original Contribution

Here for the first time a new modulation scheme called DH-PIM is proposed for use over optical wireless links. To the author's best knowledge, no work has ever been reported on the proposed scheme, and this thesis investigates its properties, characteristics and performance. The original contributions are as follows:

- DH-PIM symbol structure, expressions for pulse train, transmission bandwidth requirements, transmission rate and capacity, and system simulation (Chapter 3).

- Mathematical derivation and computer simulation of the Fourier transform and power spectral density of DH-PIM signal (Chapter 4).

- Mathematical derivation and computer simulation of the slot and packet error rates together with optical power requirement formulas for non-dispersive channels (Chapter 5).

- Mathematical derivation and computer simulation of the optical power requirement and penalty formulas for multipath channel (Chapter 6).

1.4 List of Publications

1.4.1 Refereed journals

[1] N. M. ALDIBBIAT, Z. GHASSEMLOOY and R. McLAUGHLIN: "Dual header pulse interval modulation for dispersive indoor optical wireless communication systems", (Submitted to IEE Proceedings - Circuits, Devices and Systems).

[2] N. M. ALDIBBIAT, Z. GHASSEMLOOY and R. McLAUGHLIN: "Spectral characteristics of dual header pulse interval modulation (DH-PIM)", IEE Proceedings Communications, October 2001, Vol. 148, No. 5, pp. 280-286.

[3] N. M. ALDIBBIAT, Z. GHASSEMLOOY and R. McLAUGHLIN: "Error performance of dual header pulse interval modulation (DH-PIM) in optical wireless communications", IEE Proceedings Optoelectronics, April 2001, Vol. 148, No. 2, pp. 91-96.

1.4.2 Conferences

[4] N. M. ALDIBBIAT, Z. GHASSEMLOOY and R. McLAUGHLIN: "Multipath dispersion in optical wireless networks employing DH-PIM", ICINASTe'2001 conference, Minsk, Belarus, October 2001, Vol. 1, pp. 22-26.

[5] N. M. ALDIBBIAT, Z. GHASSEMLOOY, R. McLAUGHLIN & C. LU: "The characteristics of dual header pulse interval modulation (DH-PIM) in indoor optical wireless systems", SCI 2001, Florida, USA, July 2001, Vol. IV, No. 151, pp. 24-28.

[6] Nawras M. ALDIBBIAT: "DH-PIM as a commercially viable scheme for optical wireless communications", Innovative Futures Poster Competition, Sheffield, UK, May 2001.

[7] N. M. ALDIBBIAT, Z. GHASSEMLOOY & R. McLAUGHLIN: "Optical wireless networks employing dual header-pulse interval modulation (DH-PIM)", ICSECIT 2001, Chile, April 2001.

[8] N. M. ALDIBBIAT, Z. GHASSEMLOOY and R. McLAUGHLIN: "Performance of dual header-pulse interval modulation (DH-PIM) for optical wireless communication systems", Proceedings of SPIE, February 2001, Vol. 4214, USA, pp. 144-152.

[9] N. M. ALDIBBIAT and Z. GHASSEMLOOY: "Dual header-pulse interval modulation (DH-PIM) for optical communication systems", CSNDSP 2000, Bournemouth, UK, July 2000, pp. 147-152.

[10]   N. M. ALDIBBIAT, Z. GHASSEMLOOY and R. SAATCHI: "Pulse interval modulation – dual header (PIM-DH)", ICICS'99, Singapore, December 1999.

Chapter 2

INDOOR OPTICAL WIRELESS SYSTEMS

2.1   Introduction

This chapter presents a literature review of the recent research and development on the fundamentals of indoor optical wireless communication systems. In section 2.2, indoor optical wireless systems are compared with radio systems and it is shown that optical systems are viable alternatives to radio based system. In section 2.3, indoor optical link configurations are presented. In section 2.4, the issue of eye safety is discussed. Optoelectronic components are presented in section 2.5 and ambient light noise is discussed in section 2.6. Intensity modulation and direct detection (IM/DD) is presented in section 2.7. Section 2.8 is devoted to the modulation schemes, which are used on current optical wireless systems such as OOK, PPM and DPIM. Infrared data association, IEEE 802.11 working group, free space optical wireless systems and the RF Bluetooth specifications are briefly presented in section 2.9. The chapter concludes with a short summary.

2.2   Comparison of Optical Wireless and Radio Links

Indoor optical and radio wireless links are both attractive and viable solutions for providing a low cost, reliable, high speed and low power consumption wireless point-to-point and network connectivity in indoor environments. However, as a medium for short-range indoor applications, non-directed optical wireless communication systems have been shown to be a viable alternative to radio based system [1-6,14].

Table 2.1 shows a comparison between radio and infrared systems for indoor wireless communications [4].

Property	Radio	Infrared	Implication for infrared
Bandwidth regulated?	Yes	No	Approval not required. Worldwide compatibility.
Passes through walls?	Yes	No	Inherently secure. Carrier reuse in adjacent rooms.
Multipath fading	Yes	No	Simple link design.
Multipath dispersion	Yes	Yes	Problematic at high data rates
Dominant noise	Other users	Background light	
Range/coverage	High	Low	Short range.

Table 2.1: Comparison between radio and infrared for indoor wireless communication.

As a transmission medium, optical wireless offers vast-unlicensed bandwidth, high data rates and immunity to electromagnetic interference. Also, since the optical signal

(infrared) does not pass through walls, indoor optical wireless links are relatively secure systems and it is possible to reuse the same spectrum in adjacent rooms [1,4,7,13-14].

In multipath propagation, the signal may undergo many reflections from the walls, ceiling and other object within the transmission area before arriving into the receiver. As a result, the received electric field may undergo severe amplitude fades on the scale of a wavelength, therefore, a detector area smaller than the wavelength would experience multipath fading. However, multipath fading is prevented in optical systems when intensity modulation and direct detection (IM/DD) is employed. This is because the total generated photocurrent is proportional to the integral of the optical power over the entire photodetector surface area, which is larger than the optical wavelength, this provides an efficient inherent spatial diversity, thus preventing multipath fading. [16].

Both radio and optical wireless channels are still subject to multipath induced distortion, which results in intersymbol interference (ISI) [4,7,14]. Multipath propagation becomes more problematic as the data rate increases [4]. The dominant noise source in radio frequency systems is the interference caused by other users. However, in optical wireless systems, the main source of noise is the intense amount of ambient light, arising from both natural and artificial sources, which gives rise to shot noise in the receiver, which is the dominant noise source even when optical filtering is used [1,4-6,14,16].

2.3 Link Configurations

There are many different configurations for designing an indoor infrared link. These links can be classified in terms of their directionality and whether or not the link require line-of-sight (LOS) transmission, as illustrated in Fig. 2.1 [4].
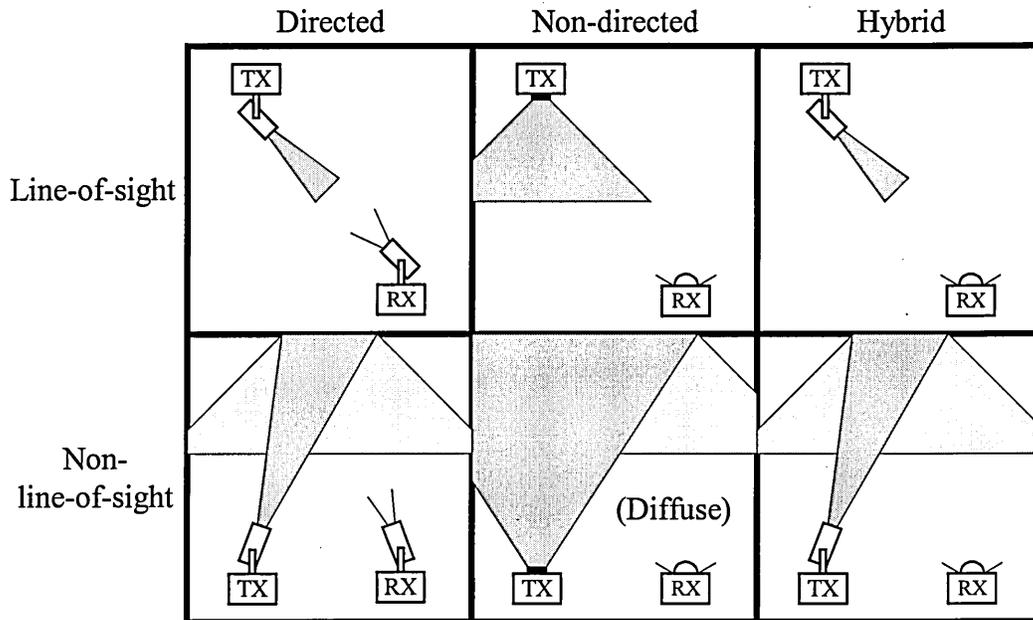
Fig. 2.1: Classification of optical wireless systems.

In directed links, the power efficiency is maximised by utilising narrow beam transmitters and narrow field of view (FOV) receivers but must be aimed. However, in the non-directed links, wide-angle transmitters and receivers can be used without a need for pointing them, thus more convenient to use and increased coverage area. The hybrid links combine transmitters and receivers with different degrees of directionality [4].

In line-of-sight (LOS) systems, there must be an uninterrupted line of sight path between the transmitter and receiver, whereas such a path is not required in non-LOS systems where reflections of light from the ceiling and walls of the room are essential to establish the link. Measurements have shown that materials used in typical office environments are between 40 – 90 % efficient at reflecting infrared radiation [5]. Non-LOS links have the advantages of ease of use and high link robustness, allowing the link to operate even if, for example, people are standing between the transmitter and receiver. The increased robustness and ease of use are achieved by the non-directed-non-LOS design, referred to as a diffuse system [4] as shown on Fig. 2.1.

Among these configurations, the directed LOS, non-directed LOS and diffuse configurations have received the most attention from researchers. In the following subsections 2.3.1, 2.3.2 and 2.3.3 these three configurations will be discussed.

2.3.1 Directed LOS configurations

Directed LOS systems do not suffer from multipath propagation, and are less susceptible to ambient background light, which means the data rate is limited only by the available power budget rather than multipath dispersion [17]. Directed LOS links have been chosen for IrDA links [18] and many directed LOS experimental links have been reported [19-22]. An example of a directed LOS link used in a local area network operating at a data rate of 50 Mbps with an average power of 1 mW over a distance of 30 m has been reported in [20]. Another example of this configuration is for low bit rate remote control applications as used in domestic electrical equipment, such as televisions and audio equipment.

The directed LOS links can be further improved using a tracking system that allows the light beam to be directed to the user [23-27]. In this system, a ceiling unit with a separate photodiode array is used to identify the location of each user, thus the corresponding laser in the down-link and the photodiode in the up-link can be activated [23]. Such a system when uses an 8 × 8 array of 0.8 mW laser diodes operating at a wavelength of 850 nm may offer a potential bit rate of 155 Mbps on both down-link and up-link, with a coverage area of 1 m by 1 m [23].

2.3.2 Non-directed LOS configurations

The non-directed LOS link suffers from multipath dispersion. It can be used for point-to-multipoint communications applications. For example, an infrared access point located on the ceiling of a room, providing connectivity to the portable devices within its coverage area employing the same wavelength.

Computer generated holograms have been used in BT laboratories as antennas to achieve a safe distribution of optical power in non-directed LOS links by emitting equal-intensity light beams which overlap in the far field to produce the required distribution in the target area [3].

Non-directed LOS systems where large rooms are divided into optical cells, each covered by a different infrared access port have been reported [28-30]. In such a system, simulation results showed that a maximum bit rate of 100 Mbps can be supported based on a cell size of 5 m^2 and a power per transmitted unit of + 13 dBm [28]. Also many different applications have been proposed such as optical telepoint systems and dealing desks. Optical telepoint, shown in Fig. 2.2, can be used in a hospital ward or an exhibition in a museum and provides a high capacity video link within a cell where the user can move within the cell boundaries [31-32].

11
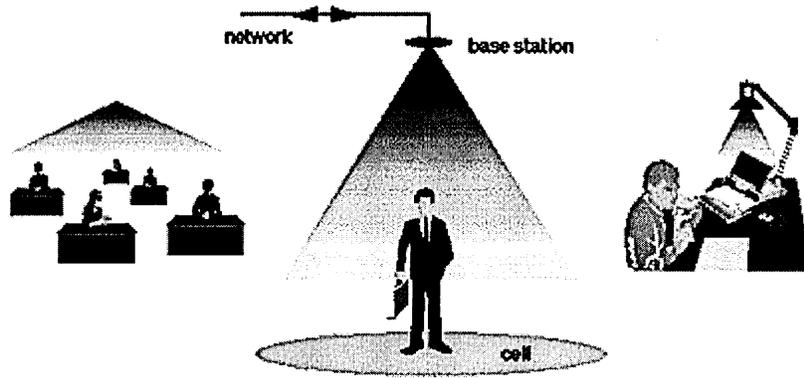
Fig. 2.2: Optical telepoint [32].

Dealing desks have been proposed by BT laboratories to intelligently work with dealers rather than merely for them by managing the input voice, data and video and presenting them to the dealers in a simple form [33].

2.3.3 Diffuse configurations

The non-directed non-line-of-sight is also known as the diffuse configuration, see Figs. 2.1 and 2.3.
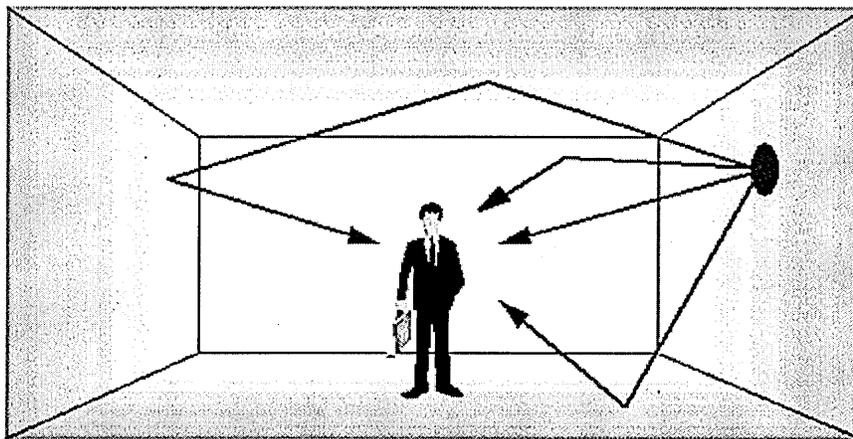
Fig. 2.3: Example of a diffuse configuration [32].

Diffuse links achieve the greatest robustness and ease of use but are more susceptible to multipath dispersion and optical path loss than other configurations [1,4, 34-36]. The flexibility comes from the fact that in diffuse systems the transmitter has a wide beam and the receiver a wide FOV, therefore pointing of the transmitter or receiver is not required. The signal may undergo one or more reflections from the ceiling, walls and any objects in the room before reaching the receiver [4-5,35].

Since the publication of the first paper on diffuse systems by Gfeller et al. in 1978 [37], diffuse links have received considerable attention from researchers worldwide who have developed models to calculate the diffuse channel impulse response [38-47]. A number of experimental diffuse links have been reported [14,48-57]. In Chapter 6 of this thesis, the ceiling-bounce model proposed by Carruthers et-al. in 1997 is chosen to study multipath propagation as it offers a simple and accurate method for predicting the power requirements given simple parameters of the room and the location of the transmitter and receiver [38].

Experimental results reported by Kahn et-al. have shown that the unshadowed diffuse links incur a high optical path loss of 53 - 64 dB for a horizontal separation distance between transmitter and receiver of 0 to 5 m [57]. The path loss is about 2-5 dB higher for a shadowed diffuse link, when the main signal path is obstructed by a person standing next to the receiver [57]. However, in the presence of shadowing diffuse links exhibit path losses that are 2-5 dB smaller compared with corresponding LOS links [57]. Diffuse links also suffer from multipath dispersion, which limits the data rate [1]. Smyth et-al. reported that, the unequalised bit rate would be limited to about 16 Mbps for a coverage volume of 10 x 10 x 3 m [28]. An experimental 50 Mbps diffuse link using OOK with decision-feedback equalisation has been reported by

Marsh *et-al.* [50,53]. Equalisation provides a resistance to intersymbol interference (ISI) due to multipath dispersion. The system achieved a low bit error rate with a range of 2.9 m in a bright skylit room [53]. The diffuse link is also the chosen link configuration for the IEEE 802.11 infrared physical layer standard [58]. Diffuse systems are commercially available such as the PC Card Wireless LAN Adapter, manufactured by Spectrix Corporation [59]. This Spectrix adapter sends and receives diffuse infrared allowing users to move freely within the service area and is specified to work over a coverage area of 1000 square feet, and achieves a data rate of 4 Mbps, which is shared between all the users within the cell [59].

To improve the performance of non-directed links (LOS and diffuse), an angle-diversity receiver can be used which can be implemented in either of two methods, non-imaging or imaging (also called 'fly-eye receiver') [2,4,60-69]. The non-imaging angle-diversity receiver consists of multiple nonimaging receiving elements oriented in different directions, each of which has its own optical concentrator [61]. An experimental 70 Mbps OOK link using a nine-element non-imaging angle-diversity receiver which achieved a 4.2 m range has been reported [61]. The main drawback of this approach is that it can lead to a bulky and costly receiver [60].

The imaging angle-diversity receiver was first proposed by Yun and Kavehrad [62]. It consists of a one imaging optical concentrator (e.g. a lens) that produces an image of the received light on a segmented photodetector array placed at its focal plane, so separating signals that arrive from different directions [60].

In both implementations, the photocurrent generated by each element is amplified separately [60]. The angle-diversity receiver not only achieves a high optical gain over a wide FOV, but it also reduces the effects of ambient noise, co-channel interference

and multipath dispersion by exploiting the fact that the unwanted signals are usually received from different directions to that of the desired signal [60].

2.4 Eye Safety

Eye safety is a very important issue in any optical wireless system due to the fact that the infrared signal can penetrate the human cornea and potentially induce thermal damage to the retina [4]. The eye safety of infrared sources is governed by the International Electrotechnical Commission (IEC) standards [70]. Infrared transmitters must conform to the Class 1 classification (inherently safe) of the British Standards number BS EN 60825-1: 1994 derived from the IEC 825-1:1993 [4,24,71]. The standard specifies that the average power for a pulse train of duration 100s must not exceed the power of a single pulse of duration 100s [71].

Although infrared transmission at wavelengths beyond 1400 nm is much less hazardous to the safety of the eye than the band $780 - 950$ nm, the band $780 - 950$ nm is now commercially preferred. This is because of the availability of cheap light-emitting diodes (LEDs) and laser diodes (LDs), and because it coincides with the peak responsivity of cheap silicon photodetectors [3-4].

2.5 Optoelectronic Components

In this section, the main components used in an optical wireless system are briefly presented. The optical transmitter can be one or more laser diodes or LEDs. The optical receiver contains an optical front end and an electrical front end. The optical

front end consists of a concentrator and filter and the electrical front end consists of one or more photodetectors followed by a wide-band preamplifier [1].

2.5.1 Optical emitters

LEDs and laser diodes are suitable as optical wireless emitters due to their characteristics such as high electro-optic conversion efficiency, a small optical bandwidth, small size, safety and fast modulation properties [2,4]. The choice between LEDs and laser diodes depends on many factors such as the cost, speed and performance of the application. Compared to laser diodes, LEDs are less expensive, require simpler drive circuitry and generally considered eye safe, on the other hand, the output of laser diodes must be diffused to classify them as eye safe [4]. This can be done, for example, by the use of computer generated holograms [17, 72] or integrating sphere diffusers [73-74]. However, laser diodes enjoy many advantages over LEDs such as 1) A good electro-optic conversion efficiency (30-70 %) while it is (10-40 %) in LEDs. 2) Wide modulation bandwidths (up to tens of GHz) compared to limited bandwidths in LEDs (up to tens of MHz) which can be increased but at the cost of reduced electro-optic conversion efficiency. 3) Very narrow spectral widths (less than 5 nm) compared to wide spectral widths in LEDs (25-100 nm), thus LEDs require wide receiver optical pass-band making them more susceptible to ambient light [2,4]. Consequently, LEDs are generally used in low-speed, low-cost applications such as IrDA serial ports, while laser diodes are preferable in high-speed links [4,75].

A potential laser emitter is the low-power vertical cavity surface emitting laser (VCSEL), which produces light from its surface [76-77].

2.5.2 Optical filters

The use of a long-pass or band-pass optical filter is essential at the receiver to reduce the unwanted ambient light [2,4]. The long-pass filters are usually made of coloured glass or plastic, and their cut-off wavelength is shorter than the operating wavelength. The combination of photodiode and long-pass filter results in a band-pass filter with a bandwidth several times that required to pass the radiation of an LED [4].

The band-pass filters, known as interference filters, are made of multiple thin dielectric layers [1,4,24]. They can achieve extremely narrow bandwidths, thus very effective when used in systems employing laser diode emitters [4]. However, such filters may not be suitable for non-directed links because the pass band of the filter shifts towards shorter wavelengths as the angle of incidence increases which results in narrowing the FOV [4].

2.5.3 Optical concentrators

The optical power detected at the receiver increases as the effective area of the photodiode increases. Enlarging the photodiode area is costly and increases the receiver noise. Therefore, optical concentrators are usually used in optical wireless receivers to increase the effective area of the detector by transforming the light incident over a large area into a set of rays that emerge from a smaller area [4,24]. High gains can be achieved using compound parabolic concentrators, but these are limited to use in directed links because of their narrow FOV. However, in non-directed links, hemispherical or truncated spherical concentrators can be used because they achieve wide FOV and an omnidirectional gain [1,4,24].

2.5.4 Photodetectors

The photodetector used in an optical wireless system must have a high responsivity to maximise the system power margin and wide bandwidth to allow for high data rates [2-3]. Two types of photodetectors can be used in infrared systems, the positive-intrinsic-negative (PIN) photodiode and the avalanche photodiode (APD).

The APDs achieve a very good performance when the ambient light is very low, i.e. LOS systems [3]. However, in non-directed infrared links, particularly diffuse links, where shot noise due to ambient light is dominant, the gain achieved by APDs decreases the SNR because the random nature of the APD's internal gain increases the variance of the shot noise by a factor greater than the signal gain [1,4]. Therefore, PIN photodiodes are preferable to APDs for use in non-directed optical wireless links [1-4]. Other advantages of silicon PIN photodiodes are low-cost, availability and large surface area, which results in improved signal-to-noise ratio (SNR) because the received signal power increases linearly with the area while the noise power increases with its square root [3]. The photocurrent produced by the PIN photodiode is given by:

$$i(t) = Rx(t),$$

(2.1)

where, $x(t)$ is the instantaneous received optical power and R is the photodiode responsivity (A/W), which is typically in the range 0.5-0.75 A/W for silicon PIN operating in the wavelength band of 800-1000 nm [2].

Throughout his Thesis, it is assumed that a PIN photodiode is used.

2.5.5 Preamplifiers

A transimpedance amplifier is the best choice as a preamplifier stage at the receiver because it achieves a wide bandwidth and large dynamic range without the need for equalisation [4,24,78-79]. The large dynamic range is important to accommodate variable link distances [78]. The choice between employing a field-effect transistor (FET) or a bipolar-junction transistor (BJT) in the preamplifier depends on many factors. For example, FETs achieve low noise at high bit rates but suffer from relatively low transconductance, whilst BJTs achieve higher transconductances leading to better power conception [4,24].

2.6 Ambient Light Noise

The environments where infrared wireless systems operate usually contain an intense amount of ambient light, which has many sources such as natural (solar), incandescent and fluorescent sources. These noise sources have high power levels at the desired optical wavelength as shown on Fig. 2.4 [4].
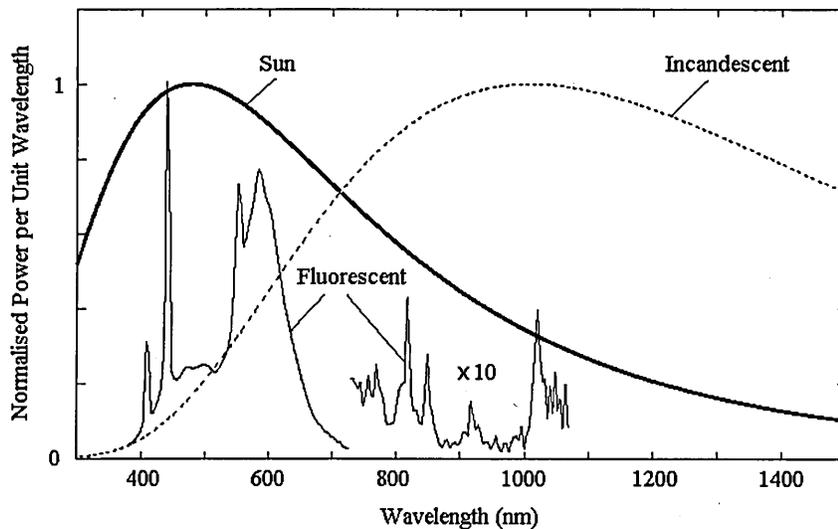
Fig. 2.4: Optical power spectrum of main ambient infrared sources [4].

The average combined power of the ambient light results in the photodetector generates a DC background photocurrent I_B giving rise to shot noise $n(t)$, which is the dominant noise source in optical wireless systems [1-4]. Even when optical filtering is used to reject ambient light sources, the received signal power is usually much lower than the power from ambient light sources [1-2]. The shot noise $n(t)$ due to ambient light is independent of the signal and can be modelled as a white Gaussian with one-sided power spectral density η, which can be given as [2,4,12,16,80]:

$$\eta = 2q_e I_B,$$

(2.2)

where q_e is the electron charge.

The other main noise source is the receiver preamplifier noise, which is also Gaussian and independent of the signal. However, preamplifier noise is dominant when little or no ambient light is present [4]. Artificial light of fluorescent lamps also induces a nearly periodic and deterministic interference, which may cause baseline wander [81-82]. This will be discussed in Chapter 6.

2.7 Intensity Modulation and Direct Detection (IM/DD)

The practical method of operation in an optical wireless system is the intensity modulation and direct detection (IM/DD) [1,4]. The term 'intensity' refers to optical power and 'modulation' to electro-optical conversion, thus 'intensity modulation' (IM) means that the instantaneous power of the optical carrier is modulated by a signal. Direct detection (DD) means that the photodetector generates a photocurrent, which is

proportional to the instantaneous received optical power [1,2,4]. An optical wireless system using IM/DD has an equivalent baseband model, which will be explained in Chapter 6.

In optical wireless systems the instantaneous optical signal $x(t)$ represents power rather than amplitude [1]. This results in two constraints on the transmitted optical signal. Firstly, $x(t)$ must be positive, i.e. $x(t) \geq 0$. Secondly, the average amplitude of $x(t)$ is limited to a specified value P_{max} because of eye safety and power consumption requirements, i.e. [1]:

$$\lim_{T_t \to \infty} \frac{1}{T_t} \int_{-T_t/2}^{T_t/2} x(t)dt \leq P_{\max},\qquad(2.3)$$

where, T_t is the truncated time.

Note that in the case of conventional electrical transmission where $x(t)$ represents amplitude rather than power, $|x(t)|^2$ must replace the term $x(t)$ in (2.3) [1]. This means that in electrical links, the SNR is proportional to the average received power, whereas in optical wireless links, it is proportional to the square of the average received optical power. Therefore, implying that relatively high optical transmit powers and a limited path loss are essential [4].

2.8 Modulation Schemes

Since the average optical power emitted by an infrared transceiver is limited, then the choice of a modulation technique, which can offer bandwidth and power efficiencies at a low cost is important. Many digital modulation schemes have been proposed for use on optical wireless systems. Among these schemes, OOK, PPM, DPIM have received

a considerable attention from researchers worldwide [1-2,4,7,14,82]. These techniques

will be presented with more details in the following subsections and also will be used

for comparison with the proposed scheme DH-PIM throughout this thesis.

2.8.1 On-off-keying (OOK)

On-off keying is a very simple digital modulation scheme, however, it is more

susceptible to multipath dispersion and artificial light interference than PPM [14].

Depending on the duty cycle, OOK can be either return-to-zero (RZ) or non-return-to-

zero (NRZ). In both OOK-RZ and OOK-NRZ a zero is represented by zero intensity,

however, in OOK-NRZ, a pulse occupies a full bit duration and in OOK-RZ, a pule

occupies a specified part of the bit duration and the rest of the bit duration is

represented by a zero intensity. Figure 2.5 shows a representation of bits "1 0" using

OOK-NRZ and OOK-RZ (50% duty cycle).

(a)   (b)
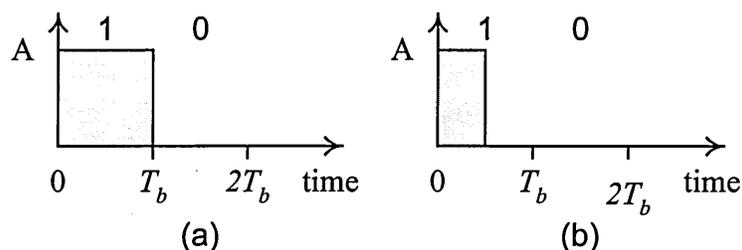
Fig. 2.5: Representation of bits "1 0" using (a) OOK-NRZ, and (b) OOK-RZ (50%

duty cycle).

There is also an inverted version of OOK-RZ called, return-to-zero-inverted (RZI)

signalling, used on some commercial applications such as the IrDA serial infrared link,

which supports optical link lengths from zero to at least one meter for data rates up to

1.152 Mbps. In RZI, a "0" is represented by a light pulse with different duty cycles depending on the data rates [83].

Due to the relatively wide pulses, OOK-NRZ achieves a good bandwidth efficiency, but at the expense of poor power efficiency compared with PPM and DPIM [7]. However, power efficiency can be improved by the use of OOK-RZ. Therefore, there should be a trade off between optical power and bandwidth efficiency when choosing the width of the OOK-RZ [2]. The performance of OOK signals on optical wireless channels has been investigated and reported in many papers, [1,2,4,7,14,50,53,84-87].

2.8.2 Digital pulse time modulation schemes

The ability to exchange optical power against bandwidth extension in pulse time modulation techniques is of increasing importance in high-speed networks. These techniques deal exclusively with a pulse format, thus there is no concern over LED or laser diode linearity. In addition, these schemes also offer simple circuit implementation [11,88-90].

In pulse time modulation techniques, one of the time-dependent features of a pulsed carrier is used to convey information, e.g. pulse position, width, interval, width and interval, frequency, etc. are varied depending on the amplitude of the modulation signal.

Analogue and digital schemes can be divided mainly into two categories, isochronous and anisochronous. In isochronous schemes, the symbol length is fixed while in

anisochronous methods the symbol length is variable [11,88-90]. Figure 2.6 shows the pulse time modulation tree [7,11].

Pulse Time Modulation

Analogue		Digital	
Isochronous	**Anisochronous**	**Isochronous**	**Anisochronous**
PWM	PIWM	DPWM	DPIWM
PPM	PIM	PPM	DPPM
	PFM	MPPM	DPIM
	SWFM	PCM	**DH-PIM**
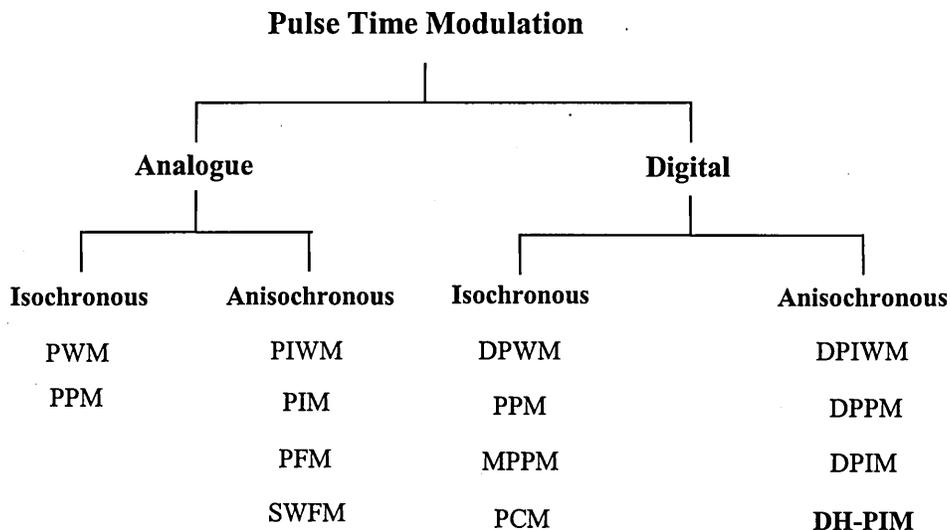
Fig. 2.6: Pulse time modulation tree.

In the following subsections, digital PPM and DPIM are presented.

2.8.2.1 *Pulse position modulation (PPM)*

PPM achieves the best optical power performance but at the expense of increased bandwidth requirement and circuit complexity since both slot and symbol synchronisation are required in the receiver in order to demodulate the signal [1-2,4,91]. When encoding an OOK input words into PPM, the higher the bit resolution, the better the average power efficiency and the larger bandwidth requirement [1,7].

In PPM, each block of M-bit word is mapped to one of L possible symbols, where $L = 2^M$. Each symbol consists of a pulse occupying one slot, and the rest of the symbol duration is empty of pulses. Therefore, the information is represented by the position of the pulse within the symbol, which is equal to the decimal value of the input binary

word [1-2,4,91]. For example to map the 4-bit word "1 0 1 0" into a PPM symbol, a symbol of $L = 16$ slots should be generated with one pulse occupying position 10 which corresponds to the decimal value of the binary word 1010 as shown in Fig. 2.7. Note that numbering starts from "0", therefore, the first slot is number "0" and the last slot is number "15".
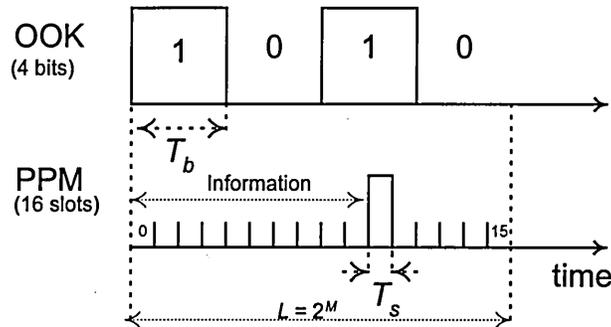
Fig. 2.7: Mapping the word "1 0 1 0" into a PPM symbol.

There are two different methods of decoding PPM signals, hard decision decoding and soft decision decoding [1,4,91], see a PPM system block diagram shown in Fig. 2.8.
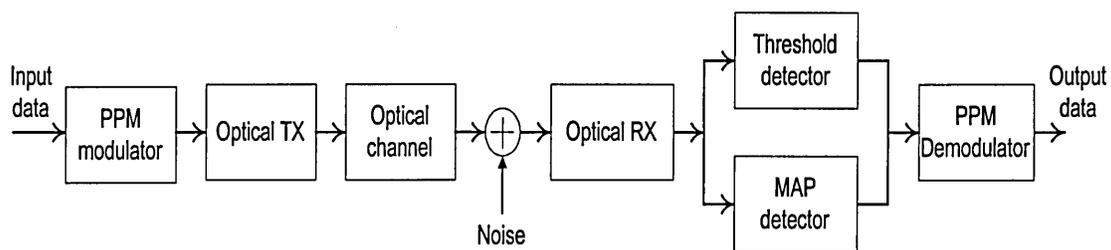
Fig. 2.8: Block diagram of the PPM system.

The hard decision decoders use a threshold detector which samples the received signal at the slot rate, and assigns a '1' or a '0' to each slot depending on whether the signal

is above or below the threshold level at the sampling instant. Soft decision decoders use a maximum-a-posterior (MAP) detector, which compares the values of all L slots within a symbol, assigns a '1' to the slot with the highest optical power and assigns "0"s to the other slots within the symbol. Soft decision decoding is the best when channels are distortion-free and AWGN is the dominant noise source [1,4,91].

PPM is used on commercial applications such as the IrDA serial infrared link, which employs 4-PPM to support optical link lengths from zero to at least 1 meter for data rates of 4 Mbps. A "1" is represented by a light pulse and the nominal pulse duration is 125 ns [83]. Also, the infrared physical layer section of the IEEE 802.11 standard on wireless LANs specifies 16-PPM for bit rate of 1 Mbps and 4-PPM for 2 Mbps [92].

The performance of PPM on optical wireless channels has been broadly investigated. Audeh *et-al.* reported that on unequalised multipath channels, the good power efficiency remains good for large values of L if the amount of ISI is small. However, as ISI increases, the power requirements increase more rapidly for PPM than for OOK especially for large L, due to the short slot duration [93]. The performance of PPM on multipath channels can be improved by the use of maximum-likelihood sequence detection (MLSD), however, MLSD is complex and as ISI increases. The power requirements of PPM increase much more rapidly than those of OOK [4, 94-95]. This has motivated many researchers to consider equalisation to improve the performance of PPM on non-directed wireless channels [1,4,34,36,56,96-98]. There are linear and decision-feedback equalisers (DFEs) operating at either the slot or symbol rates [1,4]. Audeh *et al.* have examined the performance of PPM on measured non-directed indoor infrared channels employing DFEs. They found that although the computational

complexity and storage requirements of zero-forcing DEFs (ZF-DFEs) are much less than that of the MLSD, the performance of symbol-rate ZF-DFE was very close to that of MLSD [96].

2.8.2.2 *Digital pulse interval modulation (DPIM)*

Digital pulse interval modulation has built-in symbol synchronisation and offers an improvement in bandwidth efficiency and data rate compared with PPM and power efficiency compared with OOK [11]. In DPIM, the symbol is represented by a discrete time interval between two successive pulses belonging to two consecutive symbols. Each symbol starts with a short duration pulse followed by guard band then a number of empty time slots determined by the decimal value of the input code word [11]. The guard band consists of zero or more empty slots and is important to avoid consecutive pulses when the input word is zero [11]. Unlike isochronous schemes, e.g. PPM where the symbol length is fixed, the symbol length in DPIM is variable as shown in Fig. 2.9 where the input word "1 0 1 0" is encoded into a DPIM symbol with a guard band of one time slot.
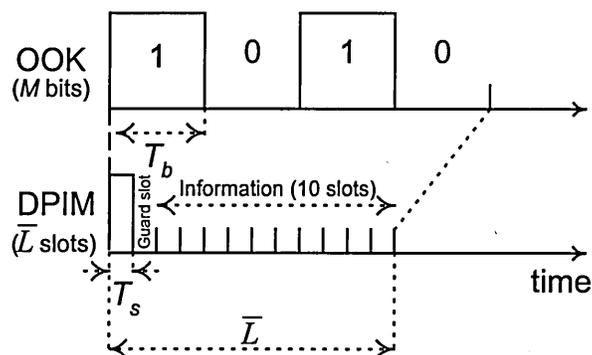
Fig. 2.9: Mapping the word "1 0 1 0" into a DPIM symbol.

The main principles and characteristics of DPIM have been studied by many researchers [7,9,11,82,100-104], and practical system implementations and results are given in [9,11,99-100]. Because of its variable symbol duration, practical implementations favour the use of simpler threshold detection receivers rather than soft decision detector [100], see a DPIM system block diagram shown in Fig. 2.10.
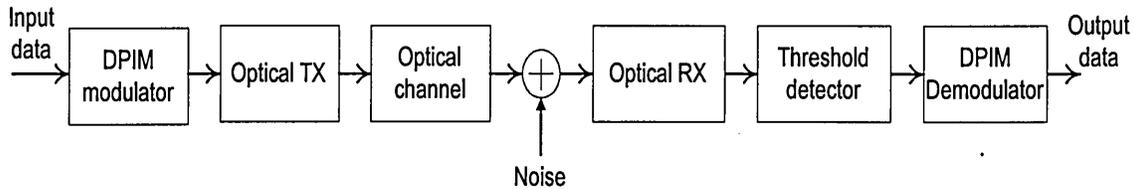
Fig. 2.10: Block diagram of the DPIM system.

The spectral properties of DPIM have been studied in [82,101-103]. Derivation of the power spectral density (PSD) is given in [82]. Unlike PPM, the PSD of DPIM and OOK do not approach zero at DC, however, DPIM is more resistant to the baseline wander than OOK [82,102].

For low bit rates around 1 Mbps with high-pass filter cut-on frequencies of the order of tens or hundreds of kHz, 8-DPIM with one guard slot offers the lowest optical power penalty compared with 8-PPM and OOK [82].

The error performance of DPIM has been studied in [7,82]. Ghassemlooy *et al.* reported a detailed analysis of the packet-error-rate (PER). They showed that for a given bandwidth, DPIM using a threshold detector outperforms both OOK and PPM in terms of PER [7].

The effect of multipath dispersion on the performance of DPIM has been analysed and results showed that DPIM without a guard band is more resistant to the effects of multipath propagation compared with PPM due to its longer slot duration. However,

the use of a guard band reduces the bandwidth efficiency but improves the performance of DPIM as the severity of the intersymbol interference increases [104].

2.9 Wireless Systems and Standards

2.9.1 Infrared data association (IrDA) systems

IrDA was founded in 1993 as a non-profit industry-sponsored International organization, headquartered in Walnut Creek, California, to create international standards for the hardware and software used in low cost infrared communication links. The IrDA standards support a broad range of appliances, computing and communications devices. International travelers can use IrDA functional devices wherever they are with minimal interference problems [75].

The IrDA standards published in 1994 include serial infrared (SIR) link specification, infrared link access protocol (IrLAP) specification, and infrared link management protocol (IrLMP) specification.

Products provided with infrared features based on IrDA standards include components, adapters, printers, PC's, personal digital assistants (PDA's), notebook computers, local area network (LAN) access, and software applications. Microsoft has added support for IrDA connectivity to Windows 95 operating system, and IrDA connectivity is being incorporated into most notebooks. IrDA featured devices are predicted to be popular in future office and home mobile environment. Future PCs will support connectivity of more than one device via a single IrDA access point [75].

2.9.2 IEEE 802.11 standards

The IEEE 802 LAN/MAN Standards Committee develops local area network (LAN) standards and metropolitan area network (MAN) standards. There are many working groups in IEEE 802, and the 802.11 is the working group on wireless LAN. The IEEE 802.11 standard defines three alternative physical interfaces, two radio frequency (direct sequence spread spectrum and frequency hopping spread spectrum) and one infrared [105-108].

The standard was finalized in 1997 after seven years of work. The spread spectrum RF products provide 1 to 2 Mbps data rates and a range from 50 feet to 1000 feet depending on the type of building construction and interference sources [107].

Unlike IrDA LOS links, the 802.11 IR links use diffuse infrared transmission. An 802.11 IR wireless LAN (WLAN) is suitable for a big, open area because it will operate at much higher power than an IrDA link. The range of 802.11 IR links will be up to about 10 meters. The basic access rate is based on 1 Mbps, with an enhanced access rate of 2 Mbps [108].

2.9.3 Free space optical wireless communications

Free space optical wireless systems have been used initially by the military and space aviation pioneers. However, in recent years, they have been used in a wider range of communication applications especially when a physical connection is impossible or costly and in cities where radio spectrum is already too crowded and expensive to license [109-115]. For example, across highways and rivers, across land not owned by the network operator, temporary connectivity [112]. Free space optical wireless systems have the ability to communicate between two fixed optical transceiver

separated by a free space LOS path to provide full duplex (bi-directional), which currently enables optical transmission of data, voice and video signal at up to 2.5 Gbps via a wireless connectivity [113].

However, in this thesis, the focus is on indoor wireless systems rather than free space systems.

2.9.4 Bluetooth specifications

Bluetooth, named after a medieval Danish king, Harald Blaatand II or Bluetooth (940-981), is sort of a cross between IEEE 802.11 and IrDA LANs. It is a computing and telecommunications industry specification for a small-form factor, low-cost radio solution and has been sanctioned as the foundation of wireless personal-area networks (WPAN) being developed by the IEEE standards body in its 802.15 specification. Bluetooth products will provide wireless connectivity between mobile computers, mobile phones, printers and other portable devices, as well as access to the Internet using a short-range wireless connection [116-121].

The Bluetooth SIG (Special Interest Group) was formed in February 1998 by 5 companies Ericsson, IBM, Intel, Nokia, Toshiba. Now there are more than 2100 members of SIG.

The products, which support Bluetooth technology, must be tested and approved by the SIG. The Bluetooth 1.1 specification consists of two documents: the Core [113], which provides design specifications, and the Profile [114], which provides guidelines. Users of Bluetooth products will be able to bye a three-in-one phone which functions

as a cellular phone, pager, and PDA, and can initiate the sending or receiving of a fax and initiate a print-out. Each Bluetooth device requires a low-cost transceiver chip, which transmits and receives in the frequency band 2.45 GHz, which is available globally. In addition to data, up to three voice channels are available. The maximum range is 10 meters. Data can be exchanged at a rate of 1 Mbps [117].

2.10 Summary

In this chapter, a review of the current indoor optical wireless systems has been presented. Comparison with the radio wireless systems showed that optical wireless systems have many advantages for short-range links. Different link configurations have been discussed and the issue of eye safety was considered. Optoelectronic components have been presented. The problem of ambient light noise, which affects transmission on optical wireless channels particularly non-directed links has been discussed. Transmission using IM/DD has been discussed. The main modulation techniques being used or proposed for use in indoor optical wireless systems were presented. OOK offers better bandwidth efficiency but poor optical power performance. Digital pulse time modulation techniques such as PPM and DPIM offer a trade off between bandwidth and optical power efficiencies. Finally, the infrared data association, IEEE 802.11 working group, free spaces optical wireless systems and Bluetooth specifications have been described briefly.

Chapter 3

DH-PIM: SYSTEM PRINCIPLES

3.1 Introduction

In this chapter for the first time a new modulation technique called dual header pulse interval modulation (DH-PIM) is introduced and its properties are presented. DH-PIM offers shorter symbol length, improved transmission rate, capacity and bandwidth requirement compared with existing pulse techniques such as DPIM and PPM. It also provides a built-in symbol synchronisation and simple slot synchronisation. Symbol structure and mathematical expression of the DH-PIM pulse train, transmission bandwidth requirement, transmission rate and capacity are presented in sections 3.2 – 3.5. The block diagrams of the complete system, transmitter and receiver of DH-PIM as well as selected simulated waveforms in the time domain are presented in section 3.6. The chapter is concluded with a summary of the results.

3.2 DH-PIM Symbol Structure

The DH-PIM principles and its difference with other pulse modulation techniques such as OOK, PPM and DPIM may be best understood by reference to Fig. 3.1 in which an example of two consecutive symbols is shown.
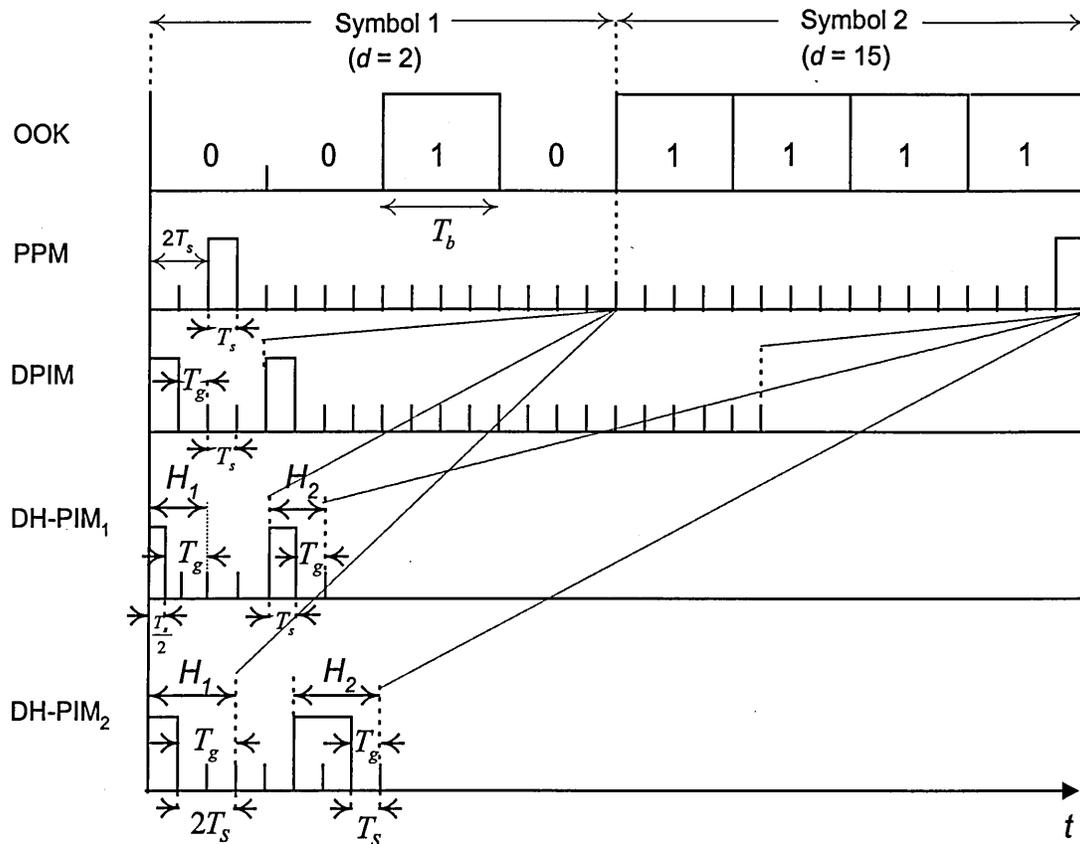
Fig. 3.1: OOK/PPM/DPIM/DH-PIM$_1$/DH-PIM$_2$ symbol structure.

In PPM, a pulse of one time slot duration is located in the slot corresponding to the information data and in DPIM the symbol length is shortened by eliminating the redundant slots which follow the PPM pulse, thus resulting in an increased data throughput [7,9,11]. The DPIM symbol starts with a pulse of duration equal to or less

than one slot duration T_s followed by a guard band of zero or more T_s and the information slots which corresponds to the decimal value of the input code word. Throughout this thesis and unless otherwise sated we will use DPIM with a guard band of one T_s for comparison purposes.

In DH-PIM, the symbol consists of two sections, a header, which initiates the symbol and an information section which concludes it. Fig. 3.2 shows the nth symbol $S_n(h_n, d_n)$ of a DH-PIM sequence, where h_n represents the header and d_n represents the information slots of the symbol S_n.
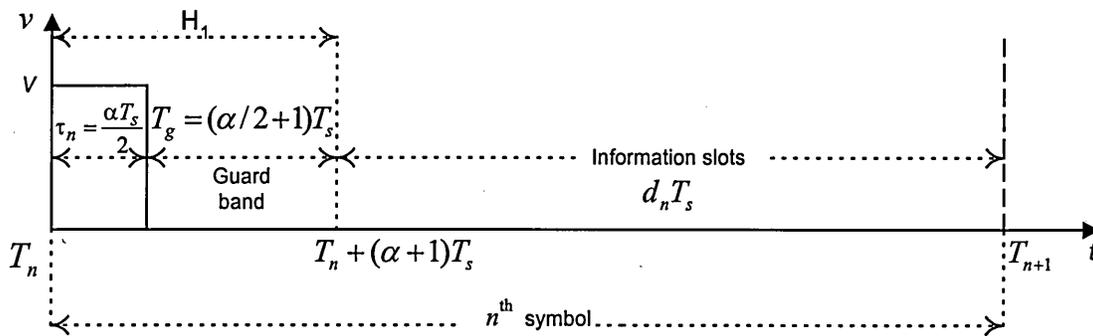
(a)
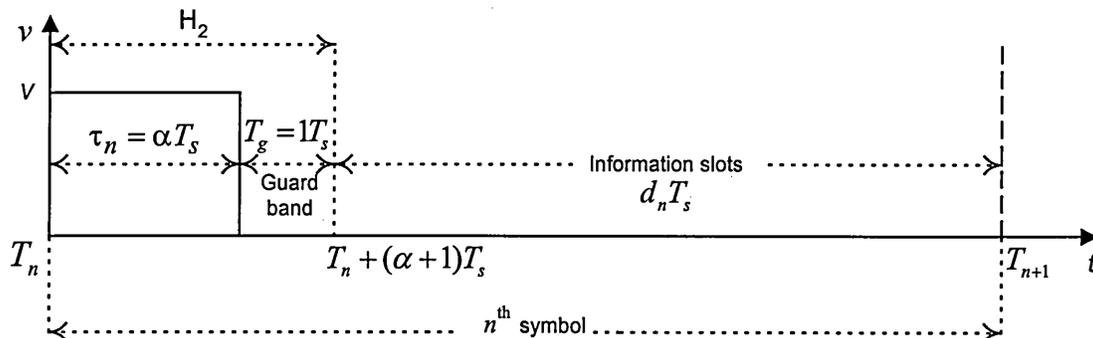
(b)

Fig. 3.2: The nth symbol of DH-PIM: (a) shows H$_1$, and (b) shows H$_2$.

Depending on the most significant bit (*MSB*) of the input word, two different headers are considered H_1 and H_2, which correspond to $MSB = 0$ and $MSB = 1$, respectively. Both H_1 and H_2 have a total duration of $T_h = (\alpha + 1)T_s$, where $\alpha > 0$ is an integer. The header h_n is composed of a pulse of duration $\frac{\alpha T_s}{2}$ in H_1 and αT_s in H_2, each followed by a guard band of appropriate length T_g so that the total duration of the both headers is $T_h = (\alpha + 1)T_s$, where $\alpha > 0$ is an integer. The guard band is important to cater for symbols representing zero, and it has a duration of $T_g \in \left\{ \left(\frac{\alpha}{2} + 1 \right) T_s, T_s \right\}$ corresponding to $h_n \in \{H_1, H_2\}$.

The information section is composed of d_n empty slots. The value of $d_n \in \left\{ 0, 1, ..., 2^{M-1} - 1 \right\}$ is simply the decimal value of the input code word when the symbol starts with H_1, or the decimal value of the 1's complement of the input code word when the symbol starts with H_2, where M is the bit resolution of the OOK input word. The header pulse plays the dual role of symbol initiation and time reference for the preceding and succeeding symbols resulting in built-in symbol synchronisation.

The DH-PIM signal can be expressed as a rectangular pulse that starts at $t = T_n$, and has duration:

$$\tau_n = (1 + h_n) \frac{\alpha T_s}{2}, \qquad (3.1)$$

where $h_n \in \{0,1\}$ indicating H_1 or H_2 respectively, and n is the instantaneous-symbol number as shown in Fig. 3.2. The DH-PIM pulse train can be expressed mathematically as:

$$x(t) = V \sum_{n=0}^{\infty} \left\{ \text{rect}\left[\frac{2(t-T_n)}{\alpha T_s} - \frac{1}{2} \right] + h_n \text{rect}\left[\frac{2(t-T_n)}{\alpha T_s} - \frac{3}{2} \right] \right\}, \qquad (3.2)$$

where, V is the pulse amplitude, and the rectangular pulse function is defined as [122]:

$$\text{rect}(u) = \begin{cases} 1 \; ; \; -0.5 < u < 0.5 \\ 0 \; ; \; \text{otherwise} \end{cases}. \qquad (3.3)$$

For $h_n = 0$, (3.2) represents DH-PIM symbols with H_1 only having a pulse duration of

$$\tau_n = \frac{\alpha T_s}{2}.$$

The start time of the nth symbol is defined as:

$$T_n = T_0 + T_s \left[n(\alpha+1) + \sum_{k=0}^{n-1} d_k \right], \qquad (3.4)$$

where, T_0 is the start time of the first pulse at $n = 0$ and $d_k \in \left\{0,1,...,2^{M-1} -1\right\}$ the number of information time slots in the kth symbol.

Throughout this thesis, DH-PIM will be referred to as L-DH-PIM$_\alpha$ according to the values of L and α, e.g. 8-DH-PIM$_1$ and 8-DH-PIM$_2$ refer to DH-PIM with $L = 8$

($M = 3$) and $\alpha = 1$ and $\alpha = 2$ respectively. Also DPIM and PPM will be referred to as L-DPIM and L-PPM according to the values of L. e.g. 8-PPM, 8-DPIM.

Table 3.1 shows the mapping of all possible combinations of a 3-bit OOK code word into 8-PPM, 8-DPIM and 8-DH-PIM$_2$ symbols.

OOK	8-PPM	8-DPIM	8-DH-PIM$_2$
0 0 0	1 0 0 0 0 0 0 0	1 0	**1 0** 0
0 0 1	0 1 0 0 0 0 0 0	1 0 0	**1 0** 0 0
0 1 0	0 0 1 0 0 0 0 0	1 0 0 0	**1 0** 0 0 0
0 1 1	0 0 0 1 0 0 0 0	1 0 0 0 0	**1 0** 0 0 0 0
1 0 0	0 0 0 0 1 0 0 0	1 0 0 0 0 0	**1 1 0** 0 0 0
1 0 1	0 0 0 0 0 1 0 0	1 0 0 0 0 0 0	**1 1 0** 0 0
1 1 0	0 0 0 0 0 0 1 0	1 0 0 0 0 0 0 0	**1 1 0** 0
1 1 1	0 0 0 0 0 0 0 1	1 0 0 0 0 0 0 0 0	**1 1 0**

Table 3.1: Mapping of OOK code into 8-PPM, 8-DPIM and 8-DH-PIM$_2$ symbols. H_1 and H_2 are shown in bold font.

Therefore, DH-PIM not only removes the redundant time slots that follow the pulse as in PPM symbol, but it also reduces the average symbol length compared with DPIM, resulting in an increased data throughput. The minimum, maximum and average symbol lengths of DH-PIM are given respectively as:

$$L_{\min} = \alpha + 1, \qquad (3.5)$$

$$L_{\max} = 2^{M-1} + \alpha, \qquad (3.6)$$

$$\overline{L} = \frac{2^{M-1} + 2\alpha + 1}{2}, \qquad (3.7)$$

and the slot duration is defined as:

$$T_s = \frac{2M}{(2^{M-1} + 2\alpha + 1)R_b}, \qquad (3.8)$$

where, R_b is the bit rate of the OOK input signal.

The symbol length of PPM (in slots) is fixed and is given by [11]:

$$L = 2^M, \qquad (3.9)$$

and the average symbol length of DPIM with one guard slot is given by [11]:

$$\overline{L}_{DPIM} = \frac{(2^M + 3)}{2}. \qquad (3.10)$$

The average symbol lengths of PPM, DPIM, DH-PIM$_1$ and DH-PIM$_2$ versus the bit resolution (M) are shown in Fig. 3.3. It can be observed from this figure that changing the value of α results in a very small improvement on the average symbol length of DH-PIM. However, both DH-PIM$_1$ and DH-PIM$_2$ display a significant improvement compared with PPM and DPIM by reducing the average length of the symbol

especially at high bit resolutions ($M > 5$) where the average symbol length of DH-PIM is about quarter that of PPM and half that of DPIM.
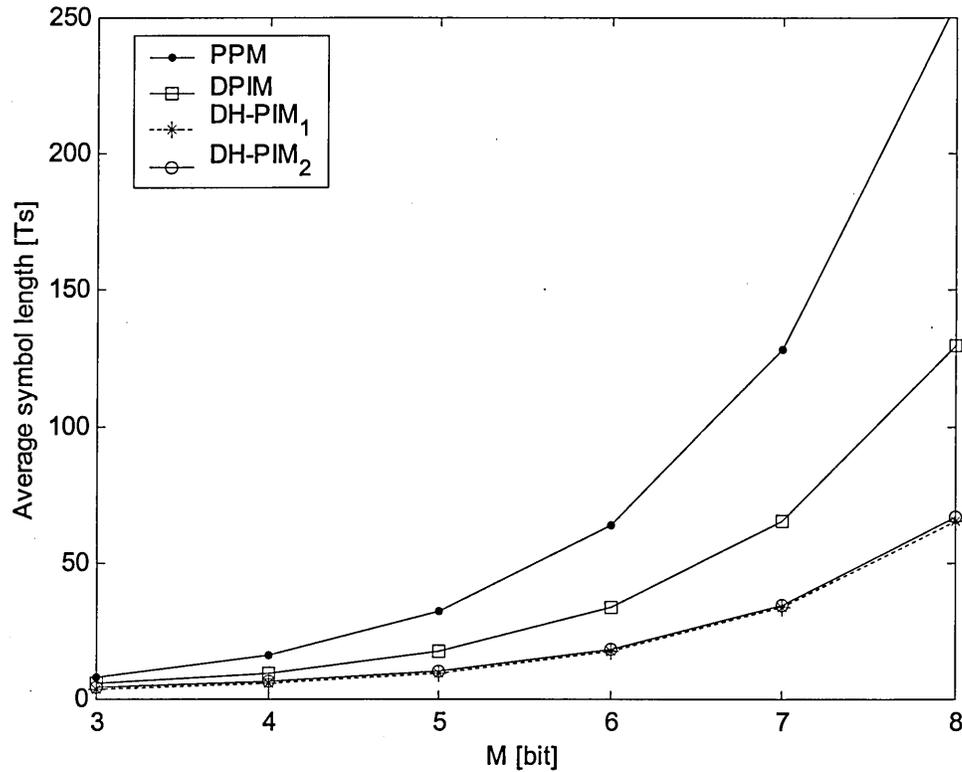
Fig. 3.3: The average symbol length of PPM, DPIM, DH-PIM$_1$ and DH-PIM$_2$ versus

M.

3.3 Transmission Bandwidth Requirements

The bandwidth requirement of any digital pulse time modulation DPTM scheme is determined by the frequency characteristics of the pulse [91].

The transmission bandwidth requirement of DH-PIM system can be expressed as:

$$B_{req} = \frac{1}{\tau_{min}}, \qquad (3.11)$$

where, τ_{min} is the minimum pulse duration which is given by (3.1) as:

$$\tau_{min} = \frac{\alpha T_s}{2}.$$ (3.12)

Therefore,

$$B_{req} = \frac{2}{\alpha T_s}.$$ (3.13)

Substituting (3.8) in (3.13) gives:

$$B_{req} = \frac{2\overline{L}R_b}{\alpha M}.$$

Therefore, from (3.7) the bandwidth requirement is given as:

$$B_{req} = \frac{R_b(2^{M-1} + 2\alpha + 1)}{\alpha M}.$$ (3.14)

The bandwidth requirement of DPIM is given by:

$$B_{req-DPIM} = \frac{R_b \overline{L}_{DPIM}}{M}.$$

Therefore, from (3.10),

$$B_{req-DPIM} = \frac{R_b(2^M + 3)}{2M}.$$ (3.15)

The bandwidth requirement of PPM is given by:

$$B_{req-PPM} = \frac{M}{R_b L}.$$

Therefore, from (3.9),

$$B_{req-PPM} = \frac{R_b 2^M}{M}. \tag{3.16}$$

The bandwidth requirements of DH-PIM given in (3.14) is plotted in Fig. 3.4 against M for $R_b = 1\text{Mbps}$ and $\alpha = 1, 2 \& 3$. The DH-PIM requires less bandwidth with α increasing particularly at high values of M (> 5). For example, with $M = 6$, DH-PIM$_1$, DH-PIM$_2$ and DH-PIM$_3$ require 5.83, 3.08 and 2.17 MHz bandwidth respectively, and at $M = 8$, they require 16.38, 8.31 and 5.63 MHz, respectively.
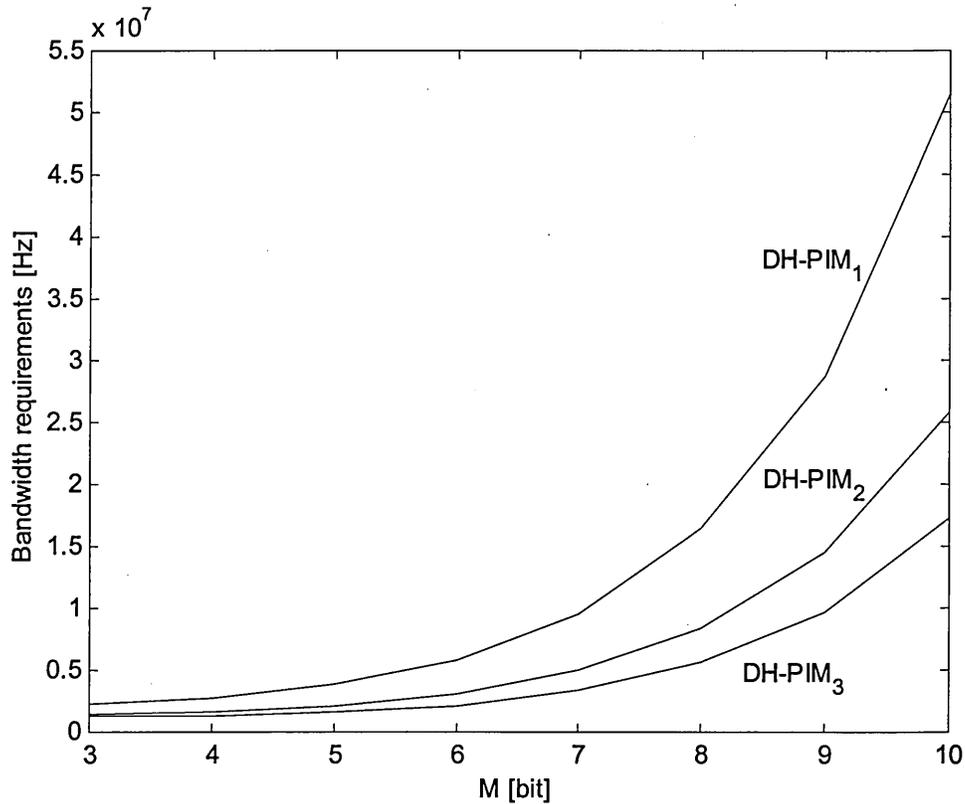
Fig. 3.4: Transmission bandwidth of DH-PIM$_1$, DH-PIM$_2$ and DH-PIM$_3$ versus M for

$$R_b = 1\text{Mbps}.$$

Figure 3.5 shows the bandwidth requirements normalised to OOK-NRZ versus bit resolution for PPM, DPIM, DH-PIM$_1$, DH-PIM$_2$ and DH-PIM$_3$. DH-PIM$_1$ has similar bandwidth requirements as DPIM but lower than PPM. For $\alpha > 1$ and $M > 5$, DH-PIM shows a considerable bandwidth improvement compared to its counterparts. For example, at $M = 6$, PPM, DPIM, DH-PIM$_1$, DH-PIM$_2$ and DH-PIM$_3$ require 10.7, 5.6, 5.8, 3.1 and 2.2 times the bandwidth of OOK-NRZ, respectively. This is because the minimum pulse width of DH-PIM increases as α increases and as M increases the symbol length of DH-PIM becomes far shorter than those of PPM and DPIM resulting in wider slot duration in the case of DH-PIM compared with its counterparts.
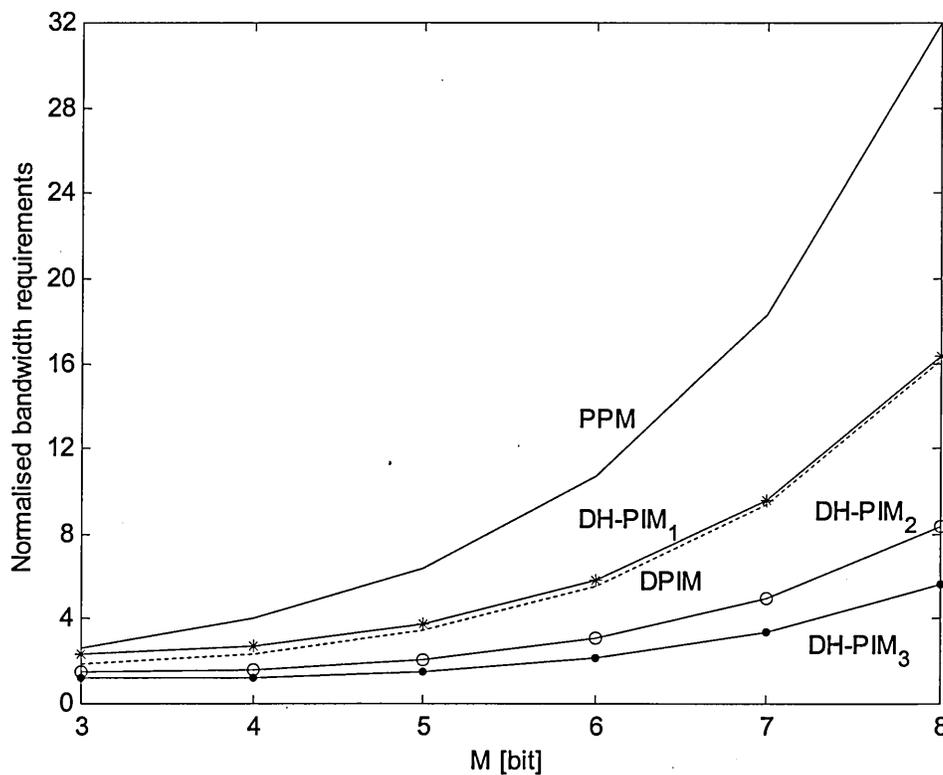
Fig. 3.5: Transmission bandwidth of PPM, DPIM, DH-PIM$_1$, DH-PIM$_2$ and DH-PIM$_3$ normalised to OOK-NRZ versus the bit resolution M.

3.4 Transmission Rate

In an anisochronous modulation scheme such as DH-PIM, the symbol length is variable and consecutive header pulses define its boundaries. Hence an error is not necessarily confined to the symbol in which it occurs. Therefore, it is convenient to base the study on the packet transmission rate rather than the bit rate.

The packet is assumed to have a fixed length of N_{pkt} bits, therefore the average length of a DH-PIM packet in time slots is given by:

$$L_{pkt} = \frac{N_{pkt}\overline{L}}{M}.$$

Substituting for $\overline{L}$,

$$L_{pkt} = \frac{N_{pkt}(2^{M-1} + 2\alpha + 1)}{2M}. \qquad (3.17)$$

The slot rate $R_s = \dfrac{1}{T_s}$ and the packet transmission rate $R_{pkt} = \dfrac{R_s}{L_{pkt}}$, therefore,

$$R_{pkt} = \frac{2M}{T_s N_{pkt}(2^{M-1} + 2\alpha + 1)}.$$

Since $T_s = \dfrac{2}{\alpha B_{req}}$ (from 3.15), then the packet transmission rate is given by:

$$R_{pkt} = \frac{\alpha M B_{req}}{N_{pkt}(2^{M-1} + 2\alpha + 1)}. \qquad (3.18)$$

For DPIM, the packet transmission rate is given by:

$$R_{pkt-DPIM} = \frac{2MB_{req-DPIM}}{N_{pkt}(2^M+3)}.$$

(3.19)

And for PPM, the packet transmission rate is given by:

$$R_{pkt-PPM} = \frac{MB_{req-PPM}}{N_{pkt}2^M}.$$

(3.20)

Figure 3.6 displays the packet transmission rate of DH-PIM$_1$, DH-PIM$_2$ and DH-PIM$_3$ versus M for a fixed bandwidth of 1 MHz and N_{pkt} = 1 kilobyte. As M increases, the transmission rate decreases because the symbol length increases, and as α increases the transmission rate increases. For example, for M = 4, the packet rate of DH-PIM$_1$, DH-PIM$_2$, and DH-PIM$_3$ are 44.4, 75.1 and 97.7 packet/sec, respectively and for M = 6, the packet rate of DH-PIM$_1$, DH-PIM$_2$, and DH-PIM$_3$ are 20.9, 39.6 and 56.3 packet/sec, respectively.
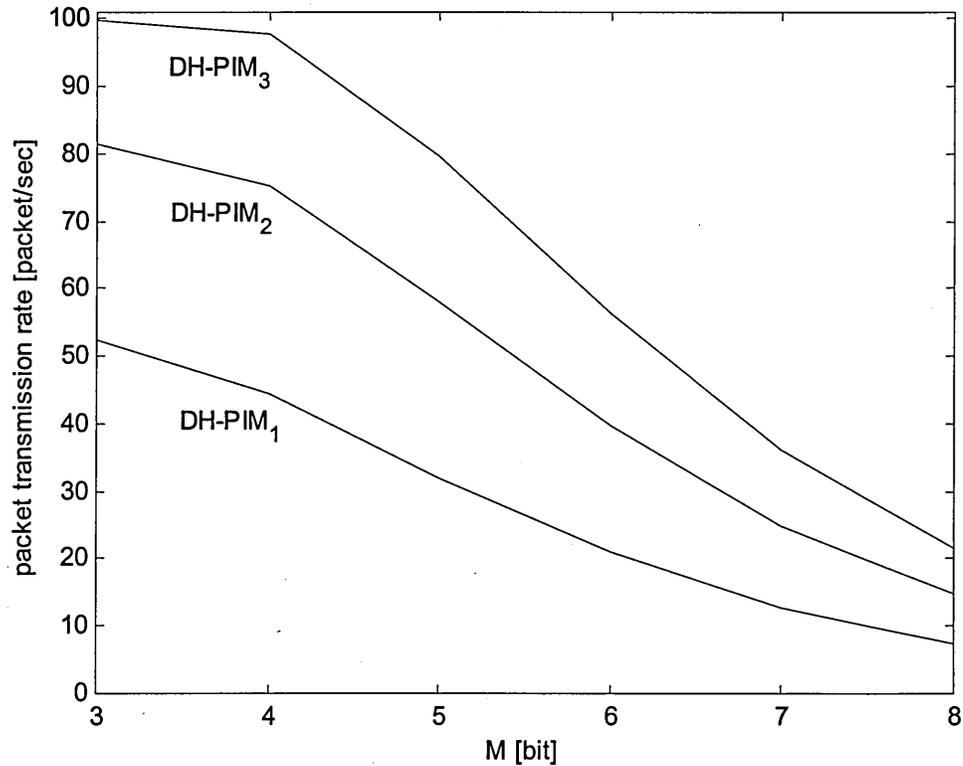
Fig. 3.6: DH-PIM₁, DH-PIM₂ and DH-PIM₃ packet transmission rate versus M for a fixed bandwidth of 1 MHz.

Figure 3.7 displays the packet transmission rate of PPM, DPIM, DH-PIM₁, DH-PIM₂ and DH-PIM₃, normalised to that of PPM versus M for a fixed bandwidth of 1 MHz. For $M > 6$, DH-PIM₁ displays similar transmission rate compared with DPIM and about twice that of PPM, however, DH-PIM₂ and DH-PIM₃ offer 4 and 6 times the transmission rate compared with PPM, respectively.
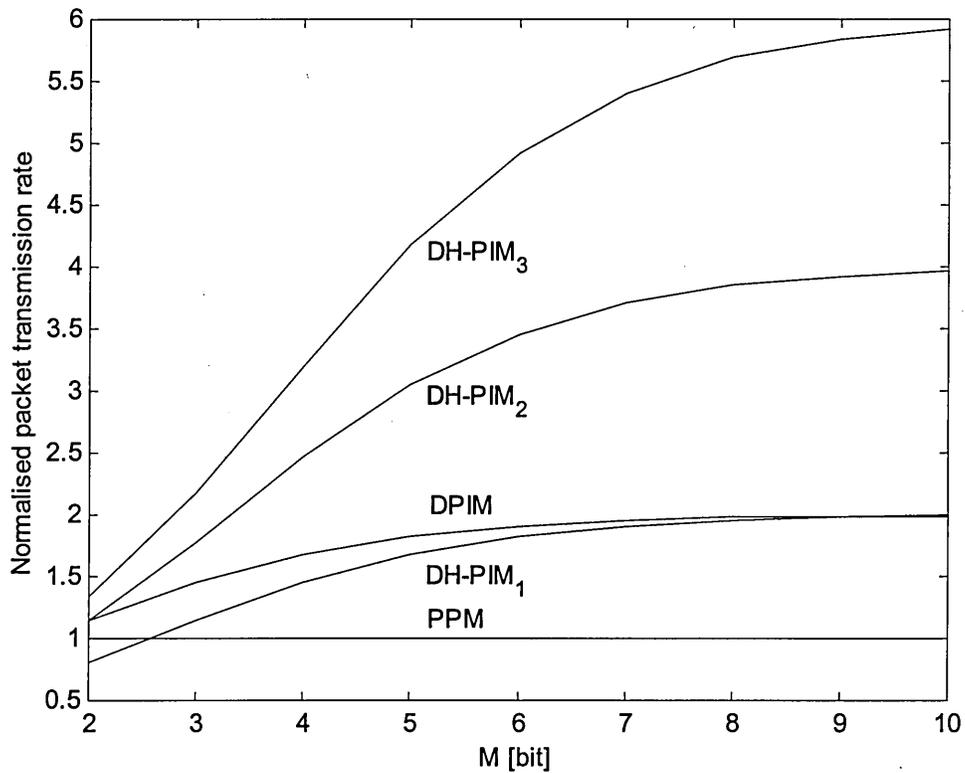
Fig. 3.7: Packet transmission rate of PPM, DPIM, DH-PIM$_1$, DH-PIM$_2$ and DH-PIM$_3$ normalised to PPM versus M for a fixed bandwidth of 1 MHz.

Figure 7.8 shows the packet transmission rate of 32-PPM, 32-DPIM, 32-DH-PIM$_1$, 32-DH-PIM$_2$ and 32-DH-PIM$_3$ versus the bandwidth requirements. It shows that 32-DH-PIM$_2$ and 32-DH-PIM$_3$ provide higher transmission rate than 32-PPM and 32-DPIM for a given bandwidth requirement. For example, for a bandwidth requirement of 6 MHz, 32-PPM, 32-DPIM, 32-DH-PIM$_1$, 32-DH-PIM$_2$ and 32-DH-PIM$_3$ achieve transmission rates of 114.3, 208.3, 191.7, 350.2 and 479.3 packet/sec, respectively. The improvement becomes even more significant for $B_{req} > 6$ MHz as shown in Fig. 3.8.
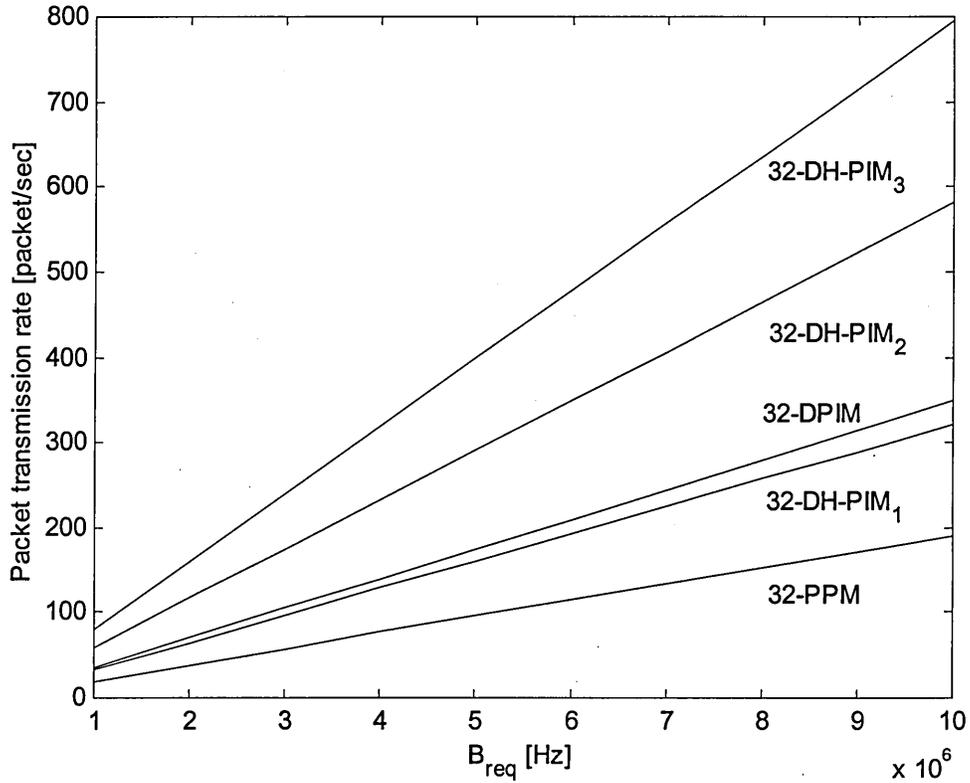
Fig. 3.8: The packet transmission rate of 32-PPM, 32-DPIM, 32-DH-PIM$_1$,

32-DH-PIM$_2$ and 32-DH-PIM$_3$ versus the bandwidth requirements.

3.5 Transmission Capacity

The transmission capacity for pulse modulation schemes is defined as [10,123]:

$$C_{Tp} = \frac{L_{\max}}{\bar{L}} R_b Log_2 \left(\text{no. of valid codes}\right). \tag{3.21}$$

In the case of DH-PIM, DPIM and PPM and assuming an M-bit input word, the number of valid code combinations is given as L.

From (3.9), (3.21) can be written as:

$$C_{Tp} = \frac{L_{\max}}{\bar{L}} R_b Log_2\left(2^M\right),$$

thus,

$$C_{Tp} = \frac{MR_b L_{\max}}{\bar{L}}. \tag{3.22}$$

From (3.6), (3.7) and (3.22), the transmission capacity of DH-PIM is given as:

$$C_T = \frac{2MR_b\left(2^{M-1} + \alpha\right)}{2^{M-1} + 2\alpha + 1}. \tag{3.23}$$

From (3.8), and (3.13), (3.24) can be rewritten as:

$$C_T = \frac{2\alpha M^2 B_{req}\left(2^{M-1} + \alpha\right)}{\left(2^{M-1} + 2\alpha + 1\right)^2}. \tag{3.24}$$

The transmission capacity of DPIM is given as [11,124]:

$$C_{T,DPIM} = \frac{4M^2 B_{req}\left(2^M + 1\right)}{\left(2^M + 3\right)^2}. \tag{3.25}$$

From (3.21), (3.9) and (3.16), the transmission capacity of PPM is given as:

$$C_{T,PPM} = \frac{M^2 B_{req}}{2^M}. \tag{3.26}$$

The transmission capacity of DH-PIM$_1$, DH-PIM$_2$ and DH-PIM$_3$ versus M for bandwidth requirement of 1 MHz is shown in Fig. 3.9. The capacity increases as M increases until $M = 5$, then starts to drop. This can be understood by reference to (3.24) where the denominator contains M to the power of 2. As α increases, higher capacity can be achieved. For example, at $M = 5$, a transmission capacity of 2.34, 4.06 and 5.36 Mbps is achieved for DH-PIM$_1$, DH-PIM$_2$ and DH-PIM$_3$, respectively.
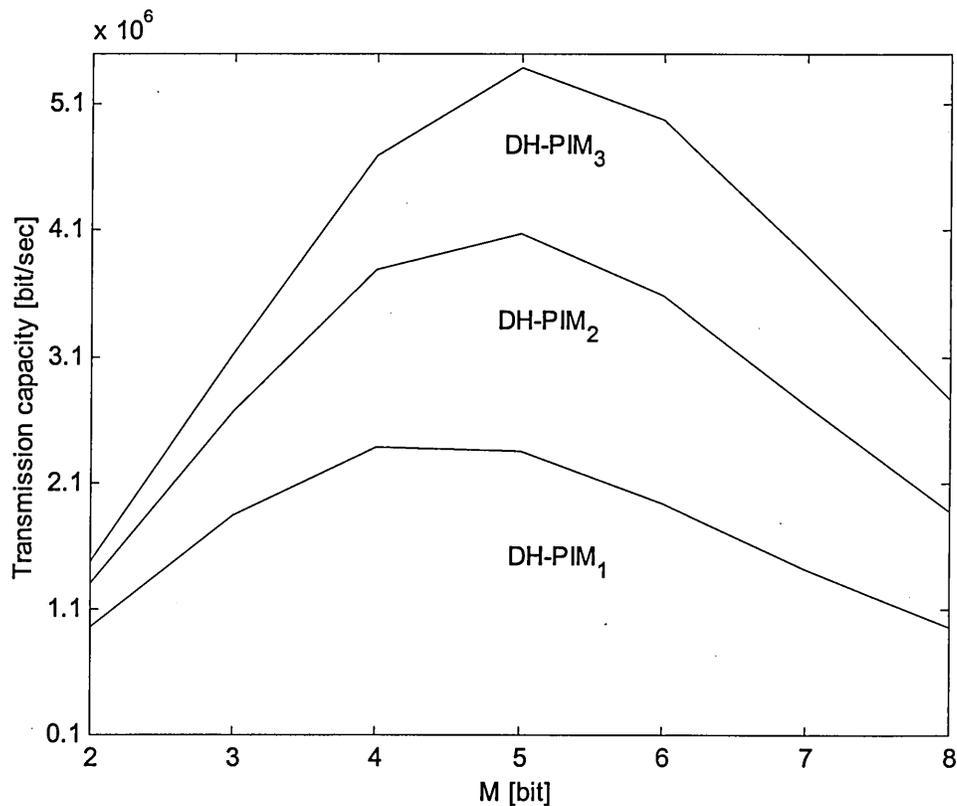
Fig. 3.9: Transmission capacity of DH-PIM$_1$, DH-PIM$_2$ and DH-PIM$_3$ versus M for bandwidth requirements = 1 MHz.

Figure 3.10 shows the transmission capacity of PPM, DPIM, DH-PIM$_1$, DH-PIM$_2$ and DH-PIM$_3$ normalised to PPM versus M for bandwidth requirements of 1 MHz. For $M > 6$, DH-PIM$_1$ and DPIM offer similar capacity, which is about four times that of

PPM. DH-PIM$_3$ and DH-PIM$_2$ achieve even higher capacity, which is about 8 and 12 times that of PPM, respectively.
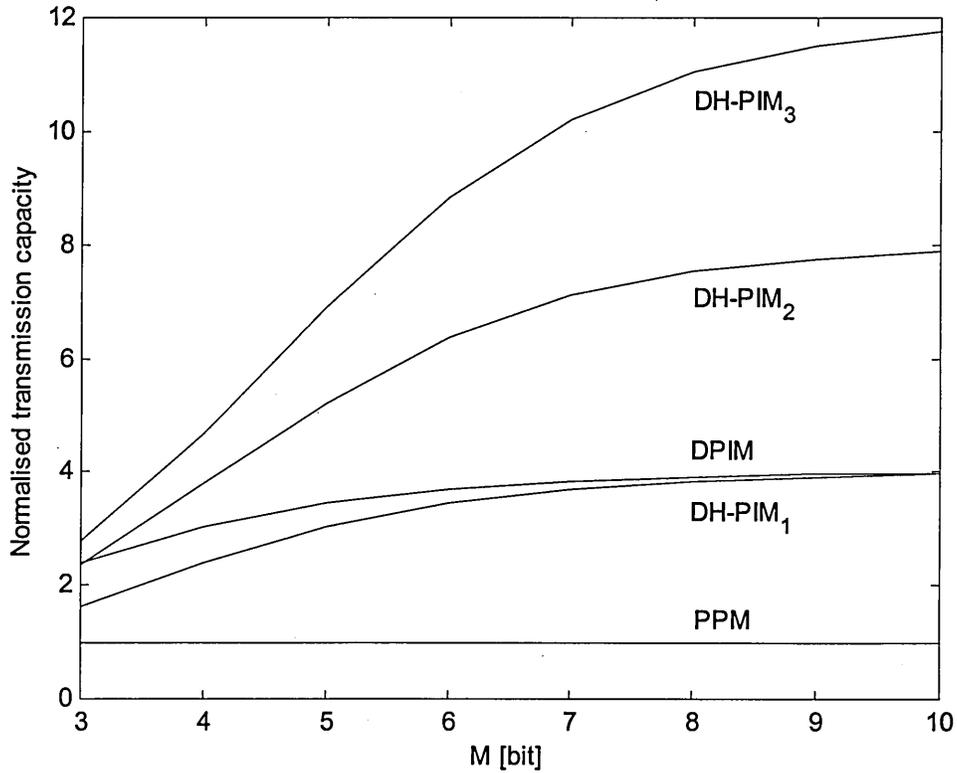
Fig. 3.10: Transmission capacity of PPM, DPIM, DH-PIM$_1$, DH-PIM$_2$ and DH-PIM$_3$ normalised to PPM versus M for bandwidth requirements = 1 MHz.

3.6 System Simulation

A general block diagram of an optical system employing DH-PIM is shown in Fig. 3.11. The DH-PIM modulator encodes every M-bit input word into a DH-PIM signal, which is used by the optical transmitter to drive the optical source. The optical source could be a laser diode or light-emitting diode (LED).
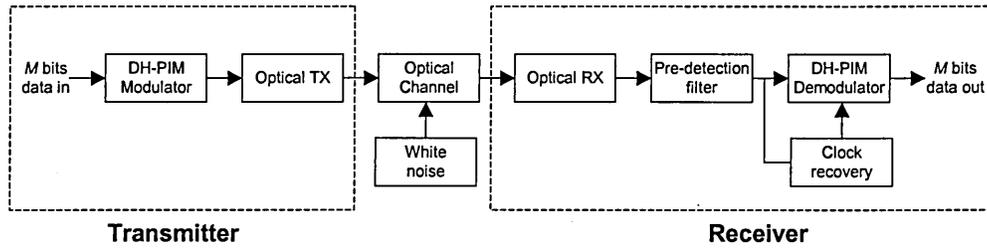
Fig. 3.11: System block diagram of DH-PIM.

The optical wireless channel adds noise, which is dominated by the background light shot noise. The shot noise is modeled as a white Gaussian noise. In addition for diffuse systems, multipath channel leads to intersymbol interference (ISI), which is significant at high bit rates > 10 Mbps [95,125]. The effect of multipath dispersion is studied in Chapter 6.

The optical receiver, typically a p-intrinsic-n (PIN) diode or avalanche photodiode (APD) converts the received optical signal into an electrical DH-PIM signal. The signal is then passed through a pre-detection filter, the output of which is passed to the demodulator in order to recover the OOK bits. Also shown is the clock recovery unit, which can be used for synchronisation, as explained in details in Chapter 4.

3.6.1 DH-PIM transmitter

The DH-PIM transmitter block diagram is shown in Fig. 3.12. The latch fetches an M-bit word. If $MSB = 0$, the decimal value of the binary word (d) is calculated, otherwise the word is inverted using a simple NOT logic gate before the decimal value (d) is calculated. A pulse generator generates the header pulse of duration $\dfrac{\alpha T_S}{2}$ corresponding to H_1 if $MSB = 0$, or αT_S corresponding to H_2 for $MSB = 1$. The generated pulse is fed into an optical transmitter. The latch will fetch the next input

word after a delay period of $(d + \alpha + 1)T_s$, which is the duration of transmitting the present symbol as shown in Fig. 3.12.
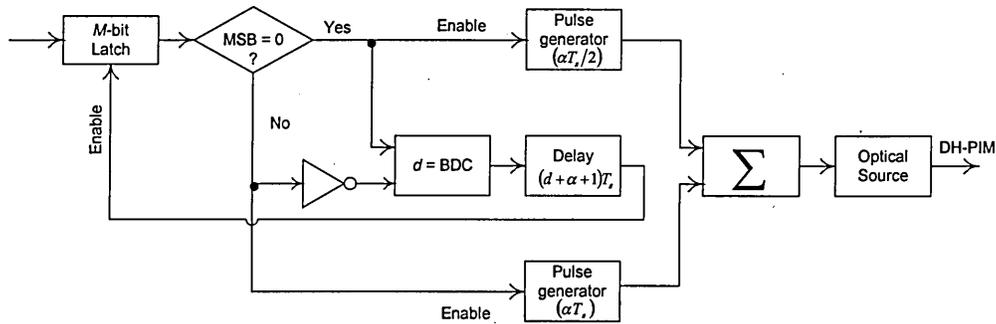
Fig. 3.12: Block diagram of DH-PIM transmitter.

3.6.2 DH-PIM receiver

The DH-PIM demodulator block diagram is shown in Fig. 3.13. At the demodulator each individual symbol length is determined by simply counting the number of time slots between the received header pulses, a process which requires no symbol synchronisation to interpret the encoded values. The regenerated electrical signal is passed through the pre-detection filter, which consists of a matched filter, sampler and the decision circuit.
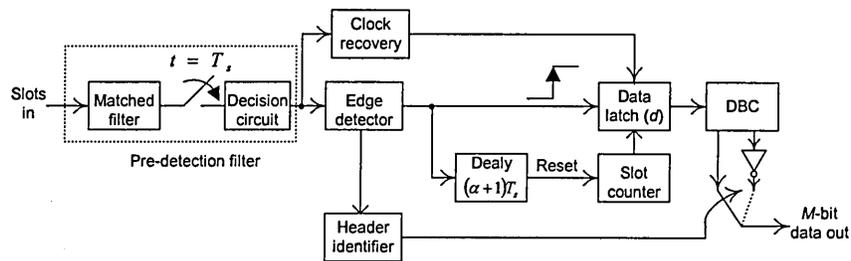
Fig. 3.13: Block diagram of DH-PIM receiver.

The output of the matched filter is sampled at the slot frequency $f_s = \dfrac{1}{T_s}$, then a simple threshold detector produces a pulse or empty slot depending on the level of the signal.

The regenerated DH-PIM signal is passed to the demodulator in order to recover the input binary words.

Once a pulse is detected, the following will happen:

- On the leading edge of the pulse, the data latch will latch the data from the slot counter which represents the information slots (d) of the previous symbol.

- After a delay of $(\alpha + 1)T_s$, the duration of the header, the slot counter will reset and start counting the number of information slots for the new symbol.

- The header identifier will measure the duration of the pulse and decides the type of header (H_1 or H_2).

- A decimal-to-binary converter will convert the number d into the binary equivalent, which will represent the input data word if the header is H_1 or its 1's complement if the header is H_2. Therefore it is required to invert the binary word if the header is H_2.

The header identifier drives the switch of the data output between the two DBC outputs according to the header detected.

The complete system, shown in Fig. 3.11 has been simulated using MATLAB. Simulation flow charts are shown in Appendix A. In the simulation, random bits of resolutions $M = 4$ and 6, have been used as input data to the transmitter at a bit rate of 1 bps. White Gaussian noise has been generated and filtered to simulate the optical channel. The level of noise has been chosen so that a slot error rate of 10^{-9} is achieved.

Figures 3.14, 3.15, 3.16 and 3.17 display selected waveforms of the first 4 symbols for 16-DH-PIM$_1$, 16-DH-PIM$_2$, 64-DH-PIM$_1$ and 64-DH-PIM$_2$, respectively. The random data generated can have any decimal values between $(0-15)$ for 16-DH-PIM and $(0-63)$ for 64-DH-PIM as explained in section 3.2. Here, the symbols shown in Figs. 3.14 and 3.15 represent the decimal values (14, 13, 7 and 0) and in Figs. 3.16 and 3.17 the values (3, 60, 9 and 15). The waveforms shown in Figs. 3.14 – 3.17 are as follows: (a) input data, (b) transmitted DH-PIM signal (c) received DH-PIM signal with noise, (d) matched filter output, (e) recovered DH-PIM signal, and (f) recovered data.
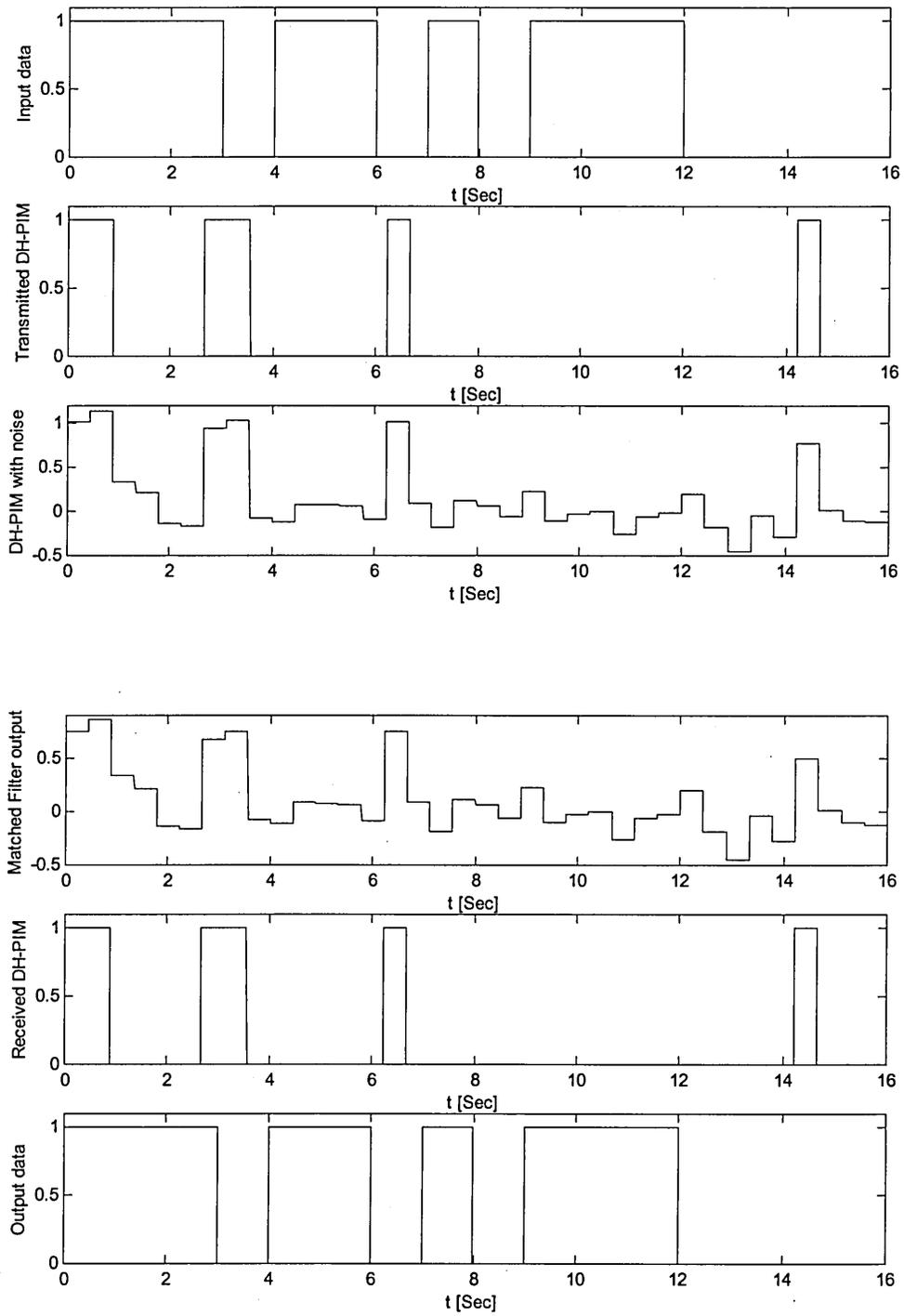
Fig. 3.14: Selected simulated waveforms for 16-DH-PIM$_1$ at a bit rate of 1 bps.

56
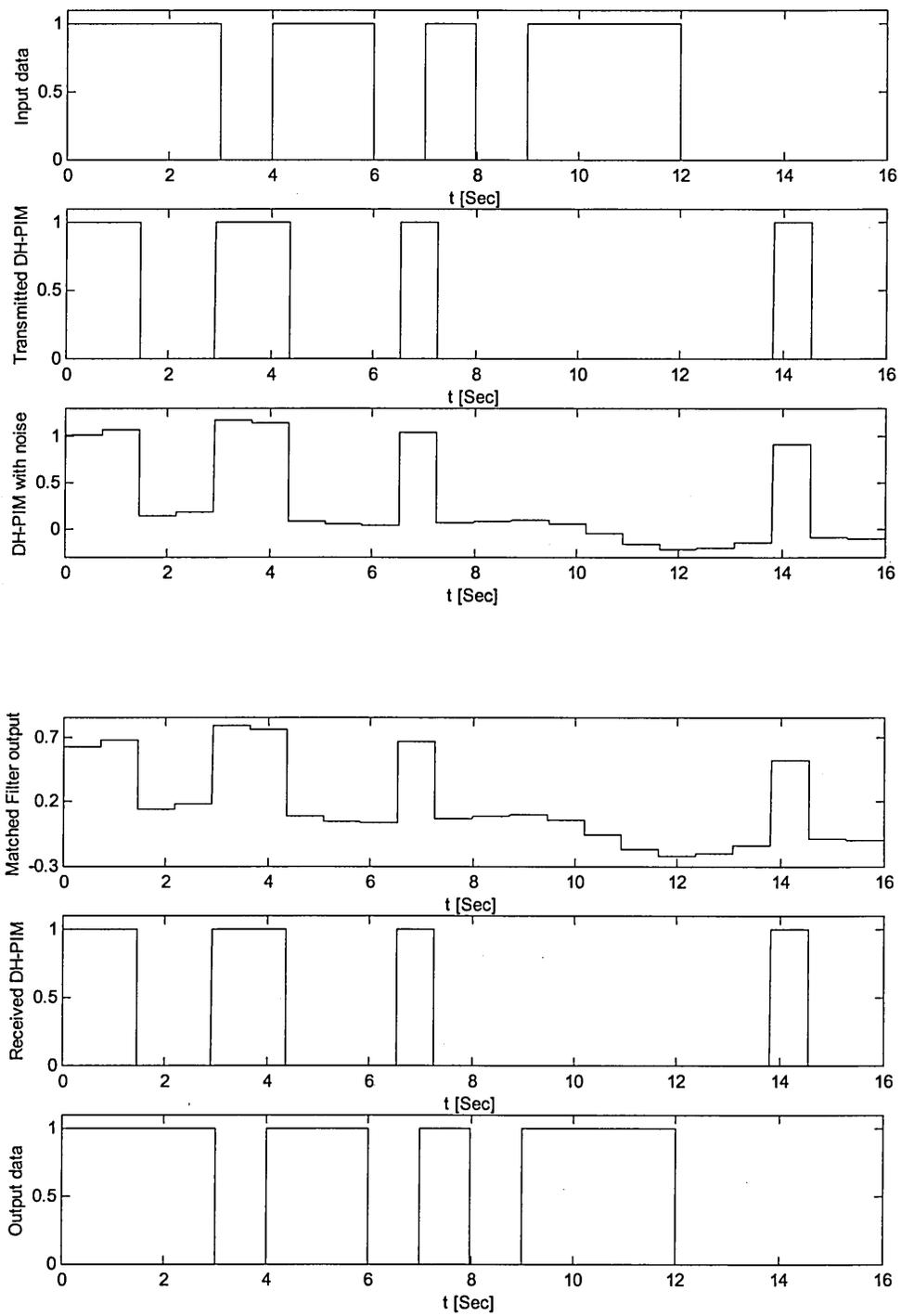
Fig. 3.15: Selected simulated waveforms for 16-DH-PIM$_2$ at a bit rate of 1 bps.
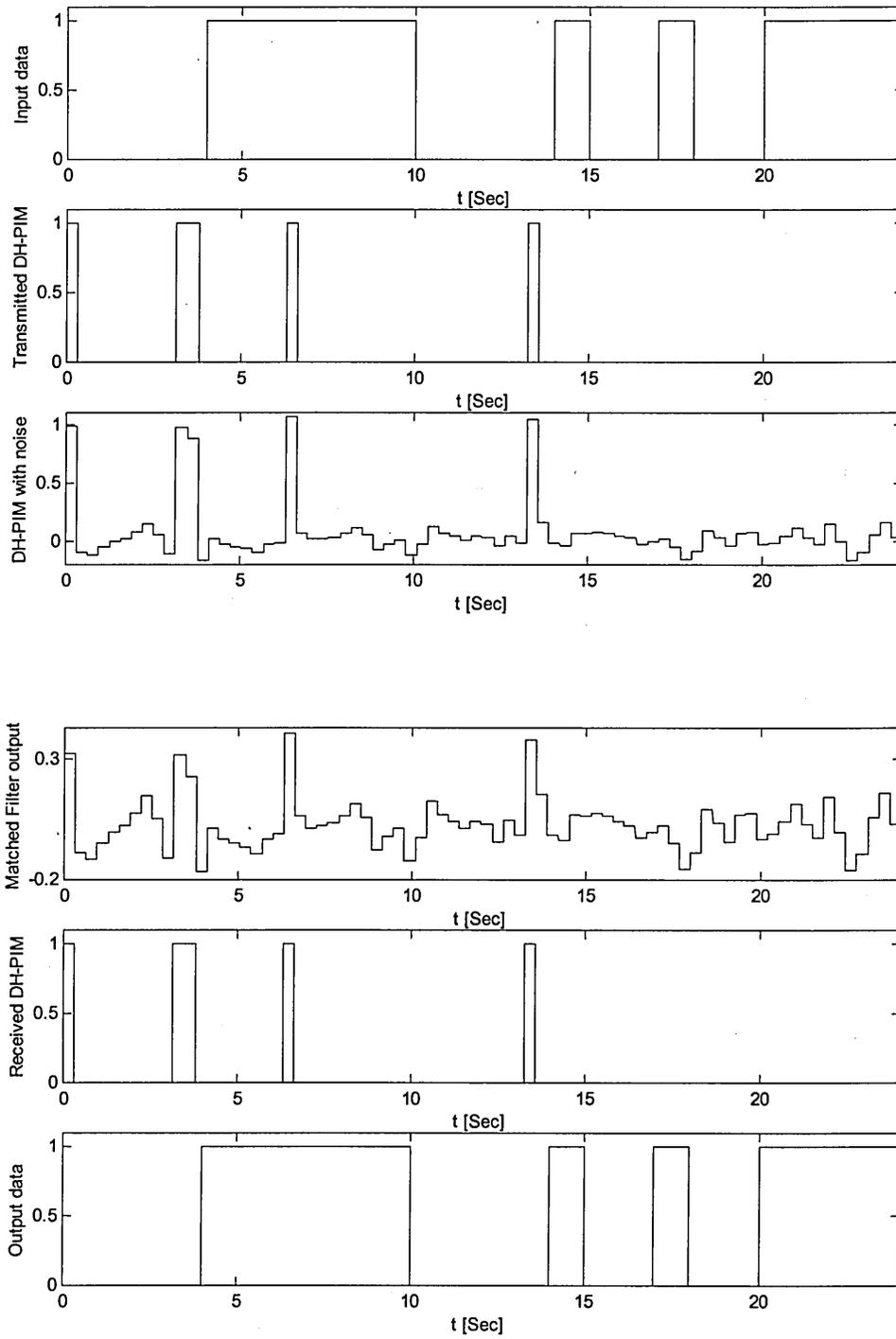
Fig. 3.16: Selected simulated waveforms for 64-DH-PIM$_1$ at a bit rate of 1 bps.
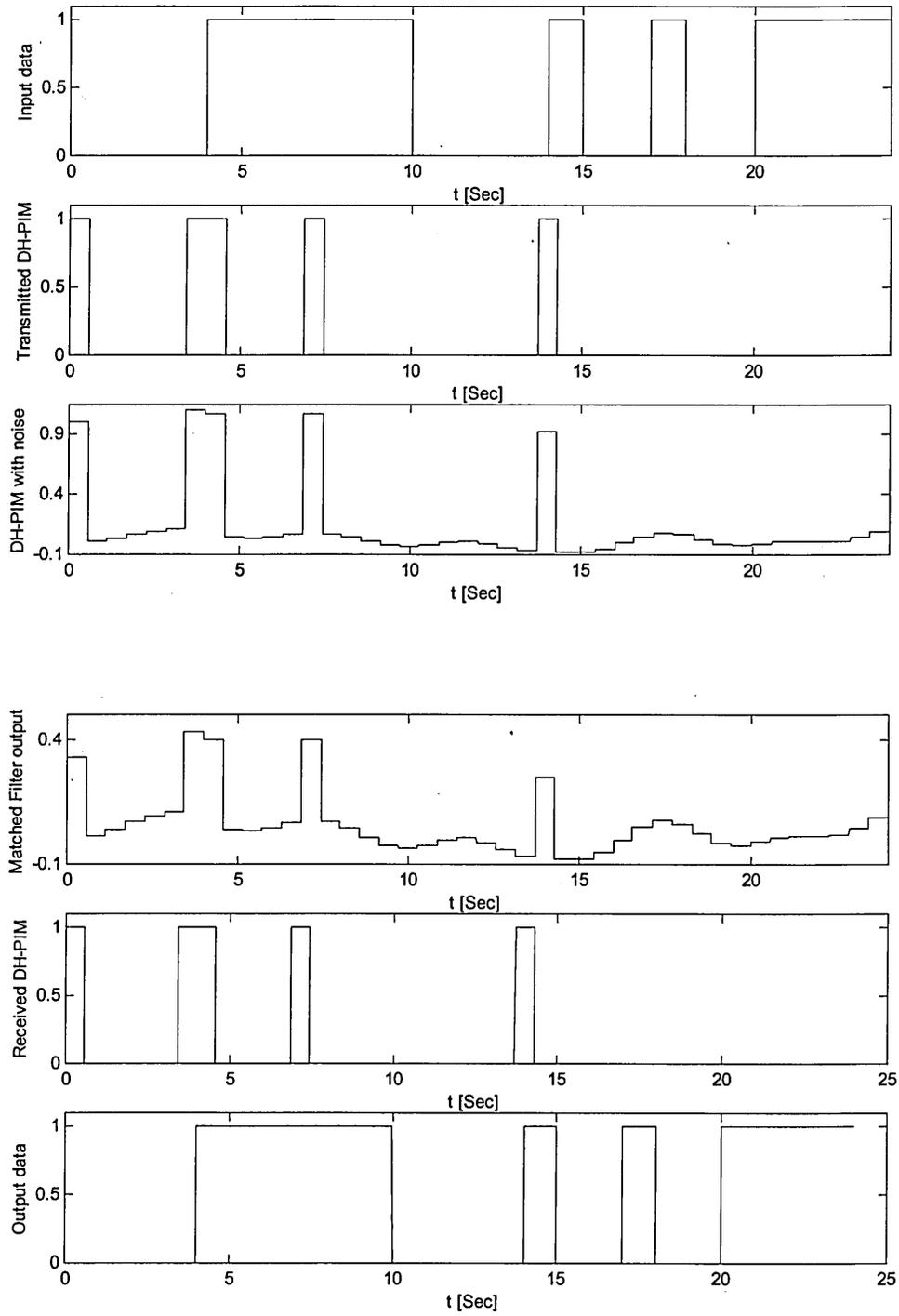
Fig. 3.17: Selected simulated waveforms for 64-DH-PIM$_2$ at a bit rate of 1 bps.

3.7 Summary

A new modulation scheme, dual header pulse interval modulation (DH-PIM), has been introduced in this chapter. The properties of the DH-PIM code, expressions to describe the pulse train, a system block diagram and simulated waveforms have been presented. Results show that DH-PIM offers shorter symbol length, improved transmission rate, capacity and bandwidth requirement compared with existing pulse techniques such as DPIM and PPM. It also provides a built-in symbol synchronisation and simple slot synchronisation. Results show that as the duration of the pulses increase (i.e. as α increases), the performance of DH-PIM improves in terms of bandwidth requirements, transmission rate and capacity. However the average symbol length increases slightly as α increases. Also discussed is the system simulation using MATLAB.

Chapter 4

SPECTRAL CHARACTERISTICS

4.1 Introduction

The spectral properties of DH-PIM pulse train are studied in this chapter. To confirm the validity of the theoretical analysis, a computer simulation model is developed and the results presented are in close agreement with the predicted results.

In section 4.2, the Fourier transform of DH-PIM pulse train is presented. Section 4.3 is devoted to a full mathematical derivation of the formula for the power spectral density of DH-PIM. A further discussion of the PSD formula is presented in section 4.4 with regard to the DC and slot spectral components and recovery of the slot components. Section 4.5 is dedicated to the results obtained from simulation and theoretical analysis. Results show that the PSD profile of DH-PIM contains a DC component, which tends to infinity when the number of symbols used in the investigation tends to infinity. The PSD profile of the DH-PIM also contains a slot component, which can be used for slot synchronisation. The locations of the slot component and its harmonics are dependent on α. Moreover, these components are distinct only when α is odd and

are masked by the nulls when α is even. Simulation of the PSD of PPM and DPIM shows a similarity to DH-PIM in the PSD profile. Concluding remarks are presented in section 4.6.

4.2 Fourier Transform of DH-PIM

The mathematical model of a DH-PIM pulse train has been presented in section 3.3. The truncated transmitted signal $x_N(t)$ of N symbols is given by (3.8) as:

$$x_N(t) = V \sum_{n=0}^{N-1} \left\{ \text{rect} \left[\frac{2(t - T_n)}{\alpha T_s} - \frac{1}{2} \right] + h_n \text{rect} \left[\frac{2(t - T_n)}{\alpha T_s} - \frac{3}{2} \right] \right\}, \qquad (4.1)$$

where V is the pulse amplitude, $h_n \in \{0,1\}$ indicating H_1 or H_2 respectively, n is the instantaneous-symbol number and T_n is the start time of the nth symbol defined in (3.10) as shown in figure 3.1.

The Fourier transform of the truncated signal (4.1) can be written as:

$$X_N(\omega) = V \sum_{n=0}^{N-1} \int_{-\infty}^{+\infty} \left\{ \text{rect} \left[\frac{2(t - T_n)}{\alpha T_s} - \frac{1}{2} \right] + h_n \text{rect} \left[\frac{2(t - T_n)}{\alpha T_s} - \frac{3}{2} \right] \right\} \cdot e^{-j\omega t} dt, \quad (4.2)$$

Where ω is the angular frequency.

Therefore,

$$X_N(\omega) = V \sum_{n=0}^{N-1} \left\{ \int_{T_n}^{T_n + \frac{\alpha T_s}{2}} e^{-j\omega t} dt + h_n \int_{T_n + \frac{\alpha T_s}{2}}^{T_n + \alpha T_s} e^{-j\omega t} dt \right\}, \qquad (4.3)$$

Thus, the Fourier transform of the truncated DH-PIM signal can be written as:

$$X_N(\omega) = \frac{V}{j\omega} e^{(-j\omega T_0)} (1 - e^{-j\omega T_s \alpha/2}) \sum_{n=0}^{N-1} \left[(1 + h_n e^{-j\omega T_s \alpha/2}) e^{-j\omega T_s n(\alpha+1)} e^{-j\omega T_s \sum_{k=0}^{n-1} d_k} \right]$$

. (4.4)

4.3 Power Spectral Density of DH-PIM

The power spectral density of the signal can be obtained by averaging over a large number of symbols N and then performing the limiting operation as given in [91]:

$$P(\omega) = \lim_{N \to \infty} \frac{E[X_N(\omega) \cdot X_N^*(\omega)]}{E[T_N - T_0]}, \qquad (4.5)$$

where $E[x]$ is the expected value of x and $X_N^*(\omega)$ is the complex conjugate of $X_N(\omega)$.

From (3.10), the expected value of $(T_N - T_0)$ is given by:

$$E[T_N - T_0] = NT_s \left[1 + \alpha + \frac{2^{M-1} - 1}{2} \right], \qquad (4.6)$$

63

and,

$$E[X_N(\omega) \cdot X_N^*(\omega)] = \left(\frac{V}{\omega}\right)^2 \left(\frac{e^{(-j\omega T_0)}}{j} \cdot \frac{e^{(j\omega T_0)}}{-j}\right)\left[\left(1 - e^{-j\omega T_s\alpha/2}\right)\left(1 - e^{+j\omega T_s\alpha/2}\right)\right] \cdot S_N(\omega),$$

$$E[X_N(\omega) \cdot X_N^*(\omega)] = 4V^2 \frac{\sin^2\left(\frac{\alpha\omega T_s}{4}\right)}{\omega^2} \cdot S_N(\omega), \tag{4.7}$$

where,

$$S_N(\omega) = E\left[\sum_{n=0}^{N-1}\sum_{q=0}^{N-1}\left((1 + h_n e^{-j\omega T_s\alpha/2})(1 + h_q e^{j\omega T_s\alpha/2})e^{-j\omega T_s(\alpha+1)(n-q)}e^{-j\omega T_s\left[\sum_{k=0}^{n-1}d_k - \sum_{k=0}^{q-1}d_k\right]}\right)\right]. \tag{4.8}$$

Expression (4.8) is best evaluated by splitting it into three regions:

(i) $S_{N1}(\omega)$, where $q < n$

(ii) $S_{N2}(\omega)$, where $q = n$

(iii) $S_{N3}(\omega)$, where $q > n$

and then summing them up as:

$$S_N(\omega) = S_{N1}(\omega) + S_{N2}(\omega) + S_{N3}(\omega). \tag{4.9}$$

Here we set out to find the expressions for $S_{N1}(\omega)$, $S_{N2}(\omega)$, and $S_{N3}(\omega)$ as outlined in (4.9).

(i)   Taking $q < n$ in (4.8) gives:

$$S_{N1}(\omega) = \sum_{n=1}^{N-1}\sum_{q=0}^{n-1} E\left[(1+h_n e^{-j\alpha\omega T_s/2})(1+h_q e^{j\alpha\omega T_s/2})e^{-j\omega T_s(\alpha+1)(n-q)}e^{-j\omega T_s\sum_{k=q}^{n-1}d_k}\right],$$

(4.10)

$$S_{N1}(\omega) = \sum_{n=1}^{N-1}\sum_{q=0}^{n-1} E\left[\left(1+h_n h_q + h_n e^{-j\alpha\omega T_s/2} + h_q e^{j\alpha\omega T_s/2}\right)\cdot e^{-j\omega T_s(\alpha+1)(n-q)}e^{-j\omega T_s\sum_{k=q}^{n-1}d_k}\right],$$

(4.11)

$$S_{N1}(\omega) = \sum_{n=1}^{N-1}\sum_{q=0}^{n-1}\left\{E\left(1+h_n h_q + h_n e^{-j\alpha\omega T_s/2} + h_q e^{j\alpha\omega T_s/2}\right)E\left[e^{-j\omega T_s\sum_{k=q}^{n-1}d_k}\right]e^{-j\omega T_s(\alpha+1)(n-q)}\right\}.$$

$h_n \in \{0,1\}$ and $h_q \in \{0,1\}$ so the expected values of h_n and h_q are:

$$E[h_n] = E[h_q] = \frac{1}{2}.$$

(4.12)

Furthermore, $h_n h_q \in \{0,0,0,1\}$ so the expected value of $h_n h_q$ is:

$$E[h_n h_q] = \frac{1}{4}, \qquad (4.13)$$

Consequently, the first factor reduces to:

$$E\left[1 + h_n h_q + h_n e^{-j\alpha\omega T_s/2} + h_q e^{j\alpha\omega T_s/2}\right] = 1 + \frac{1}{4} + \frac{e^{j\alpha\omega T_s/2} + e^{-j\alpha\omega T_s/2}}{2},$$

$$E\left[1 + h_n h_q + h_n e^{-j\alpha\omega T_s/2} + h_q e^{j\alpha\omega T_s/2}\right] = \frac{5}{4} + \cos\left(\frac{\alpha\omega T_s}{2}\right) = \frac{9}{4} - 2\sin^2\left(\frac{\alpha\omega T_s}{4}\right), \qquad (4.14)$$

and the second factor to:

$$E\left(e^{-j\omega T_s \sum_{k=q}^{n-1} d_k}\right) = E\left[\prod_{k=q}^{n-1}\left(e^{-j\omega T_s d_k}\right)\right] = \prod_{k=q}^{n-1}\left(\frac{1}{2^{M-1}} \sum_{d=0}^{2^{M-1}-1} e^{-j\omega T_s d}\right),$$

$$E\left(e^{-j\omega T_s \sum_{k=q}^{n-1} d_k}\right) = \prod_{k=q}^{n-1}\left[\frac{1}{2^{M-1}}\left(\frac{1 - e^{-j\omega T_s 2^{M-1}}}{1 - e^{-j\omega T_s}}\right)\right],$$

$$E\left(e^{-j\omega T_s \sum_{k=q}^{n-1} d_k}\right) = \left[\frac{1}{2^{M-1}}\left(\frac{1 - e^{-j\omega T_s 2^{M-1}}}{1 - e^{-j\omega T_s}}\right)\right]^{n-q}. \qquad (4.15)$$

Substituting (4.14) and (4.15) into (4.11) gives:

66

$$S_{N1}(\omega) = \sum_{n=1}^{N-1}\sum_{q=0}^{n-1}\left\{\left[\frac{9}{4}-2\sin^2\left(\frac{\alpha\omega T_s}{4}\right)\right]\cdot\left(\frac{1}{2^{M-1}}\cdot\frac{1-e^{-j\omega T_s 2^{M-1}}}{1-e^{-j\omega T_s}}\right)^{n-q}e^{-j\omega T_s(n-q)(\alpha+1)}\right\},$$

$$S_{N1}(\omega) = \left[\frac{9}{4}-2\sin^2\left(\frac{\alpha\omega T_s}{4}\right)\right]\sum_{n=1}^{N-1}\sum_{q=0}^{n-1}\left(\frac{1-e^{-j\omega T_s 2^{M-1}}}{1-e^{-j\omega T_s}}\cdot\frac{e^{-j\omega T_s(\alpha+1)}}{2^{M-1}}\right)^{n-q}. \qquad (4.16)$$

Now letting,

$$G = \left(\frac{1-e^{-j\omega T_s 2^{M-1}}}{1-e^{-j\omega T_s}}\cdot\frac{e^{-j\omega T_s(\alpha+1)}}{2^{M-1}}\right). \qquad (4.17)$$

and using the result,

$$\sum_{n=1}^{N-1}\sum_{q=0}^{n-1}G^{n-q} = \frac{G}{(1-G)^2}\left[N(1-G)-(1-G^N)\right], \qquad (4.18)$$

in (4.16) gives:

$$S_{N1}(\omega) = \left[\frac{9}{4}-2\sin^2\left(\frac{\alpha\omega T_s}{4}\right)\right]\frac{G}{(1-G)^2}\left[N(1-G)-(1-G^N)\right]. \qquad (4.19)$$

(ii) Taking $q = n$ in (4.8) gives:

$$S_{N2}(\omega) = \sum_{n=0}^{N-1}E\left[\left(1+h_n e^{-j\omega T_s\alpha/2}\right)\left(1+h_n e^{j\omega T_s\alpha/2}\right)\right],$$

$$S_{N2}(\omega) = \sum_{n=0}^{N-1} E\left[\left(1 + h_n^2 + h_n e^{-j\omega T_s \alpha/2} + h_n e^{j\omega T_s \alpha/2}\right)\right].$$

$h_n^2 \in \{0,1\}$, thus,

$$E[h_n^2] = \frac{1}{2}. \tag{4.20}$$

Hence, $S_{N2}(\omega)$ can be written as:

$$S_{N2}(\omega) = \sum_{n=0}^{N-1}\left[\frac{3}{2} + \cos\left(\frac{\alpha\omega T_s}{2}\right)\right],$$

thus,

$$S_{N2}(\omega) = \frac{N}{2}\left[5 - 4\sin^2\left(\frac{\alpha\omega T_s}{4}\right)\right]. \tag{4.21}$$

(iii) Taking $q > n$ in (4.8) gives:

$$S_{N3}(\omega) = \sum_{n=0}^{N-2}\sum_{q=n+1}^{N-1} E\left[(1 + h_n e^{-j\omega T_s \alpha/2})(1 + h_q e^{j\omega T_s \alpha/2})e^{-j\omega T_s(\alpha+1)(n-q)}e^{j\omega T_s \sum_{k=n}^{q-1}d_k}\right],$$

which can be rewritten as:

$$S_{N3}(\omega) = \sum_{q=1}^{N-1}\sum_{n=0}^{q-1} E\left[(1 + h_n e^{-j\omega T_s \alpha/2})(1 + h_q e^{j\omega T_s \alpha/2})e^{j\omega T_s(\alpha+1)(q-n)}e^{j\omega T_s \sum_{k=n}^{q-1}d_k}\right],$$

Interchanging the letters q & n gives:

$$S_{N3}(\omega) = \sum_{n=1}^{N-1}\sum_{q=0}^{n-1} E\left[(1+h_q e^{-j\omega T_s \alpha/2})(1+h_n e^{j\omega T_s \alpha/2})e^{j\omega T_s(\alpha+1)(n-q)}e^{j\omega T_s \sum_{k=q}^{n-1} d_k}\right].$$

(4.22)

Therefore,

$$S_{N3}(\omega) = S_{N1}^{*}(\omega),$$

(4.23)

and,

$$S_{N1}(\omega) + S_{N3}(\omega) = 2\,\mathrm{Re}[S_{N1}(\omega)].$$

(4.24)

Substituting (4.19), (4.21) and (4.24) into (4.9) will result in:

$$S_N(\omega) = \frac{N}{2}\left[5 - 4\sin^2\left(\frac{\alpha\omega T_s}{4}\right)\right] + \left[\frac{9}{2} - 4\sin^2\left(\frac{\alpha\omega T_s}{4}\right)\right]\mathrm{Re}\left\{\frac{G}{(1-G)^2}\left[N(1-G) - (1-G^N)\right]\right\},$$

(4.25)

with G given in (4.17).

The power spectral density of the truncated signal can be obtained by substituting (4.6) and (4.7) into (4.5) to produce:

$$P(\omega) = \frac{4V^2 \sin^2\left(\dfrac{\alpha\omega T_s}{4}\right)}{\omega^2 T_s\left[1+\alpha+\dfrac{2^{M-1}-1}{2}\right]} \cdot \lim_{N\to\infty}\left\{\frac{S_N(\omega)}{N}\right\}. \tag{4.26}$$

To simplify (4.26), the possible values of $S_N(\omega)$ must be investigated as given in (4.25), which largely depend on G.

G can be rewritten from (4.17) as:

$$G = \frac{1}{2^{M-1}}\left\{1+e^{-j\omega T_s}+e^{-j2\omega T_s}+\cdots+e^{-j\omega(2^{M-1}-1)T_s}\right\}\cdot e^{-j\omega(\alpha+1)T_s}.$$

Therefore, the absolute value of this is given as:

$$|G| = \frac{1}{2^{M-1}}\left|1+e^{-j\omega T_s}+e^{-j2\omega T_s}+\cdots+e^{-j\omega(2^{M-1}-1)T_s}\right|, \tag{4.27}$$

hence,

$$|G| \leq \frac{1}{2^{M-1}}\left\{1+\left|e^{-j\omega T_s}\right|+\left|e^{-j2\omega T_s}\right|+\cdots+\left|e^{-j\omega(2^{M-1}-1)T_s}\right|\right\}, \tag{4.28}$$

thus,

$$|G| \leq 1. \tag{4.29}$$

Therefore, only two cases needed to be investigated as outlined below.

Case 1: where $|G| < 1$

From (4.27) & (4.28), $|G| < 1$ when $e^{-j\omega T_s} \neq 1$, i.e. $\omega \neq \dfrac{2\pi K}{T_s}$ where K is a positive integer.

Here, $\lim\limits_{N \to \infty} G^N = 0$ and therefore, from (4.25):

$$\lim_{N \to \infty} \left[\frac{S_N(\omega)}{N} \right] = \frac{1}{2} \left\{ \left[5 - 4\sin^2\left(\frac{\alpha \omega T_s}{4}\right) \right] + \left[9 - 8\sin^2\left(\frac{\alpha \omega T_s}{4}\right) \right] \mathrm{Re}\left[\frac{G}{1-G} \right] \right\}, \qquad (4.30)$$

substituting (4.30) into (4.26) results in:

$$P(\omega) = \frac{4V^2 \sin^2\left(\dfrac{\alpha \omega T_s}{4}\right)\left\{ \left[5 - 4\sin^2\left(\dfrac{\alpha \omega T_s}{4}\right) \right] + \left[9 - 8\sin^2\left(\dfrac{\alpha \omega T_s}{4}\right) \right] \mathrm{Re}\left(\dfrac{G}{1-G}\right) \right\}}{\omega^2 T_s \left(2^{M-1} + 2\alpha + 1 \right)}. \qquad (4.31)$$

Expression (4.31) gives the PSD profile of the DH-PIM signal when it is finite. (Here, $|G| \neq 1$ and $\omega \neq 0$).

Case 2: where $G = 1$

From (4.27), $G = 1$ when $e^{-j\omega T_s} = 1$, i.e. $\omega = \dfrac{2\pi K}{T_s}$ where K is a positive integer.

Here, expression (4.25) is indeterminate, but applying L'Hôpital's rule [126] with $G \to 1$ gives:

71

$$\lim_{G \to 1} \left\{ \frac{G}{(1-G)^2} \cdot \left[N(1-G) - (1-G^N) \right] \right\} = \frac{N(N-1)}{2},$$

thus from (4.25):

$$S_N(\omega) = \frac{N}{4} \left\{ \left[10 - 8\sin^2\left(\frac{\alpha\omega T_s}{4}\right) \right] + (N-1)\left[9 - 8\sin^2\left(\frac{\alpha\omega T_s}{4}\right) \right] \right\}. \qquad (4.32)$$

Substituting (4.32) into (4.26) results in:

$$P(\omega) = \frac{2V^2 \sin^2\left(\frac{\alpha\omega T_s}{4}\right)}{\omega^2 T_s \left(2^{M-1} + 2\alpha + 1\right)} \lim_{N \to \infty} \left\{ \left[10 - 8\sin^2\left(\frac{\alpha\omega T_s}{4}\right) \right] + (N-1)\left[9 - 8\sin^2\left(\frac{\alpha\omega T_s}{4}\right) \right] \right\}. \quad (4.33)$$

Depending on the value of K, (4.33) will tend to 0 or ∞, as discussed below:

1. For $K = 0$, $\omega = 0$, and applying L'Hôpital's rule (since at $\omega = 0$, (4.33) is indeterminate) (4.33) will tend towards infinity with N as:

$$P(0) = \lim_{N \to \infty} \left\{ \frac{2V^2 \{9N+1\}}{T_s \left(2^{M-1} + 2\alpha + 1\right)} \lim_{\omega \to 0} \left[\frac{\sin^2\left(\frac{\alpha\omega T_s}{4}\right)}{\omega^2} \right] \right\}, \qquad (4.34)$$

$$P(0) = \frac{\alpha^2 V^2 T_s}{8\left(2^{M-1} + 2\alpha + 1\right)} \lim_{N \to \infty} \{9N+1\} \to \infty. \qquad (4.35)$$

72

2. For $K = \dfrac{2\upsilon}{\alpha}$ where $\upsilon \neq 0$ is an integer, $\omega = 2\upsilon \dfrac{2\pi}{\alpha T_S}$ (i.e. even multiple of the slot

   frequency), (4.33) reduces to zero ($P(\omega) = 0$), thus contributing to all the nulls in

   the spectrum. The location of the nulls thus depends upon α.

3. For all other frequencies of the form $\omega = \dfrac{2\pi K}{T_S}$,

$$\sin^2 \left(\frac{\alpha \omega T_S}{4} \right) = 1,$$

therefore, (4.33) reduces to:

$$P(\omega) = \frac{V^2 T_S}{2\pi^2 K^2 \left(2^{M-1} + 2\alpha + 1 \right)} \lim_{N \to \infty} (N+1), \qquad (4.36)$$

therefore,

$$P(\omega) \to \infty.$$

Thus giving the potential distinct slot component and its harmonics at $\omega = 2\pi \dfrac{K}{T_S}$,

which correspond to the case when α is an odd integer and K is an odd integer.

Therefore, the spectrum consists of a *sinc* envelope when $\dfrac{\omega T_S}{2\pi}$ is not integer, distinct

frequency components at the slot frequency and its harmonics when $\dfrac{\alpha \omega T_S}{2\pi}$ is odd

integer and nulls when $\dfrac{\alpha \omega T_S}{2\pi}$ is even integer as discussed above. This confirms that

the presence of the slot components and the locations of nulls are affected by the pulse

shape. Depending on the values of α, the slot component and its harmonics may coincide with the nulls of the *sinc* envelope, as discussed in the next section.

The above results are best summarised by:

$$P(\omega) = \begin{cases} \dfrac{4V^2 \sin^2\left(\dfrac{\alpha\omega T_s}{4}\right)\left\{\left[5-4\sin^2\left(\dfrac{\alpha\omega T_s}{4}\right)\right]+\left[9-8\sin^2\left(\dfrac{\alpha\omega T_s}{4}\right)\right]\text{Re}\left(\dfrac{G}{1-G}\right)\right\}}{\omega^2 T_s\left(2^{M-1}+2\alpha+1\right)} & ;\ \omega \neq \dfrac{2\pi K}{T_s} \\[4ex] 0 & ;\ \omega = \dfrac{2\pi K}{T_s}\ \text{and either } K \text{ even or } \alpha \text{ even} \\[3ex] \infty & ;\ \omega = \dfrac{2\pi K}{T_s}\ \text{and both } K \text{ odd and } \alpha \text{ odd.} \end{cases}$$

$$(4.37)$$

4.4 Further Discussion of the PSD Expression

4.4.1 DC component

The DC component of the power spectral density is given in (4.35). From (4.35) and assuming N is a limited and very large number, the DC component is:

$$P_{DC} \approx \frac{\alpha^2 V^2 T_s\left(9N+1\right)}{8\left(1+2\alpha+2^{M-1}\right)}. \qquad (4.38)$$

For $M = 2$ and $\alpha = 1$, the DC component of the power spectral density of 4-DH-PIM$_1$ is given from (4.38) as:

$$P_{DC,4-DH-PIM_1} = \frac{V^2 T_s (9N+1)}{40}. \qquad (4.39)$$

Therefore, by dividing the expression in (4.38) by that in (4.39), the DC component of DH-PIM normalised to that of 4-DH-PIM$_1$ can be given by:

$$P_{DC-nor} = \frac{5\alpha^2}{1 + 2\alpha + 2^{M-1}}. \qquad (4.40)$$

Therefore, the normalised DC component depends on the values of α and M as will be shown in the results section.

4.4.2 Slot component

The amplitude of the slot component tends to infinity when N tends to infinity, and assuming N is a limited and very large number, (4.36) can be written as:

$$P_{slot}(\omega) \approx \frac{V^2 T_s (N+1)}{2\pi^2 K^2 \left(2^{M-1} + 2\alpha + 1\right)}. \qquad (4.41)$$

The peak amplitude of the fundamental slot component of 4-DH-PIM$_1$ is given from (4.41) as:

$$P_{slot,4-DH-PIM_1}(\omega) = \frac{V^2 T_s (N+1)}{10\pi^2 K^2}. \qquad (4.42)$$

Therefore, by dividing (4.41) on (4.42), the peak amplitude of the fundamental slot component of DH-PIM normalised to that of 4-DH-PIM$_1$ can be given by:

$$P_{slot-nor} = \frac{5}{1 + 2\alpha + 2^{M-1}}.$$

(4.43)

Therefore, the amplitude of the normalised fundamental slot component is a function of M and α as will be shown in the results section.

4.4.3 Slot recovery

The presence of the slot component in the spectrum suggests that the slot synchronisation can be achieved using a phase locked loop (PLL) circuit which can be employed at the receiver to extract the slot frequency directly from the incoming DH-PIM data stream similar to that in PPM and DPIM. For all even values of α, the slot components are masked by the nulls and therefore, at the receiver end a simple PLL circuit is not capable of extracting the slot frequency. However, the slot frequency can be extracted by employing a nonlinear device followed by a PLL circuit [127-128].

4.5 Results and Discussions

In this section the results obtained from the theoretical analysis and from computer simulation are presented. The predicted results have been obtained using (4.37). To confirm the predicted results, the complete DH-PIM system has been simulated using MATLAB which estimates the PSD using Welch's averaged modified periodogram method. The simulation process is explained in a flow chart as shown in Fig. 4.1.

```
                        ┌─────────────┐
                        │    Start    │
                        └─────────────┘
                               │
                               ▼
                   ┌───────────────────────┐
                   │   Select parameters   │
                   │   (M, Tₛ, V, N and α)  │
                   └───────────────────────┘
                               │
                               ▼
                   ┌───────────────────────┐
                   │ Generate N M-bit      │
                   │ symbols of random     │
                   │ data bits             │
                   └───────────────────────┘
                               │
                               ▼
                   ┌───────────────────────┐
                   │   Encode into a       │
                   │   DH-PIM sequence     │
                   └───────────────────────┘
                               │
                               ▼
                   ┌───────────────────────┐
                   │ Replace each '1' by   │
                   │ 10 '1's and each '0'  │
                   │ by 10 '0's.           │
                   └───────────────────────┘
                               │
                               ▼
                   ┌───────────────────────┐
                   │  Apply PSD function   │
                   │   on the sequence     │
                   └───────────────────────┘
                               │
                               ▼
                   ┌───────────────────────┐
                   │ Plot PSD curve vs.    │
                   │ frequency             │
                   └───────────────────────┘
                               │
                               ▼
                        ┌─────────────┐
                        │  All done   │
                        └─────────────┘
```
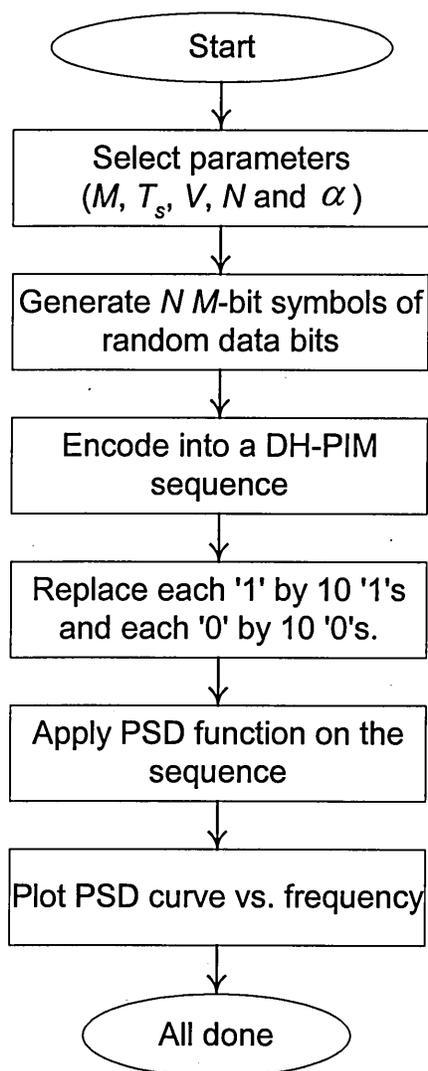
Fig. 4.1: Flow chart of the simulation process using Matlab.

A data generator has been used to obtain N consecutive input symbols of OOK-NRZ data, which were encoded by a DH-PIM modulator to produce the corresponding DH-PIM symbols. The ideal results require N to tend to infinity, however, because of computational power limitations, N is chosen to be 500 symbols. This process has been repeated for different bit resolution M and different values of α. The slot duration is chosen as $T_s = 1$ sec., thus the slot frequency is 1 Hz. Table 4.2 shows the parameters used to obtain the calculated and simulated results.

Parameter	Value
α	1, 2, 3, 4 and 5
M	2, 3, 4, 5, 6, 7 and 8 slots
N	500 symbols
T_s	1 sec
V	1 volt
Pulse duty cycle (for PPM and DPIM)	100%

Table 4.2: Parameters used in the calculation and simulation.

The PSD was obtained and the results are shown in Figs. 4.2, 4.3 and 4.4 for 8-DH-PIM$_1$, 8-DH-PIM$_2$ and 8-DH-PIM$_3$, respectively. Also the corresponding predicted results using the same simulation parameters are shown in Figs. 4.2, 4.3 and 4.4. It can be noticed from these figures that the predicted and simulated results display a very good agreement. However, at slot frequency and its harmonics, the simulated results have shorter amplitude than the predicted ones because of the limitations on the

number of symbols used in simulation, and these components should tend to infinity when N tends to infinity as explained in (4.37).

The spectral profile of DH-PIM$_1$ contains a DC component, a distinct slot component and its harmonics at odd multiples of the slot frequency, and nulls at even multiples of the slot frequency as shown on Fig. 4.2.
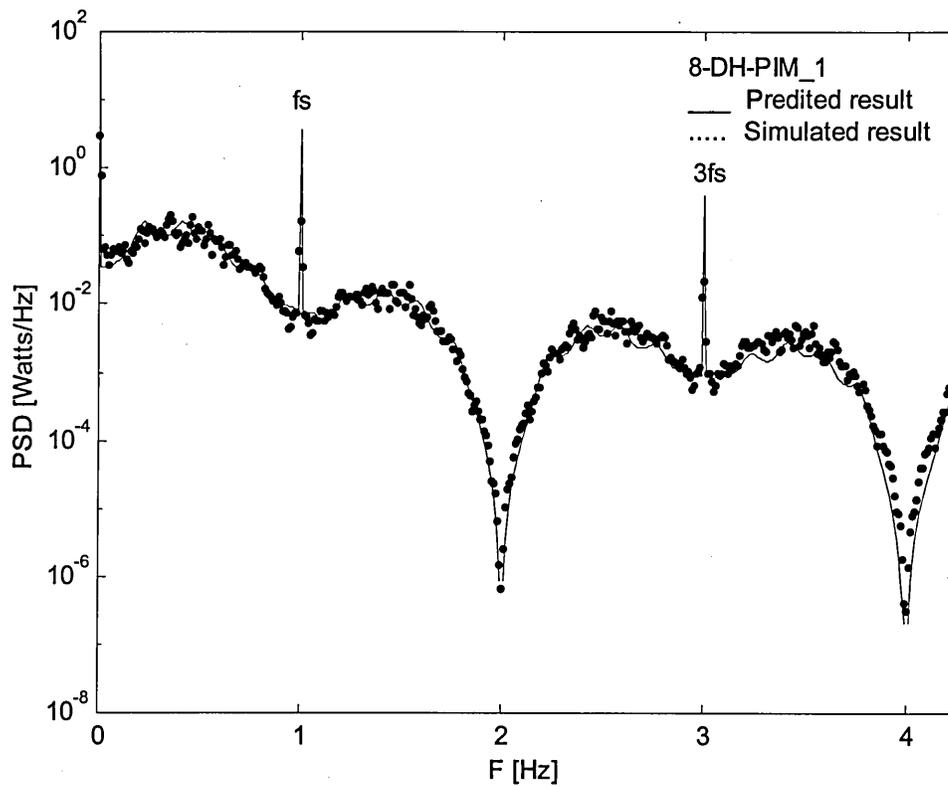
Fig. 4.2: The predicted and simulated power spectral density of 8-DH-PIM$_1$ versus the

frequency.

For DH-PIM$_2$, the nulls coincide with the slot component and its harmonics, thus suppressing them to zeros as shown in Fig. 4.3.
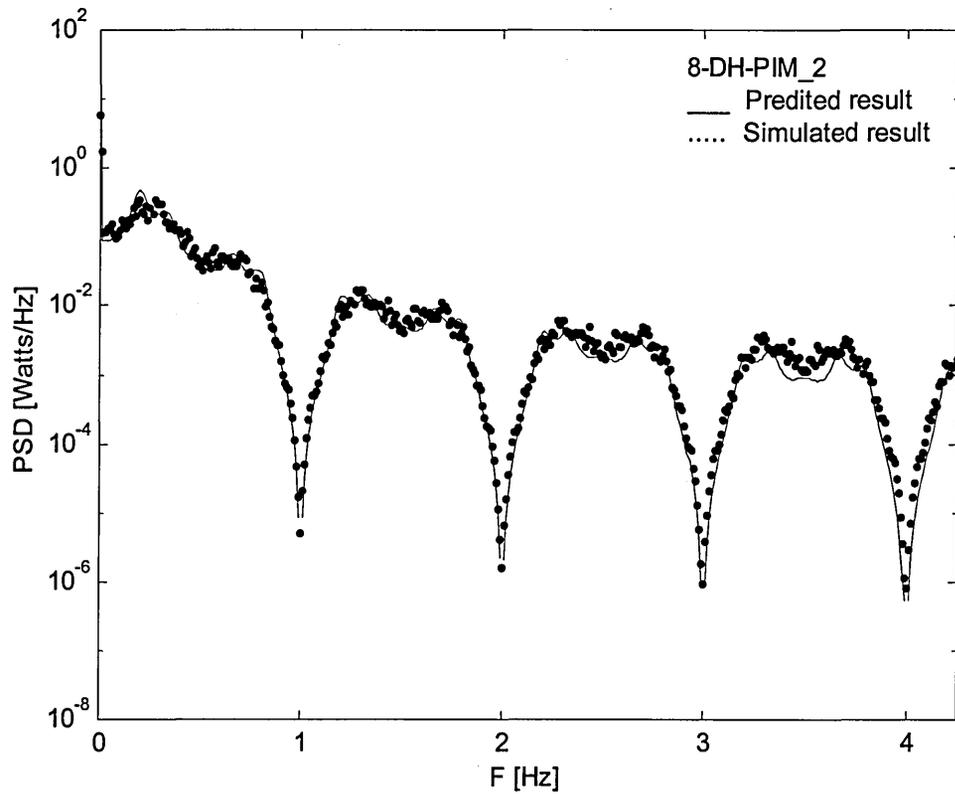
Fig. 4.3: The predicted and simulated power spectral density of 8-DH-PIM₂ versus the

frequency.

For DH-PIM₃, the slot components remain fixed in the frequency spectrum as in

DH-PIM₁, however three nulls exist between the slot component and its third harmonic

as shown in Fig. 4.4.
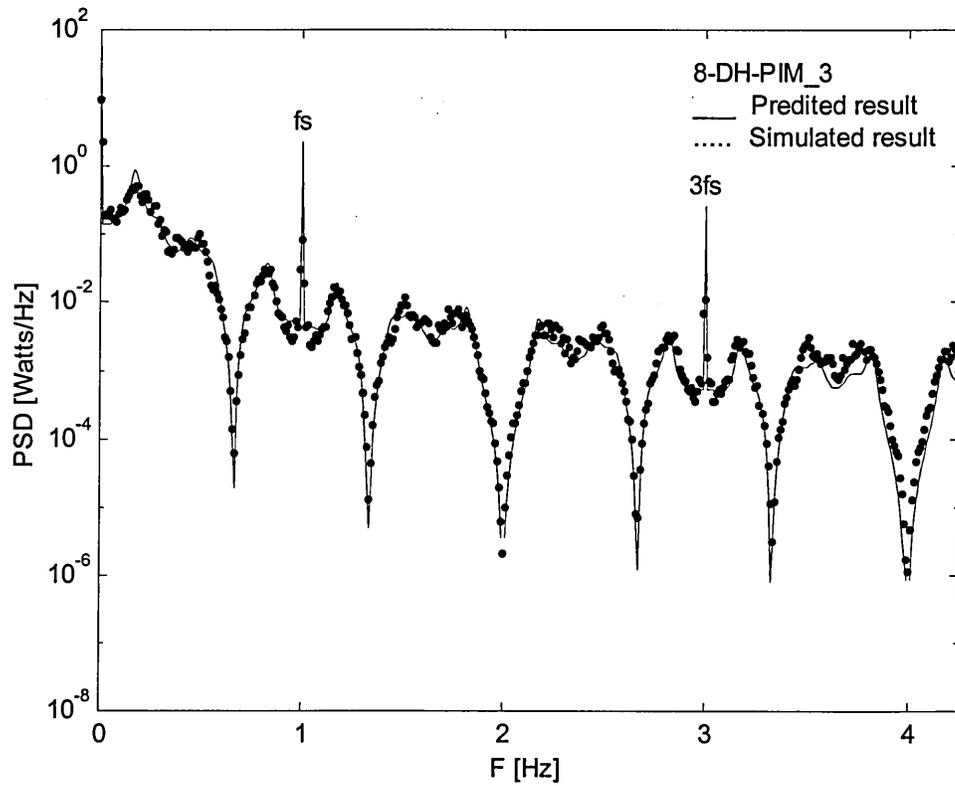
Fig. 4.4: The predicted and simulated power spectral density of 8-DH-PIM₃ versus the frequency.

For higher values of the bit resolution M, the PSD profile is similar to $M = 3$, however the amplitude decreases as M increases. This is best illustrated in Figs 4.5 and 4.6 where 3-D plots of the simulation results for DH-PIM₁ and DH-PIM₂ are presented. Figs. 4.5 and 4.6 incorporate essential features of Figs. 4.2, 4.3 and 4.4 as already discussed. Notice the disappearance of the slot components at high values of M (i.e. $M > 7$). Thus, making the clock recovery process a complex one.
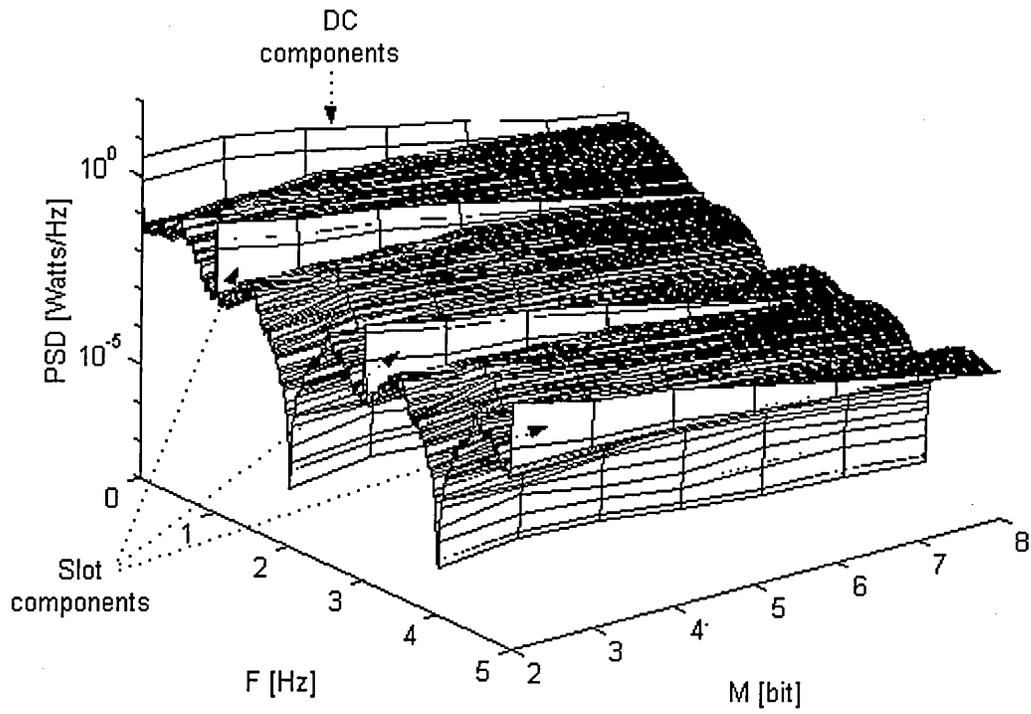
Fig. 4.5: 3-D simulated power spectral density of DH-PIM$_1$ versus the bit resolution
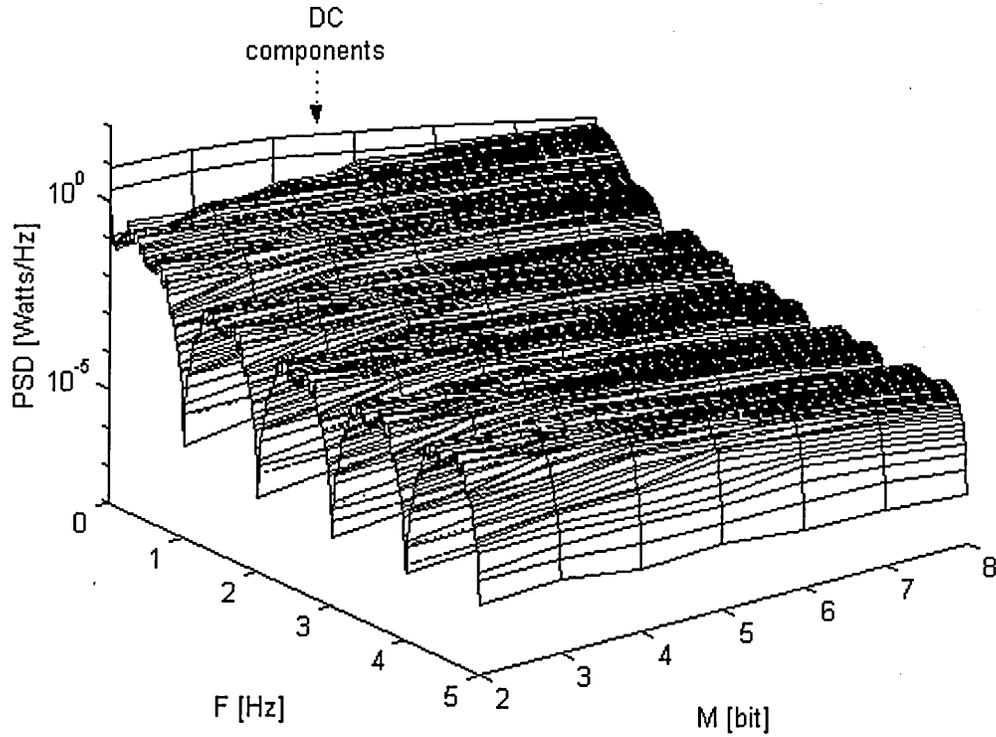
(*M*) and the frequency.

Fig. 4.6: 3-D simulated power spectral density of DH-PIM$_2$ versus the bit resolution

(M) and the frequency.

For $\alpha > 3$ the spectral profile is broadly similar to the above results.

The PSD profile of DH-PIM contains a distinct DC component, which tends to infinity when N tends to infinity as given in (4.35). From (4.40), the normalised DC component decreases as α decreases and M increases. Figure 4.7 shows the predicted DC component of DH-PIM$_1$, DH-PIM$_2$, DH-PIM$_3$, DH-PIM$_4$ and DH-PIM$_5$ normalised to that of 4-DH-PIM$_1$ versus the bit resolution M.
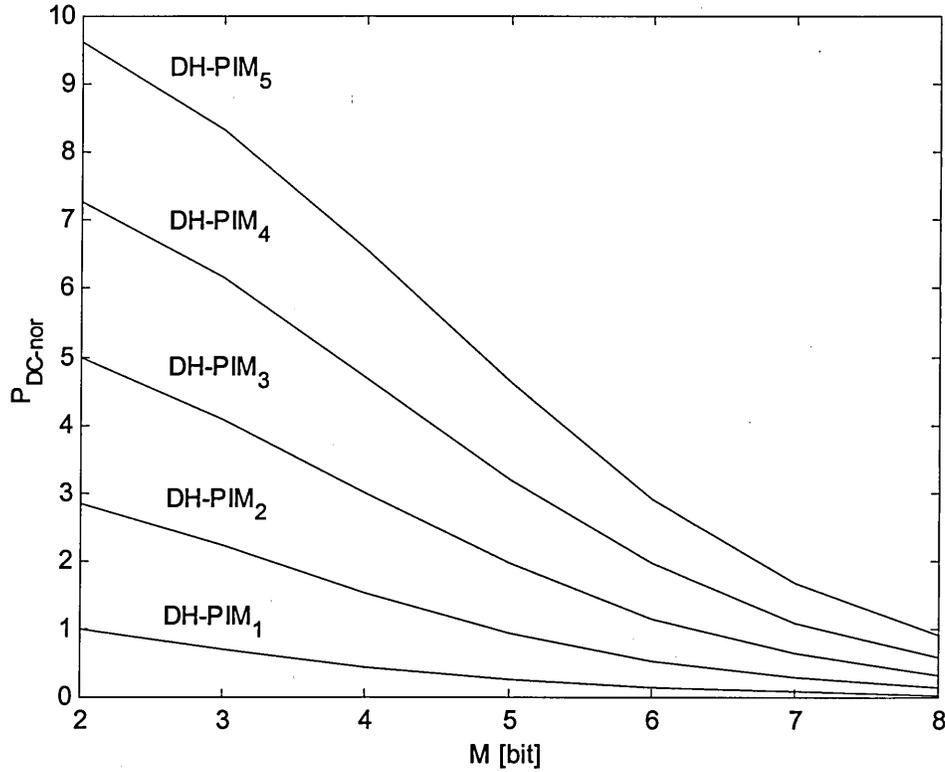
Fig. 4.7: Predicted DC component of DH-PIM$_1$, DH-PIM$_2$, DH-PIM$_3$, DH-PIM$_4$ and

DH-PIM$_5$ normalised to that of 4-DH-PIM$_1$ versus the bit resolution M.

Changing the value of α has an effect on the amplitude of the normalised DC component when M is small ($M < 6$), however, P_{DC-nor} becomes less dependant on α for $M > 6$. For example, at $M = 3$, the normalised DC level of DH-PIM$_1$ is about 1.5, 3.4, 5.5 and 7.6 less than DH-PIM$_2$, DH-PIM$_3$, DH-PIM$_4$ and DH-PIM$_5$, respectively. However, at $M = 8$, the normalised DC level of DH-PIM$_1$ is about 0.11, 0.29, 0.54 and 0.85 less than DH-PIM$_2$, DH-PIM$_3$, DH-PIM$_4$ and DH-PIM$_5$, respectively as shown in Fig. 4.7.

The slot component of DH-PIM is distinct only when α is odd, and is masked by the nulls when α is even. From (4.43), the amplitude of the normalised slot component ($P_{slot-nor}$) decreases as α and M increase. Figure 4.8 shows the predicted slot components of DH-PIM$_1$, DH-PIM$_3$ and DH-PIM$_5$ normalised to that of 4-DH-PIM$_1$ versus M as given in (4.43).
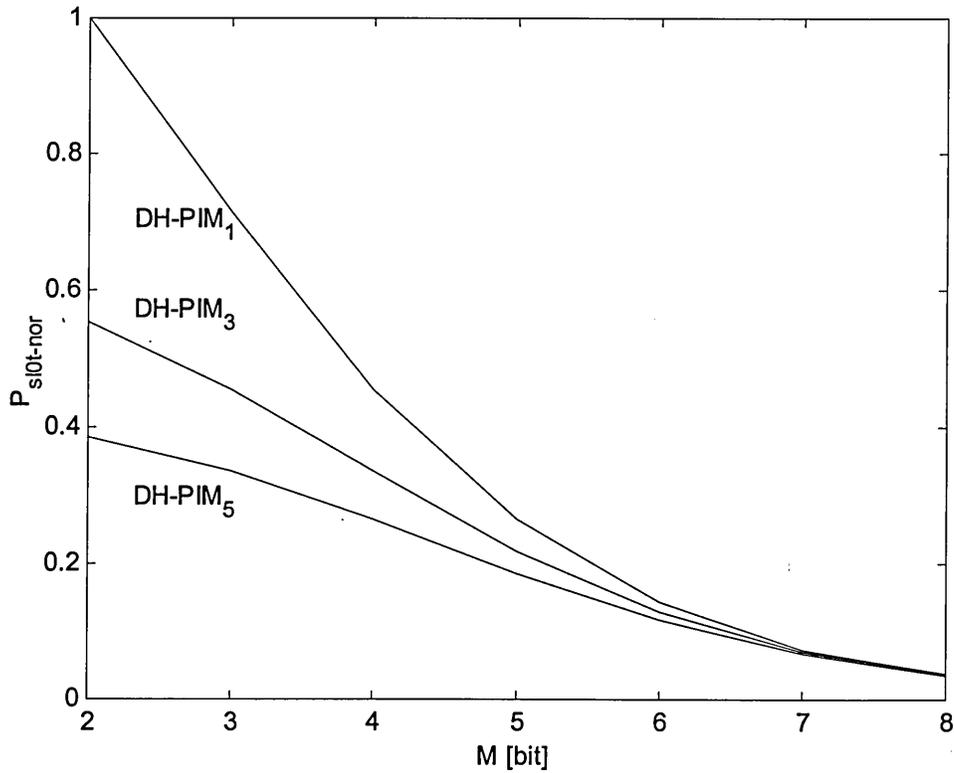
Fig. 4.8: Predicted fundamental slot component of DH-PIM$_1$, DH-PIM$_3$ and DH-PIM$_5$ normalised to that of 4-DH-PIM$_1$ versus the bit resolution M.

$P_{slot-nor}$ depends strongly on α when M is small ($M < 4$) decreasing with higher values of α. However, at higher bit resolution ($M > 4$), the slot component becomes less distinct and less dependent on α as shown in Fig. 4.8.

For example, For $M = 3$, the normalised slot amplitude of DH-PIM$_1$ is ~ 0.26 and ~ 0.38 greater than DH-PIM$_3$ and DH-PIM$_5$, respectively. However, for $M = 6$, the normalised slot amplitude of DH-PIM$_1$ is ~ 0.015 and ~ 0.027 greater than DH-PIM$_3$ and DH-PIM$_5$, respectively as shown in Fig. 4.8.

To compare the PSD of DH-PIM with those of PPM and DPIM, the later two systems have been simulated following the same procedure explained in Fig. 4.1 and the same parameters as in DH-PIM system. The pulse duty cycle is chosen to be 100%, thus the slot components are masked by the nulls. The PSD profile for 8-DH-PIM$_2$, 8-PPM and 8-DPIM versus the frequency is shown in Fig. 4.9. The PSD curve of 8-DH-PIM$_2$ is similar to those of 8-DPIM and 8-PPM, however, 8-DH-PIM$_2$ has a slightly higher PSD profile. This results from the fact that, the slot duration of DH-PIM is wider than those of DPIM and PPM, and, unlike PPM and DPIM where the symbol contains one pulse only, each DH-PIM symbol may contain one or two pulses. This suggests that the effect of baseline wander, which arises from the use of a high-pass filter to mitigate ISI caused by fluorescent lighting [16,81-82,129], on DH-PIM will be slightly worse than it on PPM and DPIM.
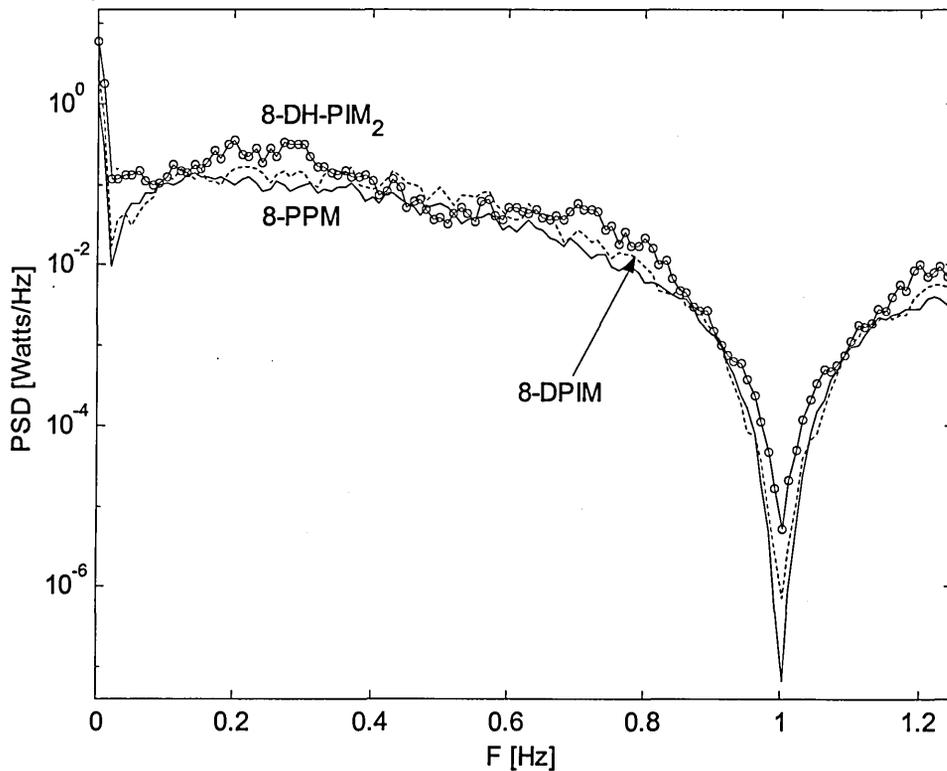
Fig. 4.9: Simulated power spectral density of DH-PIM₂, DPIM and PPM versus the

frequency.

4.6 Summary

A complete mathematical model has been developed to investigate the spectral

behaviour of DH-PIM pulse train has been presented. Simulation results presented are

in close agreement with the theoretical predictions, thus validating the DH-PIM

spectral model.

It is shown that DH-PIM contains a DC component, which tends to infinity when the

number of symbols tends to infinity. The normalised DC component decreases as α

decreases and M increases and is very much dependant on the value of α for $M < 6$.

The slot component of DH-PIM, which can be used for slot synchronisation, tends to

infinity when the number of symbols tends to infinity, however, it is distinct only when α is odd and is masked by the nulls when α is even. The amplitude of the normalised slot component decreases as α and M increase and it depends strongly on α when M is small ($M < 4$).

Simulation results showed that DH-PIM$_2$ has a slightly higher PSD profile compared with PPM and DPIM, however, the PSD profiles of the three schemes are similar.

Chapter 5

ERROR PERFORMANCE

5.1 Introduction

In this chapter, the error performance of DH-PIM in distortion-free LOS optical wireless channels is analysed. A complete derivation of the equations for slot and packet error rates for DH-PIM scheme is presented in section 5.2 as well as the corresponding formulas for DPIM, PPM and OOK. An equation for the optical power requirement of DH-PIM is also derived, and the corresponding formulas for DPIM, PPM and OOK are given in section 5.3. Section 5.4 presents results obtained from computer simulation and theoretical calculations. The simulated results match with the calculated results, confirming the validity of the theoretical analysis. The performance of DH-PIM is compared with PPM, DPIM and OOK modulation schemes. It is shown that DH-PIM offers improved error performance compared with OOK but is marginally inferior to PPM. DH-PIM$_1$ displays an improvement performance over DH-PIM$_2$ but similar performance compared with DPIM. Results also show that the

minimum optical power and bandwidth requirements are achieved for 16-DH-PIM$_1$ and 64-DH-PIM$_2$. A summary of the chapter is presented in section 5.5.

5.2 Probability of Errors

In DH-PIM, the symbol length is variable and consecutive header pulses define its boundaries. Hence an error is not necessarily confined to the symbol in which it occurs. Consider a packet of DH-PIM symbols. A pulse detected in the wrong slot would only affect symbols either side of the pulse, whereas detecting an additional pulse (i.e. false alarm) would split a symbol into two shorter length symbols. On the other hand, a pulse not detected would combine two symbols into one longer sequence of a length greater than L_{max} or otherwise. Therefore, in order to compare the performance of the DH-PIM with other schemes, it is necessary to base the analysis on the packet error rate (PER) rather than bit error rate (BER).

A non-dispersive optical wireless system model for IM/DD schemes DH-PIM, DPIM, PPM and OOK employing a threshold detector is shown in Fig. 5.1. The waveform $x(t)$ is scaled by the peak photocurrent I_p and the slot duration T_s is chosen so that the symbol in each modulation scheme has the same average transmitted optical power $\overline{P}$, which is assumed as a reference. The optical signal is transmitted over a non-dispersive channel $h(t)$. White Gaussian noise is added to the signal before being detected at the receiver. The receiver employs a unit-energy filter $r(t)$, which is matched to $x(t)$ followed by a sampler operating at a rate $f_s = \dfrac{1}{T_s}$. Finally, a simple threshold detector is employed to recover the detected symbol.
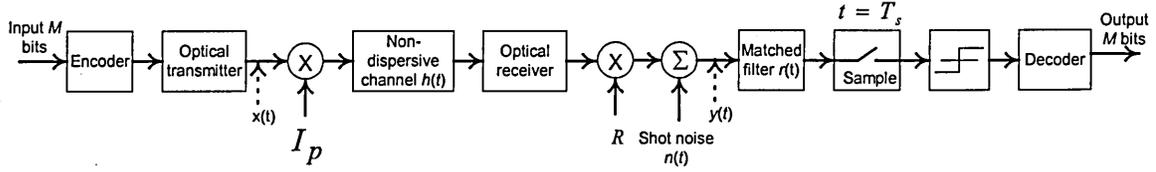
Fig. 5.1: IM/DD schemes: DH-PIM, DPIM, PPM and OOK non-dispersive optical wireless system model using a threshold detector.

In the following analysis, the following assumptions are made [7,80]:

(i)   The transmission link is a line-of-sight, and the channel imposes no multipath dispersion and no path loss.

(ii)   The noise associated with the receiver is negligible and the dominant noise source is due to background shot noise, which is assumed as a white Gaussian.

(iii)   There is no interference due to artificial light, this removes the need for a high-pass filter at the receiver and prevents baseline wander.

(iv)   There is no bandwidth limitations imposed by the transmitter and receiver.

(v) H_1 and H_2 are equally likely.

In addition, it is observed that any error in any time slot within the packet will invalidate that entire packet, thus, the probability of the packet error may be expressed as [7,125]:

$$P_{pe} = 1 - \prod_{n=1}^{Y} (1 - P_{sy_n}),$$
(5.1)

where P_{sy_n} is the probability that the nth symbol is in error, $Y = \dfrac{N_{pkt}}{M}$ is the number

of symbols within the packet, and N_{pkt} is the packet length in bits.

The detected signal at the input of the matched filter can be modeled as:

$$y(t) = \begin{cases} I_p + n(t) \; ; & pulse\,present \\ n(t) \quad\; ; & pulse\,absent, \end{cases} \tag{5.2}$$

where $n(t)$ represents the white Gaussian shot noise due to ambient light which has a

one-sided power spectral density η, zero mean and a variance of σ^2.

First we need to investigate the probability of slot error, which with reference to Fig.

5.2, is defined as [122,130]:

$$P_{se} = p_0 p_{e0} + p_1 p_{e1}, \tag{5.3}$$

where, p_{e1} is the probability of erasure error, p_{e0} is the probability of false alarm and

p_1 and p_0 are the probabilities of receiving a pulse (one) and empty slot (zero),

respectively and are given as:

$$p_1 = \frac{3\alpha}{4\overline{L}}, \tag{5.4}$$

and,

$$p_0 = 1 - p_1 = \frac{4\overline{L} - 3\alpha}{4\overline{L}}, \qquad (5.5)$$

The probability density functions for the detected signal in the absence and presence of a pulse are given respectively by [122]:

$$p_0(y) = \frac{1}{\sqrt{2\pi}\sigma} e^{-y^2/2\sigma^2}, \qquad (5.6)$$

$$p_1(y) = \frac{1}{\sqrt{2\pi}\sigma} e^{-(y-I_p)^2/2\sigma^2}. \qquad (5.7)$$
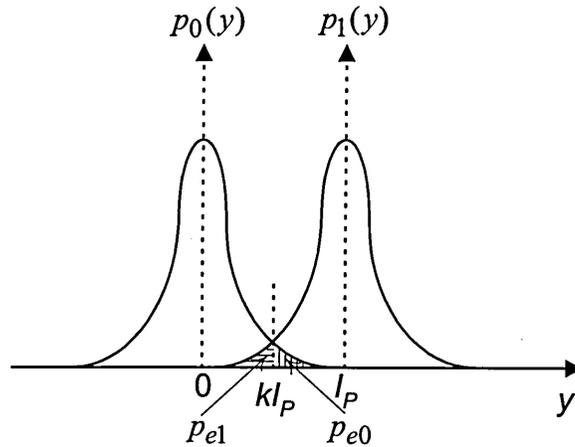
Fig. 5.2: Probability density functions for the detected signal in the absence and presence of a pulse.

Since the probability of receiving a pulse is less than the probability of receiving no pulse, then the optimum threshold level will be above $\dfrac{I_p}{2}$, and may be defined in terms of I_p as:

$$I_{th-op} = kI_p,$$
(5.8)

where, $0 < k < 1$ represents a threshold factor.

For the case of transmitting an empty slot, the probability of a false alarm is given as:

$$p_{e0} = \int_{kI_p}^{\infty} \frac{1}{\sqrt{2\pi}\sigma} e^{-y^2/2\sigma2} dy,$$

$$p_{e0} = Q\left[k\frac{I_p}{\sigma}\right].$$
(5.9)

For the case of transmitting a pulse, the probability of erasure error is given as:

$$p_{e1} = \int_{-\infty}^{kI_p} \frac{1}{\sqrt{2\pi}\sigma} e^{-(y-I_p)^2/2\sigma2} dy,$$

$$p_{e1} = Q\left[(1-k)\frac{I_p}{\sigma}\right],$$
(5.10)

where, the function $Q(X)$ is defined by [122]:

$$Q(X) = \frac{1}{\sqrt{2\pi}} \int_{X}^{\infty} e^{-z^2/2} dz.$$
(5.11)

The output of the matched filter at $t = T_s$ when a pulse is received is equal to the energy of a pulse given as:

$$E_p = I_p{}^2 T_s .$$ (5.12)

In the case of a matched filter, (5.2) can be replaced by [122]:

$$y(T_s) = \begin{cases} E_p + n(T_s) ; & \textit{pulse present} \\ n(T_s) & ; \quad \textit{pulse absent.} \end{cases}$$ (5.13)

and assuming that the output noise is Gaussian with zero mean, then the standard deviation σ has the value [122],

$$\sigma = \sqrt{\frac{\eta E_p}{2}} .$$ (5.14)

Therefore, incorporating (5.13) and (5.14) in (5.9) and (5.10), i.e. substituting E_p for I_p and $\sqrt{\frac{\eta E_p}{2}}$ for σ, gives:

$$P_{e0} = Q\left(\sqrt{\frac{2k^2 E_p}{\eta}} \right),$$ (5.15)

and,

$$P_{e1} = Q\left(\sqrt{\frac{2(1-k)^2 E_p}{\eta}} \right).$$ (5.16)

Since the channel has no path loss, then the average received optical power is equal to the average transmitted optical power $\overline{P}$. In the absence of noise and for a photodetector responsivity R, the photocurrent is given by:

$$I_p = \frac{4\overline{L}R\overline{P}}{3\alpha}.$$

(5.17)

Thus the energy of a pulse is given as:

$$E_p = \frac{16R^2\overline{P}^2M\overline{L}}{9\alpha^2 R_b}.$$

(5.18)

Substituting (5.18) in (5.15) and (5.16) gives:

$$p_{e0} = Q\left(\frac{\mu k R\overline{P}}{\sqrt{\eta R_b}}\right),$$

(5.19)

$$p_{e1} = Q\left(\frac{\mu(1-k)R\overline{P}}{\sqrt{\eta R_b}}\right),$$

(5.20)

where,

$$\mu = \sqrt{\frac{32M\overline{L}}{9\alpha^2}}.$$

(5.21)

Substituting (5.4), (5.5), (5.19) and (5.20) in (5.3) gives the probability of slot error for DH-PIM as:

$$P_{se} = \frac{1}{4\overline{L}} \left[\left(4\overline{L} - 3\alpha \right) Q \left(\frac{\mu k R \overline{P}}{\sqrt{\eta R_b}} \right) + 3\alpha Q \left(\frac{\mu(1-k)R\overline{P}}{\sqrt{\eta R_b}} \right) \right]. \qquad (5.22)$$

From (5.1), the packet error rate can be written in terms of slot error rate as:

$$P_{pe} = 1 - \left(1 - P_{se} \right)^{N_{pkt}\overline{L}/M}. \qquad (5.23)$$

For very small values of P_{se}, P_{pe} can be approximated by:

$$P_{pe} \approx \frac{N_{pkt}\overline{L}P_{se}}{M}. \qquad (5.24)$$

Thus, the probability of packet error for an N_{pkt}-bit DH-PIM packet can be given as:

$$P_{pe} \approx \frac{N_{pkt}}{4M} \left[\left(4\overline{L} - 3\alpha \right) Q \left(\frac{\mu k R \overline{P}}{\sqrt{\eta R_b}} \right) + 3\alpha Q \left(\frac{\mu(1-k)R\overline{P}}{\sqrt{\eta R_b}} \right) \right]. \qquad (5.25)$$

For comparison, the error rate formulas for DPIM, PPM and OOK are also given using the same assumptions as for DH-PIM and for the same average transmitted optical power $\overline{P}$ and photodetector responsivity R.

In DPIM, the pulse energy can be given as [7,13]:

$$E_{p-DPIM} = \frac{R^2 \overline{P}^2 M \overline{L}_{DPIM}}{R_b} . \tag{5.26}$$

The slot error rate for DPIM is given as [7]:

$$P_{se-DPIM} = \frac{1}{\overline{L}_{DPIM}} \left\{ (\overline{L}_{DPIM} - 1) Q\left(\frac{\varphi k R \overline{P}}{\sqrt{\eta R_b}} \right) + Q\left(\frac{\varphi (1-k) R \overline{P}}{\sqrt{\eta R_b}} \right) \right\}, \tag{5.27}$$

where, $\overline{L}_{DPIM}$ is given in (3.10) and φ is given by:

$$\varphi = \sqrt{2 M \overline{L}_{DPIM}} . \tag{5.28}$$

And the DPIM packet error rate using packets of N_{pkt} bits is given as:

$$P_{pe-DPIM} \approx \frac{N_{pkt}}{M} \left\{ (\overline{L}_{DPIM} - 1) Q\left(\frac{\varphi k R \overline{P}}{\sqrt{\eta R_b}} \right) + Q\left(\frac{\varphi (1-k) R \overline{P}}{\sqrt{\eta R_b}} \right) \right\}. \tag{5.29}$$

In PPM, the pulse energy can be written as [7]:

$$E_{p-PPM} = \frac{R^2 \overline{P}^2 M L}{R_b} , \tag{5.30}$$

where, L is given by (3.9) and ζ by:

98

$$\zeta = \sqrt{2ML} \,. \tag{5.31}$$

The slot error rate for PPM using a threshold detector is given as [7]:

$$P_{se-PPM} = \frac{1}{L}\left\{(L-1)Q\left(\frac{\zeta k R \overline{P}}{\sqrt{\eta R_b}}\right) + Q\left(\frac{\zeta(1-k)R\overline{P}}{\sqrt{\eta R_b}}\right)\right\}. \tag{5.32}$$

And the PPM packet error rate using packets of N_{pkt} bits is given as:

$$P_{pe-PPM} \approx \frac{N_{pkt}}{M}\left\{(L-1)Q\left(\frac{\zeta k R \overline{P}}{\sqrt{\eta R_b}}\right) + Q\left(\frac{\zeta(1-k)R\overline{P}}{\sqrt{\eta R_b}}\right)\right\}. \tag{5.33}$$

In OOK-NRZ, for $k = \dfrac{1}{2}$, the probability of bit error is given as [1,7]:

$$P_{be-OOK} = Q\left(\sqrt{\frac{2R^2\overline{P}^2}{\eta R_b}}\right). \tag{5.34}$$

And the OOK-NRZ packet error rate using packets of N_{pkt} bits is given as:

$$P_{pe-OOK} \approx N_{pkt}\, Q\left(\sqrt{\frac{2R^2\overline{P}^2}{\eta R_b}}\right). \tag{5.35}$$

Note that the OOK-NRZ electrical signal-to-noise ratio is given by:

$$SNR_{OOK} = \frac{2R^2 \overline{P}^2}{\eta R_b}.$$

(5.36)

5.3 Optical Power Requirements

The optical power requirement is an important indicator of the system performance when designing an optical wireless system. The most appropriate parameters of a system are those that result in the smallest optical power requirement at the minimum bandwidth. To simplify the study, it is assumed that the threshold level is set midway, i.e. $k = \frac{1}{2}$, thus from (5.8), the optimum threshold level is defined as:

$$I_{th-op} = \frac{I_p}{2}.$$

(5.37)

From (5.25), the DH-PIM packet error rate can be approximated by:

$$P_{pe} \approx \frac{\overline{L} N_{pkt}}{M} Q \left(\frac{\mu R \overline{P}}{2 \sqrt{\eta R_b}} \right).$$

(5.38)

and from (2.38), the average optical power requirement for DH-PIM is given by:

$$\overline{P}_{req} = \frac{2 \sqrt{\eta R_b}}{\mu R} Q^{-1} \left(\frac{M P_{pe}}{N_{pkt} \overline{L}} \right).$$

(5.39)

Using (5.29), (5.33) and (5.35), and letting $k = \dfrac{1}{2}$, the power requirements for DPIM,

PPM and OOK can be given, respectively as:

$$\bar{P}_{req-DPIM} = \frac{2\sqrt{\eta R_b}}{\varphi R} Q^{-1}\left(\frac{MP_{pe-DPIM}}{N_{pkt}\bar{L}_{DPIM}}\right), \qquad (5.40)$$

$$\bar{P}_{req-PPM} = \frac{2\sqrt{\eta R_b}}{\zeta R} Q^{-1}\left(\frac{MP_{pe-PPM}}{N_{pkt}L}\right), \qquad (5.41)$$

and,

$$\bar{P}_{req-OOK} = \sqrt{\frac{\eta R_b}{2R^2}} Q^{-1}\left(\frac{P_{pe-OOK}}{N_{pkt}}\right). \qquad (5.42)$$

5.4 Results and Discussions

The optical wireless system model shown in Fig. 5.1 has been simulated using the Matlab software for DH-PIM, DPIM, PPM and OOK schemes. The input signal is composed of binary independent, identically distributed bits of '1's and '0's. Depending on the modulation scheme, the encoder maps each word of M bits into a corresponding DH-PIM, DPIM or PPM symbol. Figure 5.3 shows a flow chart of the slot error rate simulation. As explained in section 5.2, each pulse is scaled to the peak photocurrent I_p before transmission. White Gaussian noise is added to the signal before being detected by a photodetector with a responsivity R. The regenerated

electrical signal is passed through a matched filter, the output of which is sampled at

the slot frequency $f_s = \dfrac{1}{T_s}$, followed by a threshold detector.
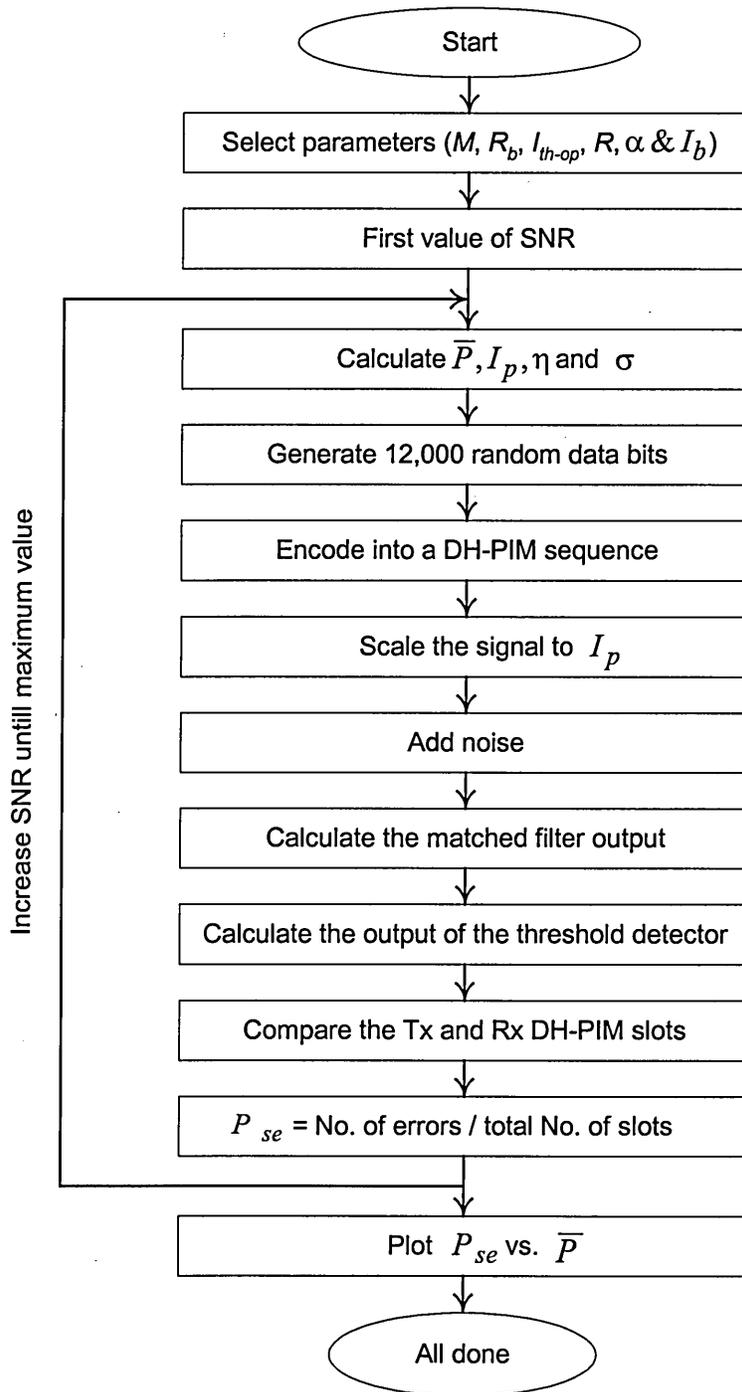
Fig. 5.3: Flow chart of the P_{se} simulation.

The flowchart contains the following elements:

- Start
- Select parameters (M, R_b, $I_{th\text{-}op}$, R, α & I_b)
- First value of SNR
- Calculate $\overline{P}$, I_p, η and σ
- Generate 12,000 random data bits
- Encode into a DH-PIM sequence
- Scale the signal to I_p
- Add noise
- Calculate the matched filter output
- Calculate the output of the threshold detector
- Compare the Tx and Rx DH-PIM slots
- P_{se} = No. of errors / total No. of slots
- Plot P_{se} vs. $\overline{P}$
- All done

Increase SNR untill maximum value

The regenerated DH-PIM signal is passed to the decoder in order to recover the data bits. Table 5.1 shows the parameters used to obtain the calculated and simulated results. The assumptions stated in section 5.2 are also used in the simulation and the packet length was chosen as $N_{pkt} = 1$ kilobyte [125]. The one-sided power spectral density η of the shot noise is calculated using (5.43) by setting the background natural (solar) light current to $I_b = 200 \mu A$ [80]:

$$\eta = 2q_e I_b, \qquad\qquad (5.43)$$

where q_e is the electron charge.

Parameter	Value
Number of random input bits	12,000 bits
α	1 and 2
M	2, 3, 4, 5, 6, 7 and 8 slots
I_{th-op}	$0.52 I_p$
Detector responsivity (R)	0.6 A/W
Background noise current (I_b)	$200 \mu A$
Packet length (N_{pkt})	1 kilobyte
Bit rate (R_b)	1, 10 and 100 Mbps
Pulse duty cycle (for OOK, PPM and DPIM)	100%

Table 5.1: Parameters used in the calculation and simulation.

Figure 5.4 shows the predicted and simulated slot error rate results for DH-PIM$_1$ and DH-PIM$_2$ versus the average optical power for a bit rate of $R_b = 1$ Mbps and different values of M. Predicted and simulated results show a good agreement for $P_{se} \geq 10^{-4}$. However, for lower values of P_{se}, the simulated results start to deviate from the predicted curves. This is because the number of data bits used in the simulation was limited to 12,000 bits due to the limited computational power.
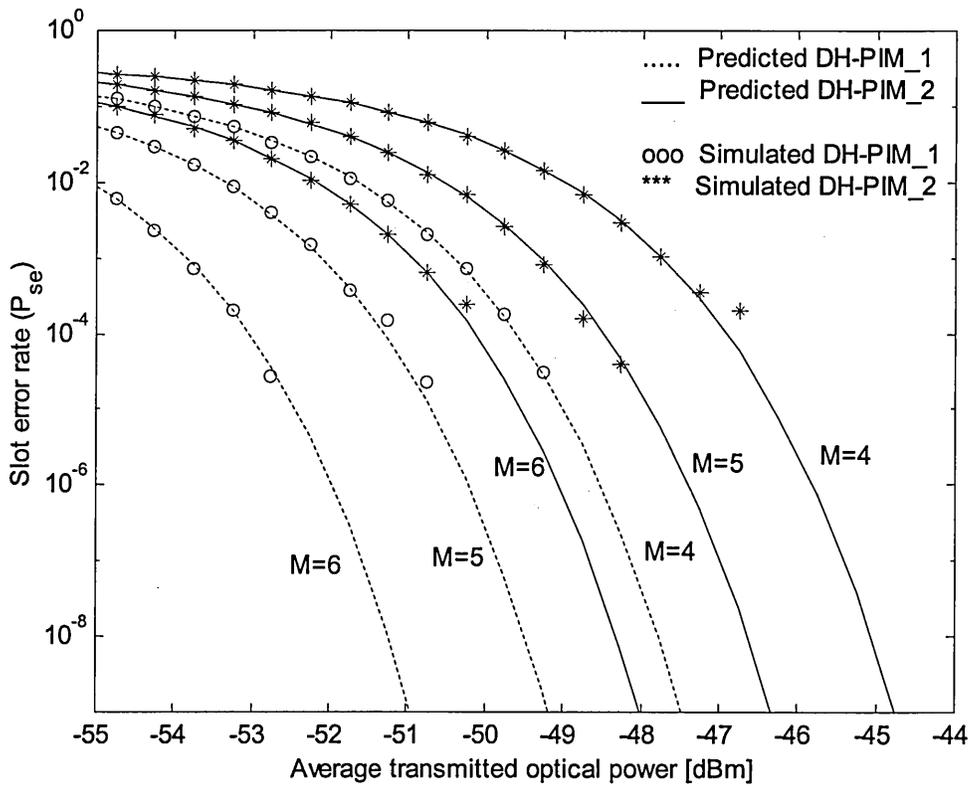
Fig. 5.4: Predicted and simulated P_{se} curves for DH-PIM$_1$ and DH-PIM$_2$ versus $\overline{P}$ for $R_b = 1$ Mbps and different values of M.

As expected, the P_{se} improves as M increases or α decreases. At $P_{se} = 10^{-9}$, the power requirement decreases by ~1.5 dBm as M increases by one. However, for the same M, DH-PIM$_1$ requires 3 dBm less optical power compared with DH-PIM$_2$. This improvement in the receiver sensitivity is offset by the increase in the transmission bandwidth for DH-PIM$_1$.

Figure 5.5 shows the P_{se} versus $\overline{P}$ for 16-DH-PIM$_1$ and 16-DH-PIM$_2$ ($M = 4$), and different values of bit rate ($R_b = 1$, 10 and 100 Mbps). For a given P_{se}, the power requirement increases by about 5 dBm each time the bit rate is increased by a decade for both schemes.
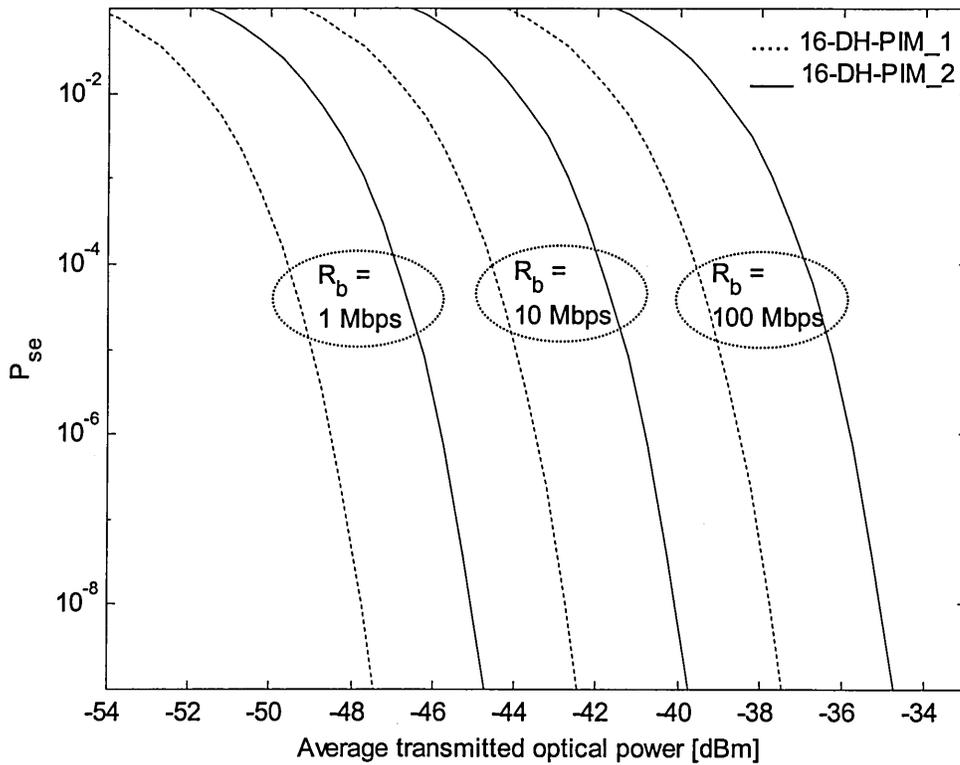
Fig. 5.5: Predicted P_{se} curves for 16-DH-PIM$_1$ and 16-DH-PIM$_2$ versus $\overline{P}$ for $R_b = 1$, 10 and 100 Mbps.

In Fig. 5.6, the slot error rate of 16-DH-PIM$_1$ and 16-DH-PIM$_2$ are compared with those of 16-DPIM, 16-PPM and OOK for $R_b = 1$ Mbps. DH-PIM displays improved performance compared with OOK. DH-PIM$_1$ error performance is similar to DPIM, but is marginally inferior to PPM requiring ~1 dBm more optical power at $P_{se} = 10^{-9}$. On the other hand DH-PIM$_2$ shows deterioration in performance compared with both DPIM and PPM, requiring 3 dBm and 4 dBm more optical power, respectively at $P_{se} = 10^{-9}$.
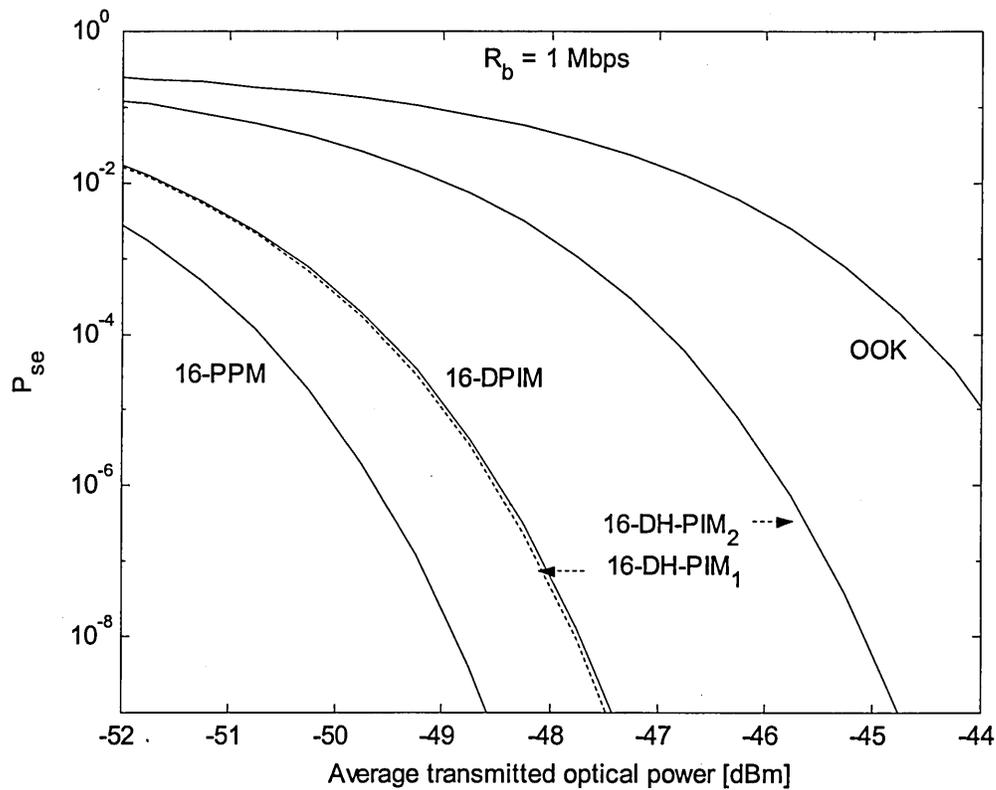
Fig. 5.6: Predicted P_{se} curves for 16-DH-PIM$_1$, 16-DH-PIM$_2$, 16-DPIM, 16-PPM and OOK versus $\overline{P}$ for $R_b = 1$ Mbps.

Figure 5.7 shows the predicted packet error rate curves versus $\overline{P}$ for $R_b = 1$ Mbps and

different values of M. For $P_{pe} = 10^{-6}$, $\overline{P}$ drops by about 1.5 dBm when M increases

by 1, and for a given M, DH-PIM$_1$ offers ~3 dBm improvement in the receiver

sensitivity compared with DH-PIM$_2$.
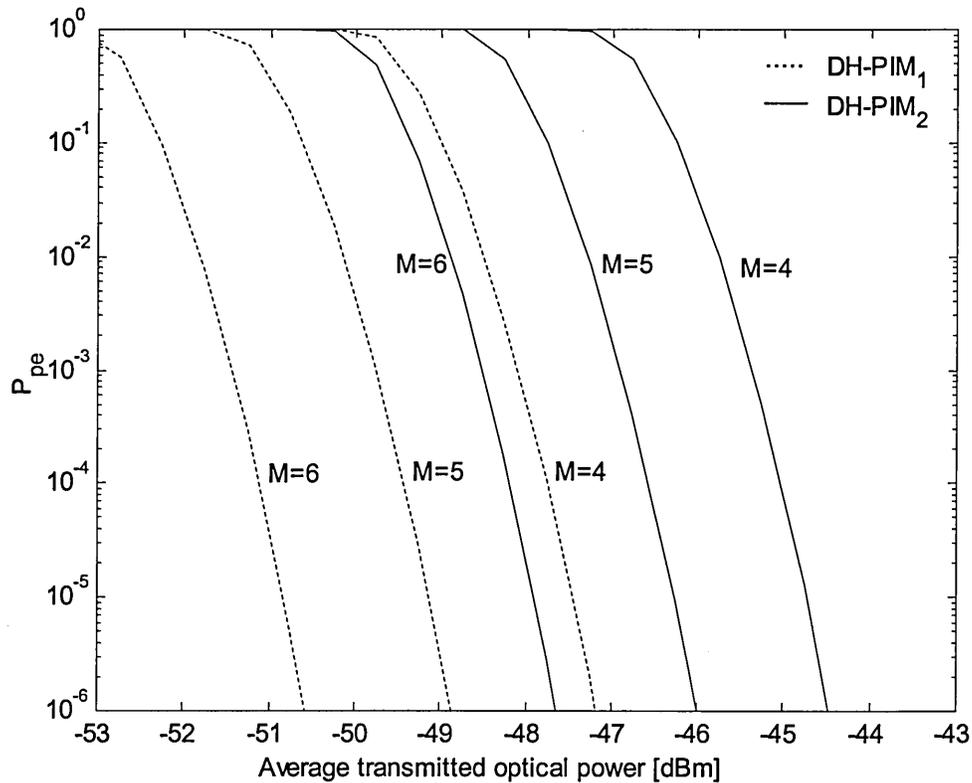
Fig. 5.7: Predicted P_{pe} curves for DH-PIM$_1$ and DH-PIM$_2$ versus $\overline{P}$ for $R_b = 1$ Mbps

and different values of M.

For both DH-PIM$_1$ and DH-PIM$_2$, the optical power requirement increases by about 5

dBm when the bit rate increases from 1 to 10 to 100 Mbps, as shown in Fig. 5.8.
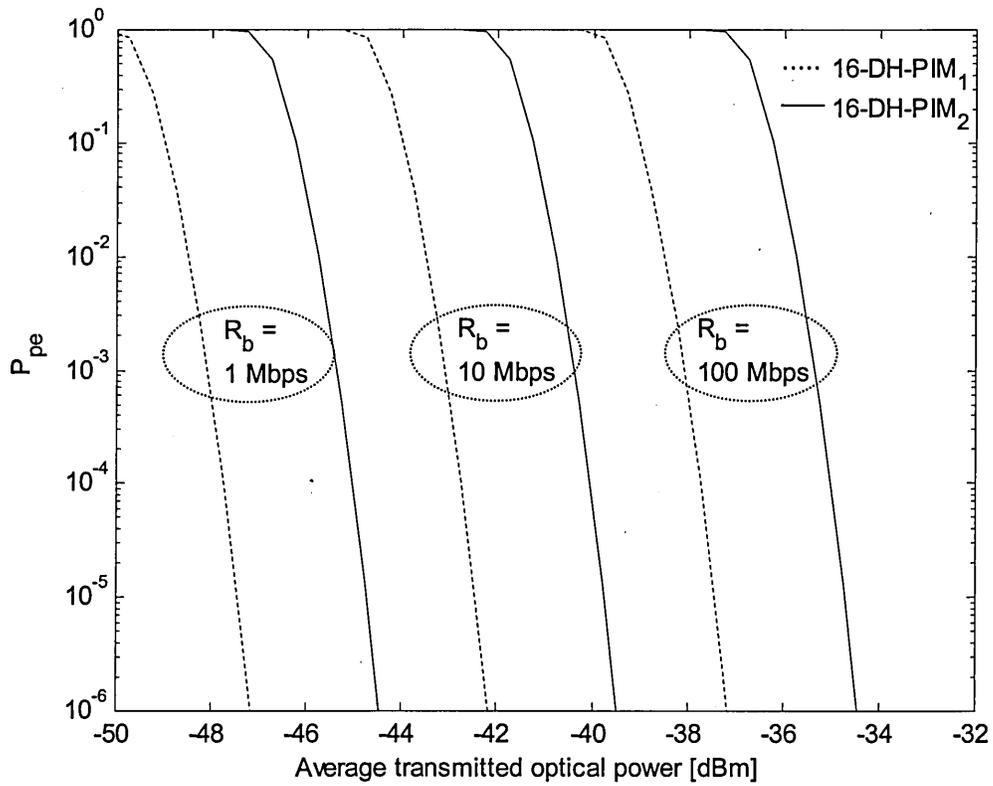
Fig. 5.8: Predicted P_{pe} curves for 16-DH-PIM₁ and 16-DH-PIM₂ versus $\overline{P}$ for

$R_b = 1$, 10 and 100 Mbps.

The packet error rate performance of DH-PIM is compared with those of DPIM, PPM and OOK-NRZ and the results are shown in Fig. 5.9. The performance characteristic is very similar to Fig. 5.6, with DH-PIM₁ displaying slightly better performance compared with DPIM, but marginally inferior to PPM. Notice that 32-DH-PIM₁ achieves ~0.5 dBm less packet error rate at $P_{pe} = 10^{-6}$ compared with 16-PPM.
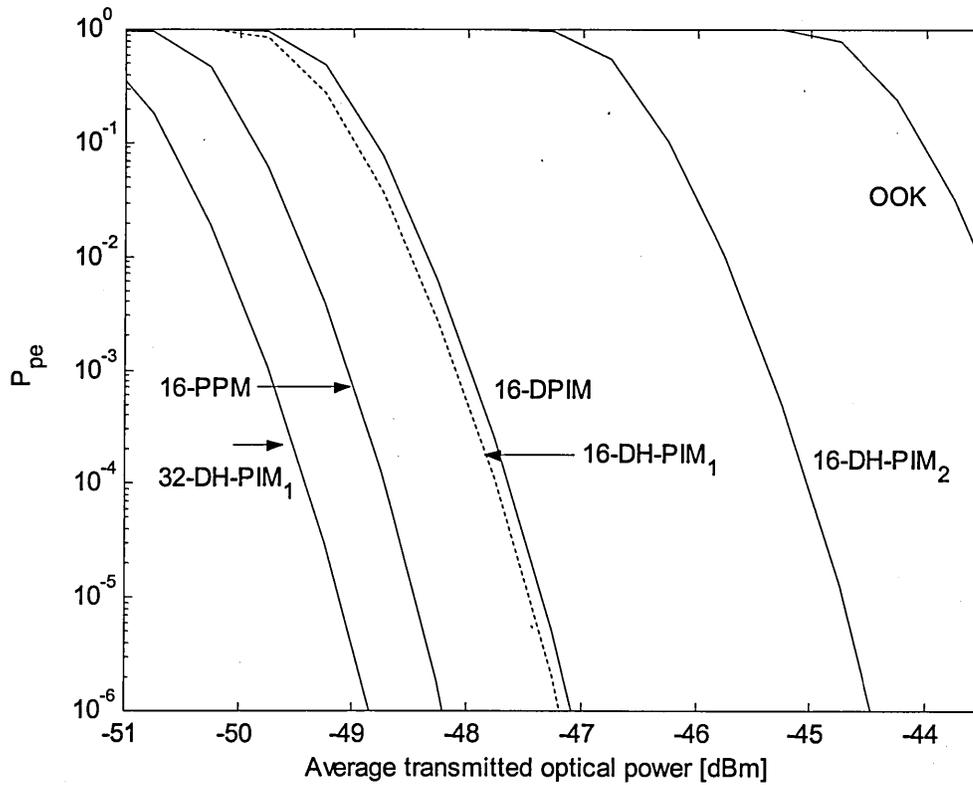
Fig. 5.9: Predicted P_{pe} curves for 16-DH-PIM$_1$, 16-DH-PIM$_2$, 16-DPIM, 16-PPM,

OOK and 32-DH-PIM$_1$ versus $\overline{P}$ for $R_b = 1$ Mbps.

The average optical power requirements for DH-PIM$_1$, DH-PIM$_2$, DPIM, PPM and

OOK normalised to that required by OOK-NRZ to send 1 kilobyte packets at a

standard $P_{pe} = 10^{-6}$ versus the bandwidth requirements normalised to the bit rate

$\dfrac{B_{req}}{R_b}$ have been calculated using (5.39) to (5.42), and the results shown in Fig. 5.10.

The numbers in Fig. 5.10 indicate the values of L and the percentage values

correspond to the OOK duty cycles.
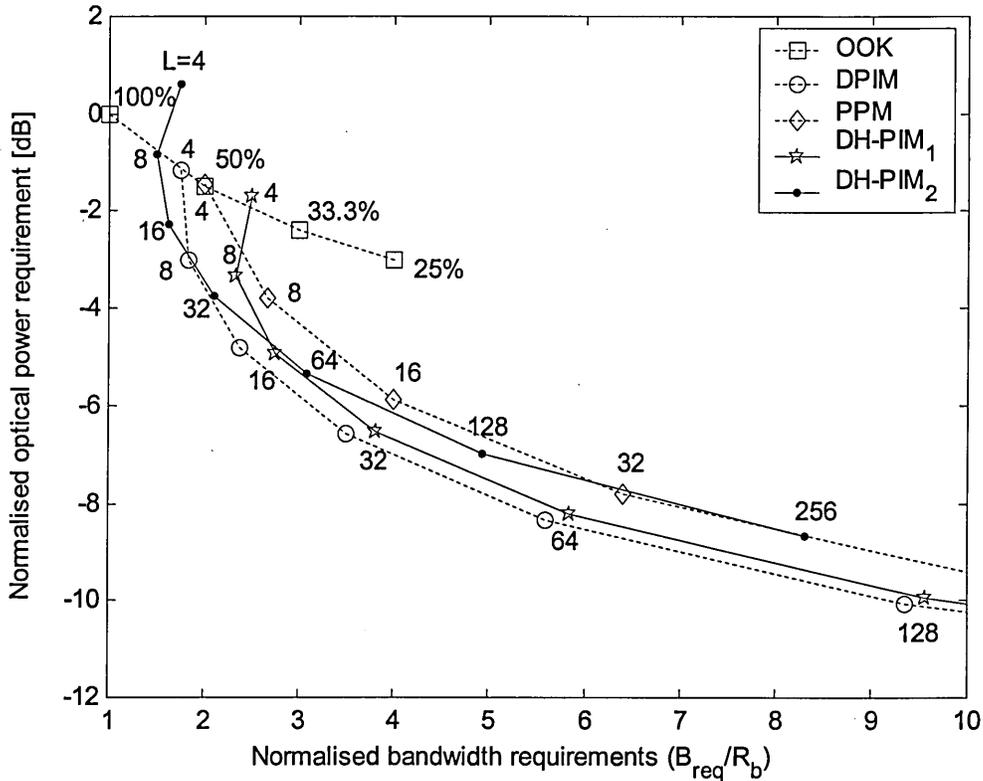
Fig. 5.10: Optical power requirements for OOK, PPM, DPIM, DH-PIM₁ and DH-PIM₂ normalised to OOK-NRZ versus bandwidth requirement normalised to the bit rate.

Regardless of bit resolution, DH-PIM₂ displays improved bandwidth efficiency compared with PPM and DPIM, but it requires more power. For example, 16-DH-PIM₂ requires ~2.6 dB, ~2.5 dB and ~3.6 dB additional optical power but ~ 1.1 dB, 0.8 dB, 2.4 dB less bandwidth compared with 16-DH-PIM₁, 16-DPIM, and 16-PPM, respectively. DH-PIM₁ displays similar power and marginally higher bandwidth requirement compared with DPIM, however, it is more bandwidth efficient than the PPM at the cost of a small increase in the power requirement. For example, 16-DH-PIM₁ requires ~0.1 dB less and ~1 dB more optical power, and ~ 0.4 dB more and 1.8 dB less bandwidth compared with 16-DPIM, and 16-PPM, respectively.

110

It is also observed that 32-DH-PIM$_1$ shows improvement in both power and bandwidth requirements compared with 16-PPM, that is 0.2 dB less bandwidth and 0.7 dB less power, and also shows improved error performance, see Fig. 5.9.

At higher bit resolution, i.e. $M = 7$ or 8, DH-PIM$_1$ is both bandwidth and power efficient compared with PPM, thus making it a more suitable scheme for optical wireless communications systems. However, the bandwidth requirements increase dramatically compared with smaller values of M. Therefore, for each scheme, the best parameters are those which result in the nearest points of the curve to the bottom left corner of Fig. 5.10. 16-DH-PIM$_1$ and 64-DH-PIM$_2$ achieve this best performance as shown in Fig. 5.10.

5.5 Summary

The error rate performance of DH-PIM has been theoretically analysed and original expressions for the slot and packet error rates, and optical power requirement have been presented. The complete system was simulated and the results obtained agree well with the theoretical predictions. Regardless of the bit resolution, DH-PIM$_1$ displays an improvement in slot and packet error rates compared with DH-PIM$_2$, which requires ~2.5 dBm more optical power to achieve $P_{se} = 10^{-9}$ or $P_{pe} = 10^{-6}$ compared with DH-PIM$_1$. For both DH-PIM$_1$ and DH-PIM$_2$, increasing the bite rate by a factor of 10 results in ~5 dBm power penalty. It is shown that DH-PIM$_2$ out-performs only OOK, whereas the DH-PIM$_1$ offers similar performance to DPIM but marginally inferior to PPM. DH-PIM$_1$ displays similar power and marginally higher bandwidth requirement compared with DPIM, and is more bandwidth efficient than PPM but at the cost of small increase in the power requirement. The best performance

of DH-PIM is achieved for 16-DH-PIM$_1$ and 64-DH-PIM$_2$ in terms of optical power and bandwidth requirements.

Chapter 6

MULTIPATH PROPAGATION

6.1 Introduction

When a signal is transmitted on a non-directed LOS or diffuse indoor wireless channel, it may undergo multiple reflections from the walls, ceiling, floor and objects within a room, before arriving at the receiver. On a diffuse optical channel, the entire transmitted signal incident on the photodetector surface experiences at least one reflection which causes the transmitted pulses to spread in time, resulting in intersymbol interference (ISI) which is significant for high bit rates (above 10 Mbps) [35].

In this chapter, the effect of multipath dispersion on DH-PIM is analysed. Novel theoretical analyses for the optical power requirements and power penalty due to ISI is presented. Both DH-PIM$_1$ and DH-PIM$_2$ are considered for calculated and simulated results. The analytical results are confirmed by the simulation of the system impulse response and eye diagrams for different values of normalised delay spread and bit

rates. The results of DH-PIM are compared with other modulation schemes such as OOK, PPM and DPIM.

The remainder of this chapter is organised as follows: The optical channel model is presented in section 6.2 and the multipath propagation of DH-PIM signal is detailed in section 6.3. A list of the parameters used to quantify the severity of the ISI, calculated and simulated results as well as a discussion of the results can be found in section 6.4. The chapter is concluded in section 6.5.

6.2 Optical Channel Model

The unequalised multipath channel can be modeled as a baseband linear system, with input optical power x(t), output current $y(t)$, and an impulse response $h(t)$ as illustrated in Fig. 6.1 [4].
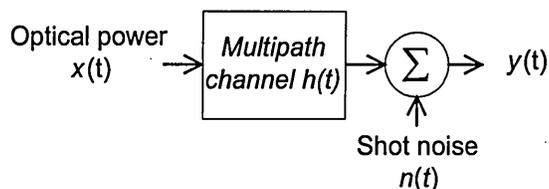
Fig. 6.1: Block diagram of unequalised multipath channel.

The channel may be described in terms of the impulse response (or frequency transfer function) $h(t) \leftrightarrow H(f)$. Normally, $h(t)$ is fixed for a given position of the transmitter, receiver and intervening reflectors, and changes significantly only when any of these are moved a distance in the order of centimetre [35]. The channel is assumed to be time invariant because of the slow movement of people and objects within a room and the relatively high bit rates involved. This means that the channel will vary

significantly on a time scale of many bit periods only. The power requirements may be separated into two factors [38]:

(a) Multipath power requirement.

(b) Optical path loss: $\dfrac{1}{H(0)}$.

Where $H(0)$ is the optical gain, which is given by:

$$H(0) = \int_{-\infty}^{\infty} h(t)\, dt.$$ (6.1)

Consideration will be limited to the optical power penalty due to multipath propagation only, therefore, we choose $H(0) = 1$ so that the channel has a path loss of $0\,\text{dB}$ [38], i.e. the average transmitted optical power $\overline{P}$ is equal to the received optical power. This is implemented in the simulation by normalising the channel impulse response to $H(0)$.

The multipath power requirement can be predicted by the normalised delay spread of the channel, which is defined as [38]:

$$D_T = \frac{D_{rms}}{T_b},$$ (6.2)

where T_b is the OOK bit duration and D_{rms} is the RMS delay spread given by:

$$D_{rms} = \sqrt{\frac{\int_{-\infty}^{\infty} (t - D_{mean})^2 h^2(t) dt}{\int_{-\infty}^{\infty} h^2(t) dt}}, \qquad (6.3)$$

where D_{mean} is the mean delay spread given by:

$$D_{mean} = \frac{\int_{-\infty}^{\infty} t h^2(t) \, dt}{\int_{-\infty}^{\infty} h^2(t) \, dt}. \qquad (6.4)$$

Similar to $h(t)$, D_{mean} is fixed for a given configuration.

Practical channel measurements by Kahn *et. al.* [57] have shown that both non-directed LOS and diffuse configurations have channel RMS delay spreads which typically range form 1 to 12 ns, with diffuse links generally being slightly larger. As one may expect, shadowing is more detrimental to non-directed LOS channels, increasing delay spreads to typically between 7 and 13 ns, whilst on diffuse channels, the increase in delay spread due to shadowing is relatively modest.

When a pulse modulation signal such as PPM, DPIM and DH-PIM is transmitted over multipath channels, the slot containing a pulse can induce interference in slots both within the same symbol (intra-symbol interference) and in the adjacent transmitted symbols (intersymbol interference). We refer to these effects collectively as ISI [4,16]. We base our study on the ceiling-bounce model [38] which was found to predict multipath power requirement for OOK, PPM and DPIM schemes on non-directed LOS and diffuse channels, with and without shadowing, with a high degree of accuracy. The impulse response of the channel using the ceiling-bounce model is given by [38]:

$$h(t) = H(0) \frac{6 \left(12 \sqrt{\frac{11}{13}} D_{rms} \right)^6}{\left(t + 12 \sqrt{\frac{11}{13}} D_{rms} \right)^7} u(t),$$
(6.5)

where $u(t)$ is the unit step function.

6.3 Multipath Propagation of DH-PIM Signal

Because of its variable symbol duration, the symbol boundaries are not known prior to detection, thus, practical implementation of maximum likelihood sequence detection for DH-PIM, and for DPIM, is infeasible, even in the absence of ISI. Therefore, the most practical implementations of DH-PIM would be to employ hard-decision detection scheme. A block diagram of the DH-PIM system over unequalised dispersive optical channels is shown in Fig. 6.2.
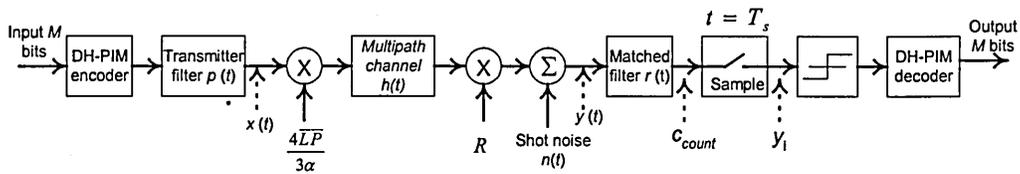
Fig. 6.2: Block diagram of unequalised DH-PIM system.

The input is a stream of OOK bits, which are assumed to be independent, identically distributed (i.i.d.) and uniform on {0, 1}. Each M-bit input block is encoded into one of L possible DH-PIM symbols according to the decimal value of the input code word, where, L is given in (3.9). The DH-PIM symbols are then passed to the transmitter

filter, which has a unit-amplitude rectangular impulse response $p(t)$ with a duration of one slot T_s. The output of the transmitter filter is scaled by the peak transmitted optical signal power $\dfrac{4\overline{LP}}{3\alpha}$, and passed through the multipath channel $h(t)$, where $\overline{P}$ is the average transmitted optical power. The received optical signal power is converted into a photocurrent by multiplying it by the photodetector responsivity R. Additive white Gaussian noise $n(t)$ with a double-sided power spectral density of $\dfrac{\eta}{2}$ is added to the detected signal, which is then passed to a unit energy filter $r(t)$ matched to $p(t)$, followed by a slot rate sampler. Depending on whether the sampled signal is above or below the threshold level, a threshold detector then assigns a one or zero to each slot. Since DH-PIM has no fixed symbol boundary format, then a single slot error not only affects the bits associated with that slot, but it will also shift the bits that follow that bit. Therefore, one cannot use the usual definition of BER to measure the DH-PIM performance. Instead, the probability of packet error (P_{pe}) needs to be calculated using the method proposed in [39], which is described as follows:

Let c_{cont} denote the continuous impulse response of the cascaded system given by:

$$c_{cont} = p(t) \otimes h(t) \otimes r(t). \tag{6.6}$$

where $\otimes$ denotes convolution.

Then the discrete-time equivalent impulse response of the cascaded system (c_k) can be given by:

$$c_k = c_{\text{cont}} \Big|_{t=kT_s} \, , \tag{6.7}$$

Suppose that c_k contains m taps. Let S_i be an m-slots DH-PIM sequence, and $s_{i,m-1}$ the value of the $(m-1)^{\text{th}}$ slot (penultimate slot) in the sequence S_i, where $s_{i,m-1} \in \{0,1\}$. Unless the channel is non-dispersive, for an S_i sequence of m slots, c_k will contain m taps: a single precursor tap, a zero tap c_0, which has the largest magnitude, and $(m-2)$ post-cursor taps. Thus, only the penultimate slot will be affected by the dispersion of the signal appearing within the S_i sequence. Sequences that fall outside the boundaries of S_i will not contribute to the dispersion on the penultimate slot of S_i. Therefore, when calculating the optical power requirement, only the penultimate slot will be considered for each sequence. Unlike the ideal channels, on a dispersive channel, the optimum sampling point may shift from the end of each slot period as the severity of the ISI changes. In order to isolate the power penalty due to ISI, two assumptions are made. First a perfect timing recovery is assumed, which is achieved by shifting the time origin so as to maximise the zero tap c_0 [39]. Secondly an optimal decision threshold is assumed.

The input signal at the threshold detector in the absence of noise is given by:

$$y_i = I_p S_i \otimes c_k \big|_{k=m} \, , \tag{6.8}$$

where, I_p is the peak photocurrent in the absence of multipath dispersion, which is given in (5.17). The energy of the penultimate slot is given by:

$$E_{p,i} = y_i^2 T_s .$$ (6.9)

The threshold level ρ is given as:

$$\rho = k\sqrt{E_{p,i}} ,$$ (6.10)

where, $0 < k < 1$.

The probability of slot error for the penultimate slot $s_{i,m-1}$ of sequence S_i is given as:

$$P_{se,i} = \begin{cases} Q\left(\dfrac{\rho}{\sqrt{\eta/2}}\right) & ; \text{ if } s_{i,m-1} = 0 \\[4mm] Q\left(\dfrac{\sqrt{E_{p,i}} - \rho}{\sqrt{\eta/2}}\right) & ; \text{ if } s_{i,m-1} = 1. \end{cases}$$ (6.11)

Multiplying the probability of slot error for each sequence by the probability of occurrence of that sequence $P_{occ,i}$ and summing up of the results for all the valid sequences give the average probability of slot error:

$$P_{se} = \sum_{\text{all } i} P_{occ,i} P_{se,i} .$$ (6.12)

For a given packet length of N_{pkt} bits, the number of DH-PIM symbols within a packet and the number of slots within the packet is given by $\dfrac{N_{pkt}}{M}$ and $\dfrac{N_{pkt}\overline{L}}{M}$, respectively. Therefore, the probability of slot error may be converted into a corresponding packet error rate as explained in Chapter 5:

120

$$P_{pe} = 1 - (1 - P_{se})^{N_{pkt}\overline{L}/M}.$$ (6.13)

To calculate the optical power requirement P_{req}, assuming c_k has m taps, we generate all the possible sequences of m-slot length and ignore all sequences that cannot be generated by DH-PIM symbols alone. Then calculate the corresponding probabilities of occurrence for each valid sequence, see a detailed flow chart in Fig. 6.3. An example of calculating the probability of occurrence is shown in Appendix B. Note that, since the slots are not i.i.d, different m-slot sequences may have different occurrence probabilities, and when $m > 2$, the total number of valid sequences is always less than 2^m.

$h(t)$ is calculated from (6.5) for different values of D_{rms} and the discrete-time impulse response of the cascaded system c_k is then determined from (6.7), with the sampling instants chosen so as to maximise c_0. From (6.13), we first calculate P_{se} in order to achieve an average packet error of 10^{-6} for all the valid sequences. Knowing the probability of occurrence of each sequence, $P_{se,i}$, $E_{p,i}$, y_i and I_p are calculated from (6.12), (6.11), (6.9) and (6.8), respectively. Finally, from (5.17), the corresponding optical power requirement P_{req} is found as:

$$P_{req} = \frac{3\alpha I_p}{4R\overline{L}}.$$ (6.14)

The optical power penalty $P_{penalty}$ is defined as the difference between the optical power required on dispersive channels P_{req} and the optical power required on ideal (dispersive-free) channels $P_{req,ideal}$ for a given value of D_{rms} and is given by:

$$P_{penalty} = P_{req} - P_{req,ideal}.$$ (6.15)

Segment of m slots: $\{s_{i,1}, s_{i+2}, ..., s_{i+m}\}$
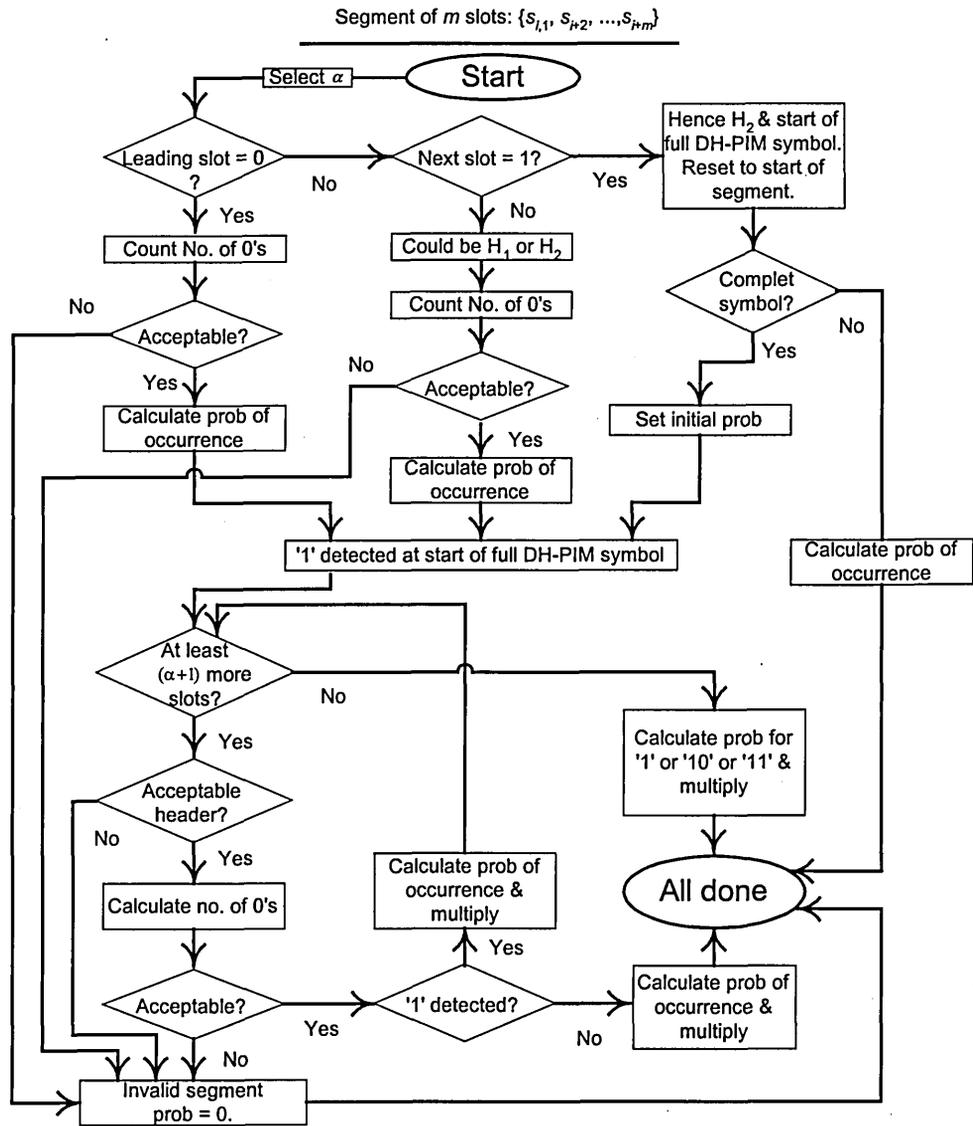
Fig. 6.3: Flow chart of generating the sequences and calculating the probabilities of

occurrence for the valid sequences.

6.4 Results and Discussion

Essentially the power requirement depends on the normalised delay spread D_T and the value of L in DH-PIM, PPM and DPIM [104-131]. The optical power requirements are normalised to the average optical power required by OOK-NRZ, operating at a bit rate of 1 Mbps to achieve a packet error rate of 10^{-6} on a non-dispersive channel using a packet length of 1 kilobyte. The results have been carried out for receivers employing threshold detectors assuming no path loss, which implies that the average transmitted optical power $\overline{P}$ is equal to the average received optical power as explained in section 6.1.

Unless otherwise stated, the parameters shown in table 6.1 have been used to obtain the results.

Parameter	Value
α	1 and 2
L	4, 8, 16 and 32 slots
m	9 slots
Threshold factor (k)	0.5
Packet length (N_{pkt})	1 kilobyte
Detector responsivity (R)	0.6 A/W
Normalised delay spread (D_T)	0.001 – 1.00
Bit rate (R_b)	1, 10 and 100 Mbps
Average optical power ($\overline{P}$)	1 W

Table 6.1: Parameters used in the calculation and simulation.

For each combination of L and α, all possible m-slot sequences are generated and the valid sequences are selected and their probabilities of occurrence are calculated as outlined in the flow chart shown in Fig. 6.3. As a trade off between realism and computation time, the number of slots over which the impulse response decays to a negligible value (i.e. < 1% of the peak value) is chosen to 9 slots (i.e. $m = 9$). The optical power requirement P_{req} is calculated from (6.13) following the procedure outlined in the previous section by varying the values of $\overline{P}$ until P_{pe} of 10^{-6} is achieved for every value of D_T using a packet length of N_{pkt} = 1 kilobyte [125]. Probabilities of errors are calculated using a fixed threshold level detector, see Fig. 6.2. It can also be observed that changing the value of the detector responsivity R doesn't affect the power requirement or the power penalty of the modulation techniques considered in this study. This is because the same value of R has been used in both the calculation and simulation for all the modulation schemes, the results have been normalised to OOK-NRZ on ideal channels.

Figure 6.4 shows the normalised optical power requirements of DH-PIM$_1$ and DH-PIM$_2$ versus the normalised delay spread D_T for various values of L, and a fixed threshold level ρ_{opt} given as:

$$\rho_{opt} = \frac{\sqrt{E_{p,i}}}{2}.$$

(6.16)

125
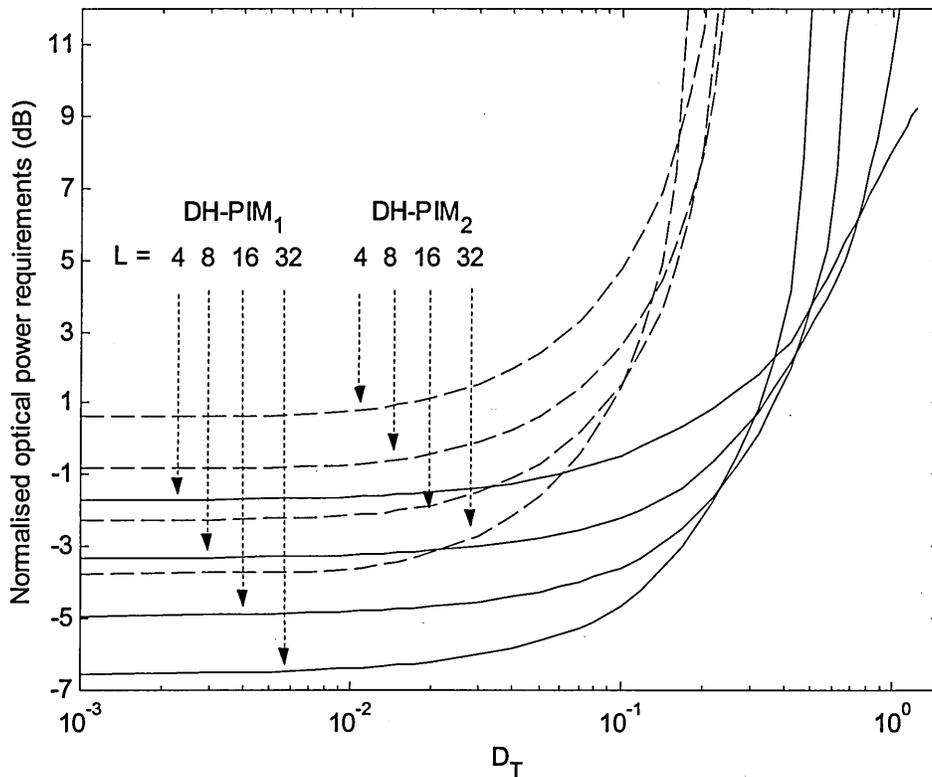
Fig. 6.4: Normalised optical power requirements for DH-PIM$_1$ and DH-PIM$_2$ versus

the normalised delay spread D_T, for L = 4, 8, 16 and 32, and R_b = 1 Mbps.

DH-PIM$_1$ displays an improvement of about 2.5 dB over DH-PIM$_2$ at low values of D_T

and this improvement increases as D_T increases, which means that DH-PIM$_1$ is less

affected by multipath dispersion than DH-PIM$_2$ especially at high values of D_T. This is

due to the fact that the pulse duration in DH-PIM$_1$ is half that of DH-PIM$_2$. For both

DH-PIM$_1$ and DH-PIM$_2$, the power requirement is reduced by $\sim$ 1.5 dB by increasing

the value of L from 4 to 8 to 16 to 32 at low values of D_T (< 0.1). This means that

32-DH-PIM$_1$ and 32-DH-PIM$_2$ offer about 3 dB improvement in power gain compared

with 8-DH-PIM$_1$ and 8-DH-PIM$_2$, respectively, but require marginally more

bandwidth (see Chapter 5). However, as the normalised delay spread increases above

0.1, the power requirement increases much more rapidly for L = 32 and 16 compared

with $L = 8$ and 4. This is due to ISI effecting larger number of shorter slots in high order L-DH-PIM$_1$ and L-DH-PIM$_2$. For example 32-DH-PIM$_1$ curve crosses 16-DH-PIM$_1$ at $D_T = 0.23$ and 32-DH-PIM$_2$ curve crosses 16-DH-PIM$_2$ at $D_T = 0.1$. Above these two values of D_T, 32-DH-PIM$_1$ and 32-DH-PIM$_2$ will require more optical power compared with 16-DH-PIM$_1$ and 16-DH-PIM$_2$, respectively.

The optical power penalty of DH-PIM$_1$ and DH-PIM$_2$ due to ISI is calculated from (6.15) and the normalised results versus D_T for different values of L are shown in Fig. 6.5. All orders of DH-PIM$_1$ and DH-PIM$_2$ display nearly the same optical power penalty for $D_T < 0.01$, which increases rapidly as D_T becomes > 0.01. DH-PIM$_1$ shows a significant improvement over DH-PIM$_2$ especially at $D_T < 0.05$. For example, at $D_T = 0.1$, 32-DH-PIM$_1$ requires $\sim$ 3.4 dB less power compared with 32-DH-PIM$_2$. Beyond $D_T = 0.1$, the improvement become even more significant.
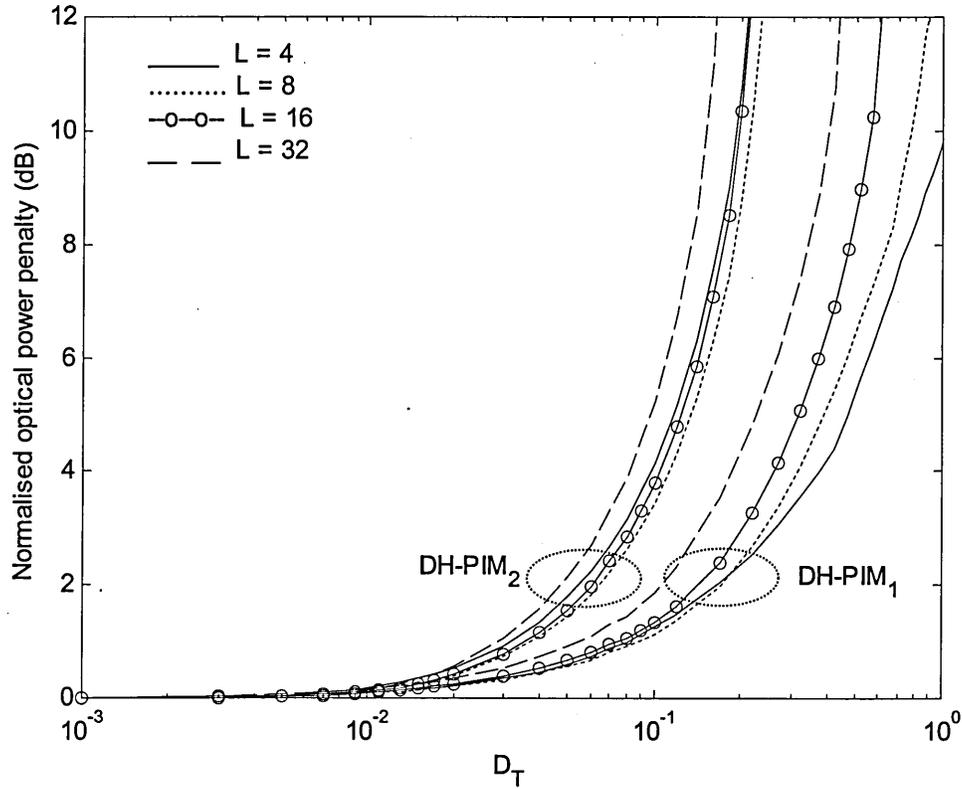
Fig. 6.5: Normalised optical power penalty for DH-PIM$_1$ and DH-PIM$_2$ versus D_T, for

L = 4, 8, 16 and 32, and R_b = 1 Mbps.

Figure 6.6 shows the normalised optical power requirements for 32-DH-PIM$_1$, 32-DH-PIM$_2$, 32- DPIM, 32-PPM and OOK-NRZ versus the normalised delay spread D_T, for R_b = 1 Mbps. At low values of D_T(< 0.02), 32-PPM requires 8, 4 and 1.2 dB less power compared with OOK-NRZ, 32-DH-PIM$_2$ and 32-DH-PIM$_1$/32-DPIM, respectively. However, as D_T increases, the power requirement increases at a much faster rate than the other schemes. For example, at D_T > 0.1, 32-PPM is outperformed by 32-DH-PIM$_1$, 32-DPIM, 32-DH-PIM$_2$ and OOK-NRZ.
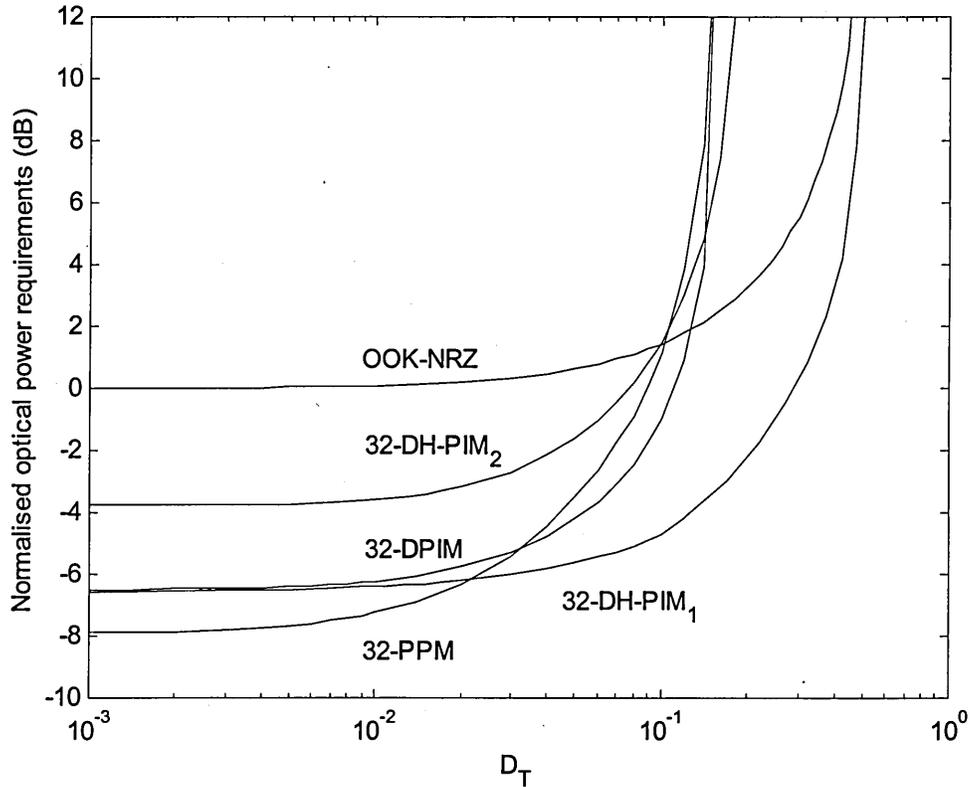
Fig. 6.6: Normalised optical power requirements for 32-DH-PIM₁, 32-DH-PIM₂, 32-DPIM, 32-PPM and OOK-NRZ versus D_T, for $R_b = 1$ Mbps.

32-DH-PIM₁ achieves the best performance for $D_T > 0.02$ compared with its counterparts. For example, at $D_T = 0.1$, 32-DH-PIM₁ requires ~ 3.8 dB less optical power compared with 32-PPM and ~ 5.9 dB less optical power compared with 32-DPIM, 32-DH-PIM₂ and OOK-NRZ. Whereas, 32-DH-PIM₂ requires more power than 32-DPIM, 32-PPM and 32-DH-PIM₁ for low values of D_T. However, it outperforms PPM and DPIM at $D_T = 0.01$ and 0.14, respectively.

The normalised optical power penalty curves for 32-DH-PIM₁, 32-DH-PIM₂, 32-DPIM, 32-PPM and OOK-NRZ versus the normalised delay spread D_T, for $R_b = 1$ Mbps are shown in Fig. 6.7.
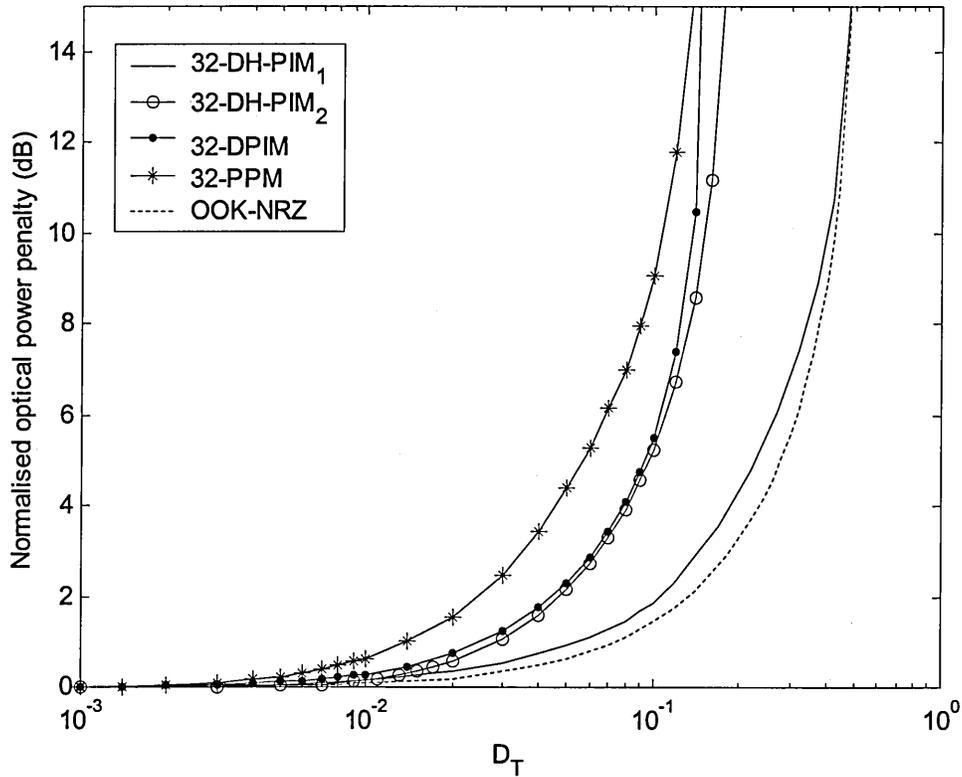
Fig. 6.7: Normalised optical power penalty for 32-DH-PIM$_1$, 32-DH-PIM$_2$, 32- DPIM,

32-PPM and OOK-NRZ versus D_T, for R_b = 1 Mbps.

From Fig. 6.7, it is observed that 32-DH-PIM$_1$ and OOK-NRZ have similar profile and offer the lowest optical power penalty compared with 32-PPM, 32-DPIM and 32-DH-PIM$_2$ over a wide range of D_T. At D_T= 0.1, 32-DH-PIM$_1$ power penalty outperforms 32-PPM, 32-DH-PIM$_2$ and 32-DPIM by 7.2, 3.51 and 3.68 dB, respectively.

Figure 6.8 shows the normalised optical power requirements for 32-DH-PIM$_1$ and 32-DH-PIM$_2$ versus the RMS delay spread D_{rms} for different bit rates.
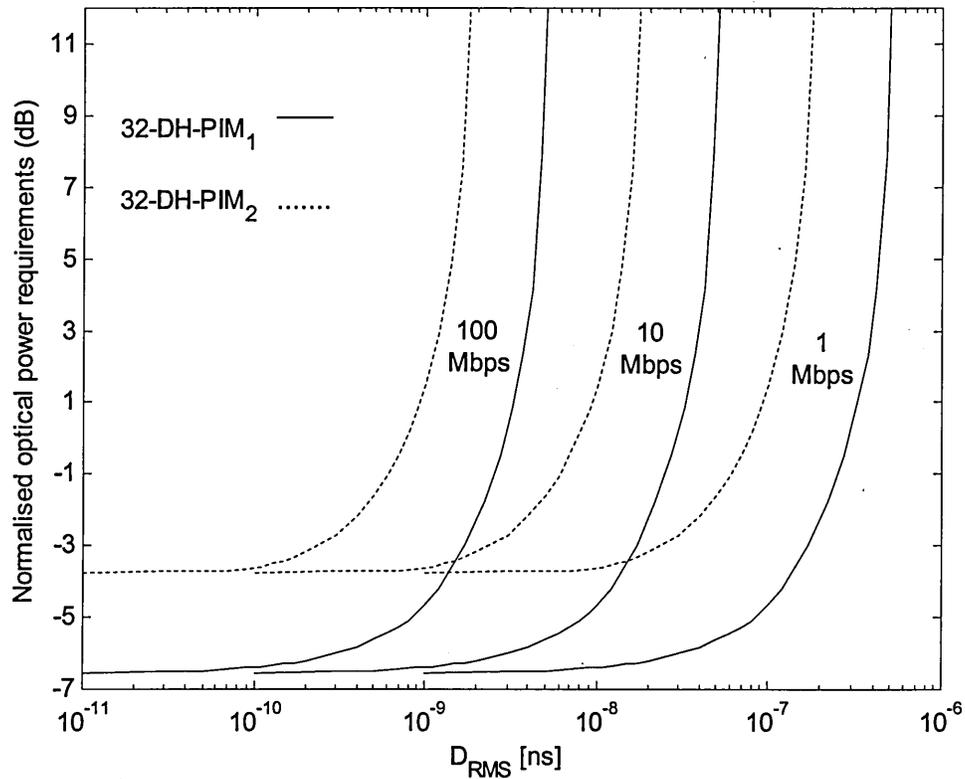
Fig. 6.8: Normalised optical power requirements for 32-DH-PIM$_1$ and 32-DH-PIM$_2$

versus D_{rms}, for $R_b = 1$, 10 and 100 Mbps.

The multipath dispersion starts to affect 32-DH-PIM$_1$ and 32-DH-PIM$_2$ at $D_{rms} > 0.1$, 1 and 10 ns for $R_b = 100$, 10 and 1 Mbps, respectively. As D_{rms} increases above these values, the effect of multipath dispersion increases significantly shifting the curves to the left.

Figure 6.9 shows the normalised optical power penalty for 32-DH-PIM$_1$ and 32-DH-PIM$_2$ versus the RMS delay spread D_{rms} for different bit rates.
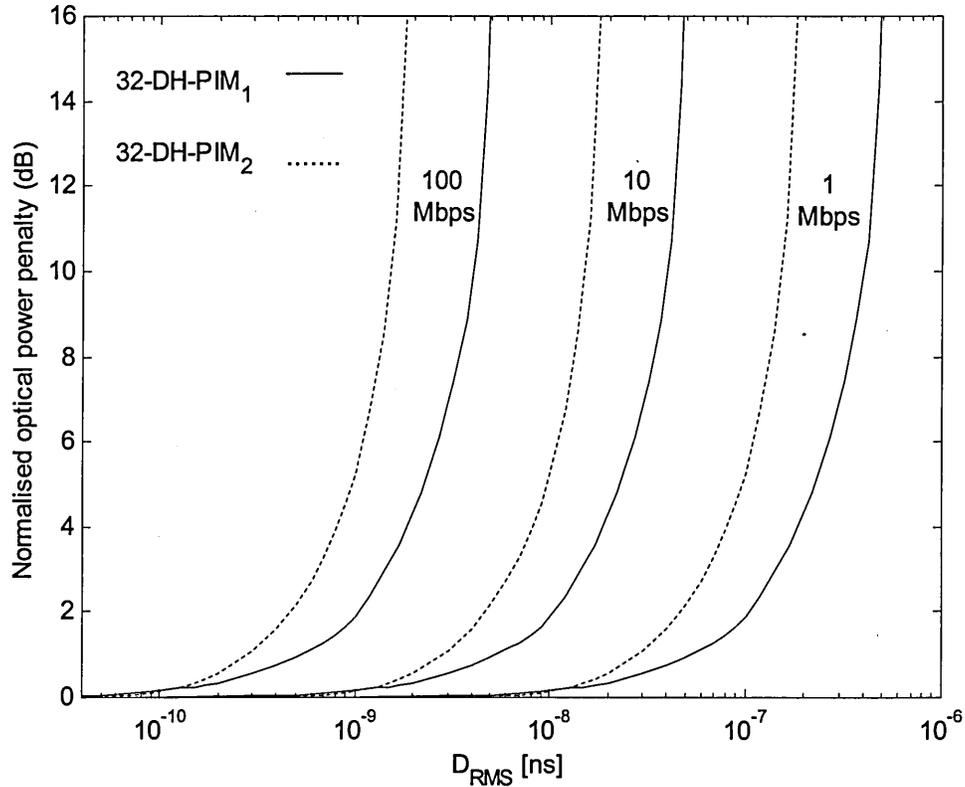
Fig. 6.9: Normalised optical power penalty for 32-DH-PIM$_1$ and 32-DH-PIM$_2$ versus D_{rms}, for R_b = 1, 10 and 100 Mbps.

Figure 6.9 shows similar results to Fig. 6.8. The multipath dispersion starts to affect 32-DH-PIM$_1$ and 32-DH-PIM$_2$ at D_{rms} > 0.1, 1 and 10 ns for R_b = 100, 10 and 1 Mbps, respectively. As expected for a given power penalty, higher bit rates require much lower delay spread compared with the lower bit rate.

The optical power requirements for 32-DH-PIM$_1$ and 32-DH-PIM$_2$ have been calculated for different threshold levels ρ given in (6.10) and the normalised results are shown in Fig. 6.10.
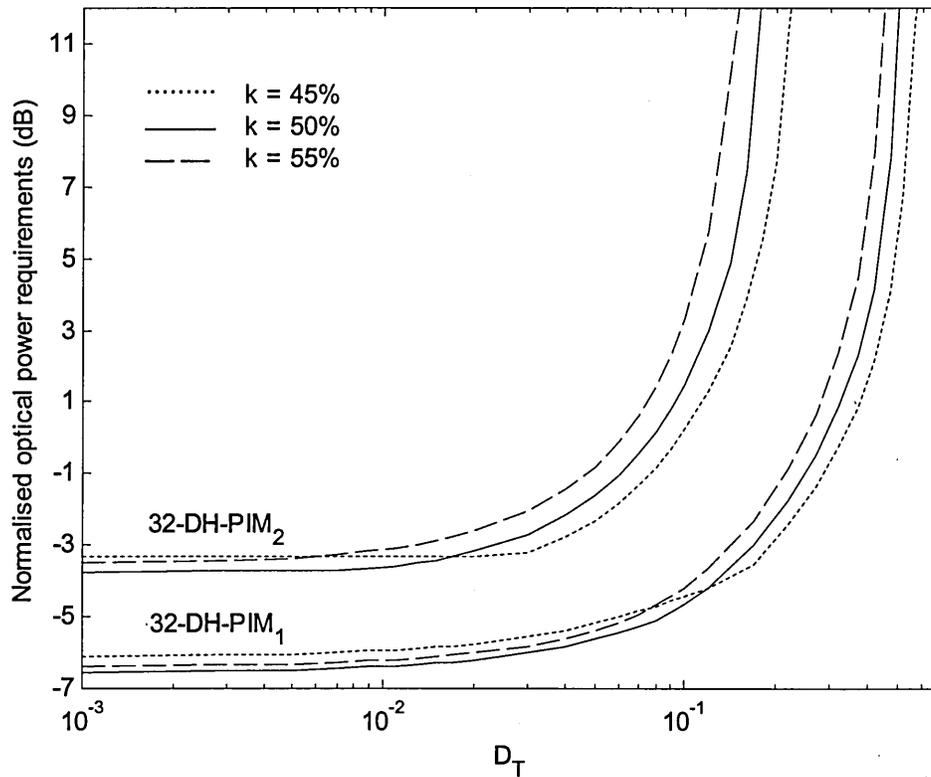
Fig. 6.10: Normalised optical power requirements of 32-DH-PIM₁ and 32-DH-PIM₂

versus D_T, for $R_b = 1$ Mbps and different threshold levels.

For low values of D_T, the lowest power requirements for both schemes are achieved at 50% threshold level. However, by increasing D_T to 0.12 and 0.02 for 32-DH-PIM₁ and 32-DH-PIM₂, respectively, the power requirement becomes the lowest for 45% threshold level. This is because for high values of the normalised delay spread, significant amount of the pulse power (optical) is dispersed and added to the next slots making the optimum threshold level slightly below the midway between zeros and ones given in (6.16). Increasing the threshold factor above 50% results in higher power requirement for DH-PIM especially at high values of D_T.

Similar results can be obtained for the optical power penalty and the normalised optical power penalty curves for different threshold levels and a bit rate of 1 Mbps versus the normalised delay spread are shown in Fig. 6.11.
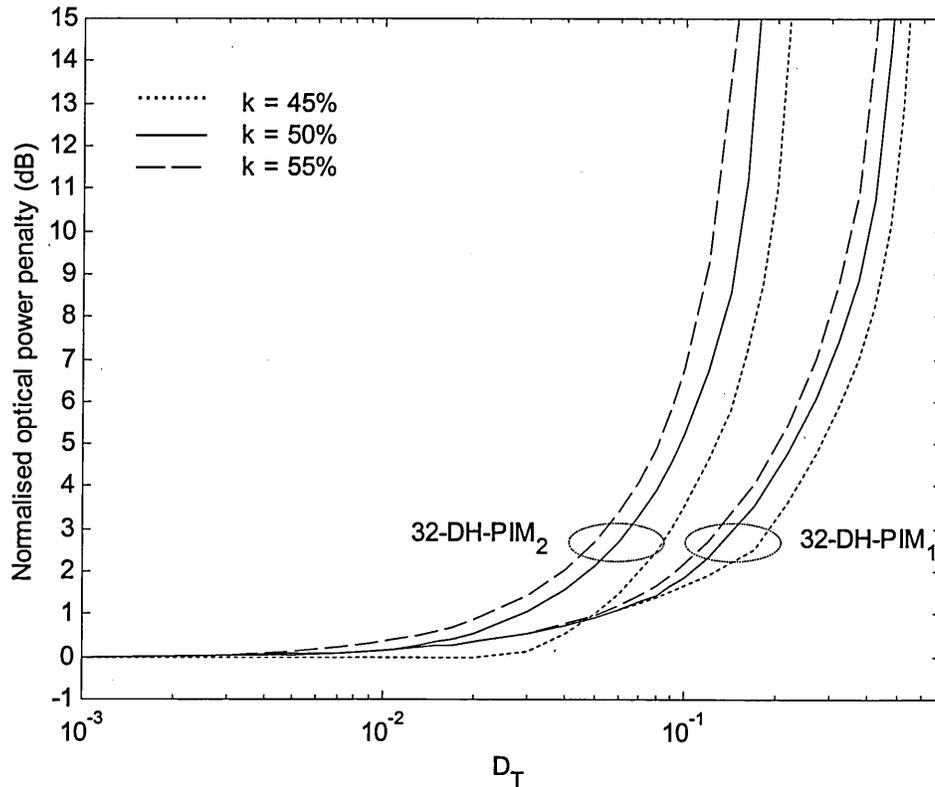
Fig. 6.11: Normalised optical power penalty for 32-DH-PIM$_1$ and 32-DH-PIM$_2$ versus D_T, for $R_b = 1$ Mbps and different threshold levels.

The optimum value for the threshold factor $k = 50\%$ in terms of power penalty is achieved for 32-DH-PIM$_1$ and 32-DH-PIM$_2$ for $D_T < 0.076$ and 0.006, respectively. However, as D_T increase above these values the optimum threshold level decrease slightly below $k = 50\%$.

The above results are confirmed by simulation of the eye diagrams at the output of the receiver filter. The eye diagrams of 32-DH-PIM$_2$ at R_b = 1 Mbps and D_T of 0.001, 0.01, 0.1 and 0.2 are shown in Fig. 6.12 a, b, c and d, respectively.
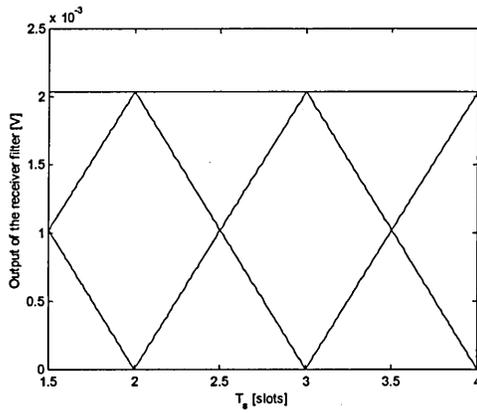
(a) 32- DH-PIM$_2$ for D_T = 0.001.
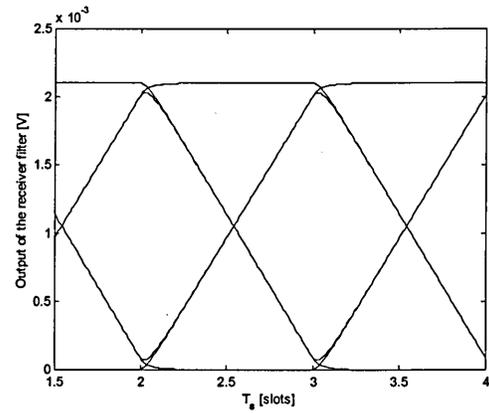
(b) 32- DH-PIM$_2$ for D_T = 0.01.
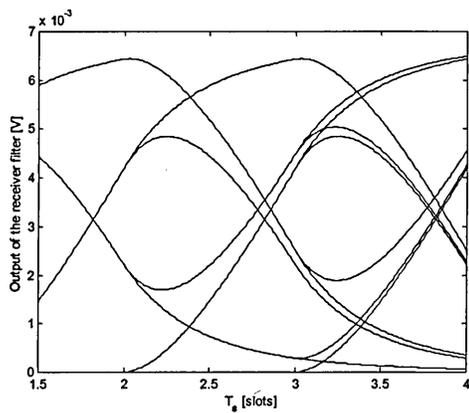
(c) 32- DH-PIM$_2$ for D_T = 0.1.
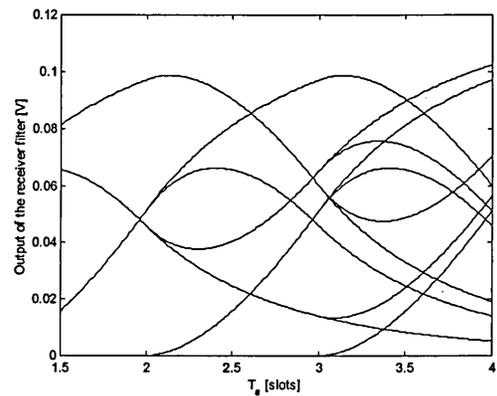
(d) 32- DH-PIM$_2$ for D_T = 0.2.

Fig. 6.12: Simulated eye diagrams at the receiver filter output for 32-DH-PIM$_2$ for different values of D_T and R_b = 1 Mbps.

Notice that the amount of eye closure increases as the normalised delay spread increases, this results in shifting the optimum sampling point from the end of the slot

135

and the optimum threshold level from the midway as the severity of ISI increases. For $D_T = 0.2$, the eye diagram clearly shows the effect of multipath dispersion, and increasing D_T further will result in a complete closure of the eye diagram.

The continuous impulse response of the cascaded system c_{cont} given in (6.6) is simulated for 32-DH-PIM$_1$ and 32-DH-PIM$_2$ over 9 slots for different values of D_T and the results are shown in Fig. 6.13.

(a) 32-DH-PIM$_1$, $R_b = 1$Mbps   (b) 32-DH-PIM$_2$, $R_b = 1$Mbps
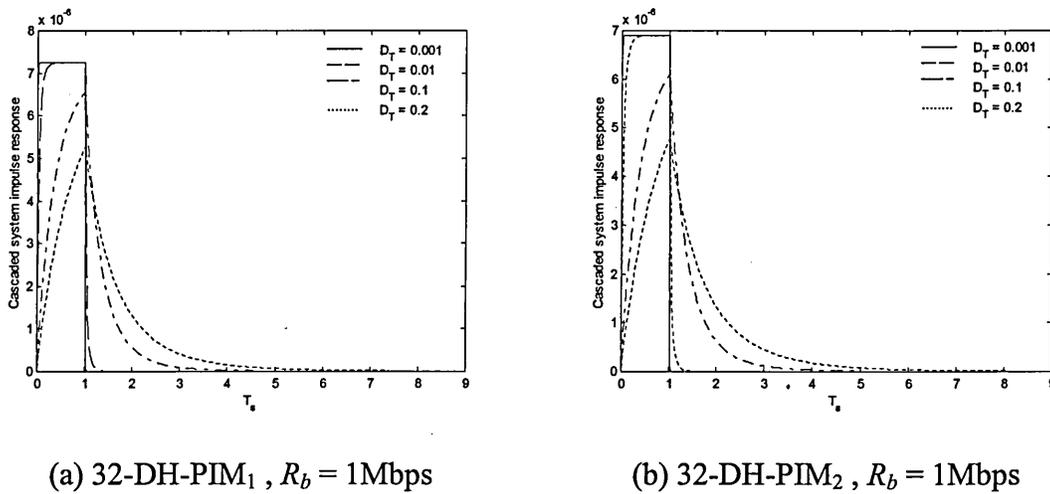
Fig. 6.13: Simulated impulse response at the receiver filter output for 32-DH-PIM$_1$ and 32-DH-PIM$_2$ for different values of D_T and $R_b = 1$Mbps.

From this figure, it can be observed that as the severity of multipath dispersion increases, and the amplitude of the zero tap (slot 1) decreases, c_{cont} spreads over many slots.

136

Increasing the bit rate results in decreasing the magnitude of the zero tap of the impulse response but the profile doesn't change. This is explained in Fig. 6.14 for 32-DH-PIM$_1$ and 32-DH-PIM$_2$ for $D_T = 0.1$ and different values of R_b (1, 10 and 100 Mbps).

(a) 32-DH-PIM$_1$, $D_T = 0.1$ (b) 32-DH-PIM$_2$, $D_T = 0.1$
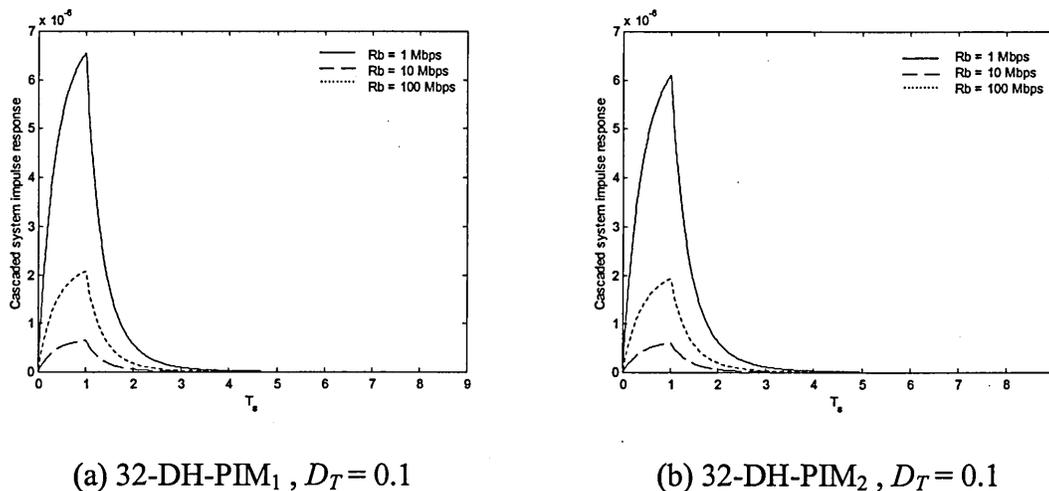
Fig. 6.14 Simulated impulse response at the receiver filter output for 32-DH-PIM$_1$ and 32-DH-PIM$_2$ for different values of R_b and $D_T = 10\%$.

6.5 Summary

The effect of multipath dispersion on DH-PIM has been theoretically analysed using the ceiling bounce model. The predicted results for both DH-PIM$_1$ and DH-PIM$_2$ have been confirmed by the simulation of the system impulse response for different values of normalised delay spread and bit rates. Results have also been compared with other modulation techniques. Results show that DH-PIM$_1$ achieves a very good performance compared with DH-PIM$_2$, DPIM and PPM in terms of optical power requirements and power penalty.

Chapter 7

CONCLUSIONS AND FURTHER WORK

7.1 Conclusions

An indoor wireless system is an attractive alternative to a wired system as it provides users with a mobile, low cost, reliable and low-power consumption line-of-sight or diffuse connectivity, which is increasingly required by users in an indoor environment. However, the combination of, a need for effective short range indoor wireless connectivity, ample unlicensed bandwidth, relative security and high transmission rate at a low cost makes an optical wireless link preferable to a radio link in many applications.

A review of indoor optical wireless system has been presented in Chapter 2 providing an insight as to the potential of this method and how it compares with an RF wireless

system. A review of the commonly used modulation schemes OOK, PPM and DPIM for indoor wireless system has been presented in Chapter 2.

The need for the effective exploitation of the characteristics of an optical wireless system has motivated the author to propose a new modulation scheme described as dual header pulse interval modulation (DH-PIM).

In Chapter 3, new expressions for the DH-PIM pulse train, symbol length, bandwidth requirement, packet transmission rate and transmission capacity have been derived. Because each symbol starts with a pulse, DH-PIM provides built-in symbol synchronisation, which is an important advantage as it simplifies the design as compared with PPM. The pulse plays the dual role of symbol initiation and a reference for the preceding and following symbols. On average, the 1's complement is taken for half the symbols when calculating the number of data slots, giving DH-PIM a much shorter symbol length compared with PPM and DPIM. At high bit resolutions ($M > 6$), the symbol length of DH-PIM is about half that of DPIM and quarter that of PPM. The value of α, which represents the number of consecutive pulses in header 2 (H_2), has less effect on the symbol length as compared to M (see equation 3.7), with average symbol length increasing slightly as α increases.

The short symbol length of DH-PIM gives an improvement in the bandwidth requirement of DH-PIM compared to its counterparts. The bandwidth requirement increases with, an increase in the data rate and the value of M, and a decrease in α. α has a pronounced effect on the bandwidth requirements especially at high M (> 6). DH-PIM$_1$ requires similar bandwidth to DPIM, but shows a marked reduction over PPM especially at high M.

The packet transmission rate increases with a decrease in packet length and M and increase in α. At high values of M, α becomes less effective on the transmission rate. Results also showed that as the bandwidth requirement increases, DH-PIM gives improved performance in terms of packet transmission rate as compared with its counterparts. Therefore, in applications where a high throughput is essential, a DH-PIM system with $M \leq 4$ and $\alpha \geq 2$ is recommended.

The peak transmission capacity of DH-PIM is reached when $M = 5$ and drops sharply either side of 5, in addition a higher α results in a higher transmission capacity. Compared with its counterparts, DH-PIM achieves higher transmission capacity especially for $\alpha > 1$ and $M > 3$.

Block diagrams of the DH-PIM transmitter/receiver have been presented along with a procedure for encoding an input data stream into DH-PIM slots and decoding received DH-PIM slots into output data. Simulated waveforms for different bit resolutions have been presented and the results indicate that the input data signal can be extracted successfully at the receiver at an appropriate SNR.

In Chapter 4, a novel mathematical derivation of the Fourier transform and power spectral density equations for DH-PIM is presented. The mathematical derivations have been confirmed by computer simulation. Results showed that the spectrum of DH-PIM consists of a *sinc* envelope, slot components and nulls. The presence of the slot components and the locations of the nulls depend on the value of α. The slot components are distinct when α is odd but are masked by the nulls when α is even. In this event a nonlinear device followed by a PLL circuit at the receiver may be used to achieve clock recovery. The slot and DC components of the DH-PIM PSD profile tend

to infinity when the number of transmitted symbols approaches infinity. The normalised slot component decreases with an increase in M and α, and the normalised DC component decreases as α decreases and M increases. DH-PIM has a similar PSD profile compared to DPIM and PPM but a slightly higher PSD, due to the use of dual headers and also the wider slot duration compared to DPIM and PPM. This power penalty is the price paid for achieving an improvement in bandwidth requirement compared with DPIM and PPM

In Chapter 5, a theoretical analysis for the error performance of DH-PIM has been presented. Original equations for the slot, packet error rates, and optical power requirement have been derived for a LOS non-dispersive optical wireless channel. Computer simulations have shown good agreement with the theoretical results. The analysis showed that the slot and packet error probabilities of DH-PIM decrease with the bit rate and α decreasing and M increasing. DH-PIM$_2$ only outperforms OOK, whereas DH-PIM$_1$ offers similar performance to DPIM but marginally inferior to PPM. Regardless of M, DH-PIM$_2$ displays improved bandwidth efficiency compared with DH-PIM$_1$, PPM and DPIM, but it requires more optical power. Thus, DH-PIM$_2$ is the preferred technique when the available bandwidth is limited and higher optical power is acceptable. DH-PIM$_1$ exhibits similar power requirements with a marginally higher bandwidth compared with DPIM, and is also more bandwidth efficient than PPM at the cost of a small increase in the power requirement. However, at higher bit resolutions, i.e. $M \geq 7$, DH-PIM$_1$ is both bandwidth and power efficient compared with PPM. The optimum parameters to minimise both the optical power and bandwidth required by DH-PIM are those of 16-DH-PIM$_1$ and 64-DH-PIM$_2$.

In Chapter 6, a theoretical analysis for the effect of multipath dispersion on DH-PIM has been presented using the ceiling bounce model. Expressions for the optical power requirement and power penalty have also been derived. Results indicate that $DH\text{-}PIM_1$ is less affected by multipath dispersion compared with $DH\text{-}PIM_2$ particularly at high levels of dispersion. This can be explained by noting that the pulse duration in $DH\text{-}PIM_1$ is half that of $DH\text{-}PIM_2$. At low dispersion (i.e. normalised delay spread $D_T < 0.1$), the power requirement of DH-PIM reduces by about 1.5 dB when M increases by one. As D_T increases above 0.1, the power requirement increases more rapidly for higher values of M due to ISI affecting a larger number of shorter slots in high order L-DH-PIM.

M has little effect on the optical power penalty at low dispersion ($D_T < 0.01$). However, the power penalty increases rapidly as D_T increases above 0.01. $DH\text{-}PIM_1$ shows a significant improvement over $DH\text{-}PIM_2$ particularly for $D_T < 0.05$. At very low dispersion ($D_T < 0.02$), the power requirements of $32\text{-}DH\text{-}PIM_1$ is, similar to 32-DPIM, considerably lower than $32\text{-}DH\text{-}PIM_2$ and OOK, and higher than 32-PPM. However, as D_T increases above 0.02, $32\text{-}DH\text{-}PIM_1$ outperforms 32-PPM and shows the best performance compared with its counterparts.

The optical power penalty of $32\text{-}DH\text{-}PIM_1$ is slightly higher than that of OOK-NRZ but lower than those of 32-PPM, 32-DPIM and $32\text{-}DH\text{-}PIM_2$. Results indicate that the higher the bit rate the higher the optical power requirement and penalty due to dispersion. The optimum threshold level lies midway between that of a pulse and an empty slot levels for low ISI, however it shifts slightly below midway for high ISI as a significant amount of the optical power is dispersed and appears in adjacent slots. Simulation of the system impulse response and eye diagram at the output of the

receiver filter verifies the theoretical results for multipath dispersion. Simulation results indicate that the amount of eye closure increases as ISI increases shifting the optimum sampling point from the end of the slot and the optimum threshold level from the midway.

Summarising, the selection of M and α optimises the characteristics of a DH-PIM system as follows:

Optimum Characteristic	M	α
Bandwidth requirement	Small	High
Packet transmission rate	Small	High
Transmission capacity	5	High
Normalised slot component of the PSD	Small	Small
Normalised DC component of the PSD	High	Small
Slot and packet error rates	High	Small
Optical power requirement on non-dispersive channel	High	Small
Optical power requirement and penalty when ISI is low	High	Small
Optical power requirement and penalty when ISI is high	Small	Small

Table 7.1: Selection of M and α for optimum characteristics of DH-PIM.

In addition, the following points can be concluded:

(i) The spectral profile contains a distinct slot component when α is odd that can be used for slot synchronisation.

(ii) The best performance of DH-PIM in terms of both optical power and bandwidth requirements is achieved for $M = 4$ and $\alpha = 1$ or $M = 6$ and $\alpha = 2$.

(iii) The optimum threshold level lies midway between zero and high pulse levels if ISI is low, and slightly below the midway otherwise.

7.2 Further Work

7.2.1. Coding

DH-PIM has got some built-in coding structure to detect errors when the received symbols are longer or shorter than the maximum and minimum symbol length, respectively. However, to further improve the probability of errors, it is recommended that some sort of channel coding be included in order to detect or detect and correct errors at the receiver. For example, channel coding can be introduced to generate even or odd DH-PIM symbols, where the number of data slots is always even or odd, respectively. A method of generating even DH-PIM can be achieved by doubling the number of data slots so that it is always even. Odd DH-PIM can be generated by doubling the number of data slots then adding one slot to make the number always odd. Channel coding provides error detection at the cost of increased symbol duration thus decreased throughput.

7.2.2. Effect of baseline wander on DH-PIM

Artificial light from fluorescent lighting induces a nearly periodic and deterministic interference that can be reduced using a high-pass filter, however this may cause baseline wander. The problem of baseline wander has been discussed briefly in Chapter 4 and it was shown that DH-PIM is slightly more susceptible to baseline wander than PPM and DPIM as it contains more optical power at low frequencies. It is recommended that further work is carried out to investigate the effect of baseline wander on DH-PIM system.

7.2.3. Equalisation

Equalisation provides a method of counteracting intersymbol interference due to multipath dispersion and therefore it improves the performance over non-directed wireless channels.

7.2.4. Hardware implementation

It was not a requirement of this PhD project to implement the DH-PIM system in hardware. However, it is recommended that any further work on DH-PIM should carry out a hardware design so that measurements can be taken. However, it is expected that measurement results will agree closely with the theoretical and simulation results.

REFERENCES

[1] J. R. BARRY: "Wireless Infrared Communications", Kluwer, 1994.

[2] R. OTTE, L. P. de JONG, and A. H. M. van ROERMUND: "Low-Power Wireless Infrared Communications", Kluwer, 1999.

[3] P. P. SMYTH, M. McCULLAGH, D. WISELY, D. WOOD, S. RITCHIE, P. EARDLEY and S. CASSIDY: "Optical wireless local area networks – enabling technologies", BT Technology J., 1993, Vol.11, No. 2, pp.56-64.

[4] J. M. KAHN and J. R. BARRY: "Wireless infrared communications", Proceedings of IEEE, 1997, Vol. 85, No. 2, pp. 265-298.

[5] F. R. GFELLER and U. BAPST: "Wireless in-house data communications via diffused infrared radiation", Proceedings of IEEE, 1979, Vol. 67, No. 11, pp. 1474-1486.

[6] A. C. BOUCOUVALAS: "Indoor ambient light noise and its effect on wireless optical links", IEE Proceedings Optoelectronics, 1996, Vol. 143, No. 6, pp. 334-338.

[7] Z. GHASSEMLOOY and A. R. HAYES: "Digital pulse interval modulation for IR communication systems-a review", Int. J. Commun. Syst., 2000, Vol. 13, pp. 519-536.

[8] J. M. KAHN and J. R. BARRY: "Wireless infrared communications", Proceedings of IEEE, 1997, Vol. 85, No. 2, pp. 265-298.

[9] Z. GHASSEMLOOY, A. R. HAYES, N. L. SEED and E. D. KALUARACHCHI: "Digital pulse interval modulation for optical communications" IEEE Communications Magazine, December 1998, Vol. 36, No. 12, pp. 95-99.

[10] R. U. REYHER: "Digital anisochronous pulse time techniques", MPhil thesis, Sheffield Hallam University, UK, 1995.

[11] E. D. KALUARACHCHI: "Digital pulse interval modulation for optical communications", PhD Thesis, Sheffield Hallam university, UK, 1997.

[12] N. M. ALDIBBIAT, Z. GHASSEMLOOY and R. McLAUGHLIN: "Error performance of dual header pulse interval modulation (DH-PIM) in optical wireless communications", IEE Proceedings Optoelectronics, April 2001, Vol. 148, No. 2, pp. 91-96.

[13] N. M. ALDIBBIAT, Z. GHASSEMLOOY and R. McLAUGHLIN: "Performance of dual header-pulse interval modulation (DH-PIM) for optical wireless communication systems", Proceedings of SPIE, February 2001, Vol. 4214, USA, pp. 144-152.

[14] K. K. WONG, T. O'FARRELL and M. KIATWEERASAKUL: 'The performance of optical OOK, 2-PPM and spread spectrum under the effects of multipath dispersion and artificial light interference", Int. J. Commun. Syst., 2000, Vol.13, pp. 551-576.

[15] M. D. KOTZIN, and A. P. VAN DEN HEUVEL: "A duplex infrared system for in-building communications", IEEE Vehic. Technol. Conf. Proc., 1986, pp. 179-185.

[16] A. M. R. MOREIRA, R.T. VALADAS and A. M. DE OLIVEIRA DUARTE: "Performance of infrared transmission systems under ambient light interference", IEE Proceedings Optoelectronics, December 1996, Vol. 143, No. 6, pp. 339-346.

[17] P. P. SMYTH, P. L. EARDLEY, K. T. DALTON, D. R. WISELY, P. McKEE and D. WOOD: "Optical wireless: a prognosis", Proceedings of SPIE, 1995, Vol. 2601, p 212-225.

[18] IrDA Infrared standard (http://www.irda.org).

[19] C. S. YEN and R. D. CRAWFORD: "The use of directed optical beams in wireless computer communications", IEEE Globecom 85, December 1985, pp. 1181-1184.

[20] T. S. CHU and M. J. GANS: "High speed infrared local wireless communication", IEEE communications magazine, Vol. 25, No. 8, August 1987, pp. 4-10.

[21] L. B. RIBEIRO: "Point-to-point optical wireless network for factory communications", Proceedings of International symposium on industrial electronics, July 1997, Guimaraes, Portugal, Vol. 1, Pt. 1, pp. 103-105.

[22] J. I. MATSUDA, T. NYU, T. SAITO and S. YAMAZAKI: "125 Mbps IR wireless link for IEEE 1394 multimedia home network", European conference on optical communication, September 1998, Madrid, Spain, pp. 343-344.

[23] J. BELLON, M. J. N. SIBLEY, D. R. WISELY and S. D. GREAVES, "Hub architecture for infra-red wireless networks in office environments", IEE Proceedings Optoelectronics, April 1999, Vol. 146, No. 2, pp. 78-82.

[24] A. M. STREET, P. N. STAVRINOU, D. C. O'BRIEN and D. J. EDWARDS, "Indoor optical wireless systems – a review", Optical and Quantum Electronics, Vol. 29, 1997, pp. 349 – 378.

[25]   A. M. STREET, K. SAMARAS, D. C. O'BRIEN and D. J. EDWARDS: "High speed wireless IR-LANs using spatial addressing", International symposium on personal indoor and mobile radio communications, Helsinki, Finland, September 1997, pp. 969-973.

[26]   E. B. ZYAMBO, D. C. O'BRIEN, G. E. FAULKNER, and D. J. EDWARDS: "Design of a High speed wireless LAN at long wavelengths", Optical Wireless Communications III, Boston, 2001, Vol. 4214, pp.115-124.

[27]   D. WISELY and I. NEILD: "A 100Mbit/s tracked optical wireless telepoint", International symposium on personal indoor and mobile radio communications, September 1997, Helsinki, Finland, pp. 964-968.

[28]   P. P. SMYTH, M. McCULLAGH, D. WISELY, D. WOOD, S. RITCHIE, P. EARDLEY and S. CASSIDY: "Optical wireless local area networks - enabling technologies", BT Technology Journal, April 1993, Vol. 11, No. 2, pp. 56 – 64.

[29]   M. J. McCULLAGH, D. R. WISELY, P. L. EARDLEY and P. P. SMYTH: "A 50 Mbit/s optical wireless LAN link using novel optical and electronic enabling technologies", International Zurich seminar on digital communications, Zurich, 1994, pp. 298-309.

[30]   M. J. McCULLAGH and D. R. WISELY: "155 Mbit/s optical wireless link using a bootstrapped silicon APD receiver", Electronics Letters, March 1994, Vol. 30, No. 5, pp.430-432.

[31]   P. NICHOLLS, S. D. GREAVES and R. T. UNWIN: "Optical wireless telepoint," IEE colloquium on optical free space communication links, London, February 1996, pp. 4/1-4/6.

[32]   D. J. T. HEATLEY and I. NEILD: "Optical wireless - the promise and the reality", IEE colloquium on optical wireless communications, London, June 1999, pp. 1/1 - 1/6.

[33]   D. J. T. HEATLEY, I. B. COCKBURN, F. T. LYNE, A. K. WILLIAMSON, K. J. FISHER, I. NEILD and N. HAQUE: "Concept 2010 – BT's new generation dealing desk", BT Technology Journal, October 1997, Vol. 14, No. 4, pp. 197-204.

[34]   D. C. LEE and J. M. KAHN: "Coding and Equalization for PPM on Wireless Infrared Channels", IEEE Trans. on Commun., 1999, Vol. 47, No. 2, pp. 255-260.

[35]   J. M. KAHN, J. R. BARRY, M. D. AUDEH, J. B. CARRUTHERS, W. J. KRAUSE and G. W. MARSH: "Non-directed infrared links for high-capacity wireless LAN's", IEEE Personal Communication Magazine, 1994, 1, pp. 12-25.

[36]   D. C. LEE and J. M. KAHN: "Coding and equalization for PPM on wireless infrared channels", IEEE Global Telecommunications Conference, 1998, Vol. 1, p 201-206.

[37]   F. R. GFELLER, H. R. MULLER and P. VETTIGER: "Infrared communication for in-house applications", IEEE COMPCON, Washington, USA, September 1978, pp. 132 – 138.

[38]   J. B. CARRUTHERS and J. M. KAHN: "Modeling of nondirected wireless infrared channels", IEEE Trans. on Commun., October 1997, Vol. 45, No. 10, pp. 1260-1268.

[39]   J. R. BARRY, J. M. KAHN, W. J. KRAUSE, E. A. LEE and D. G. MESSERSCHMITT: "Simulation of Multipath Impulse Response for Indoor Wireless Optical Channels", IEEE J. Sel. Areas in Commun., April 1993, Vol. 11, No. 3, pp. 367-379.

[40]   D. MAVRAKIS, S. R. SAUNDERS: "A Novel Modelling Approach for Wireless Infrared Links", Third International Symposium on Wireless Personal Multimedia Communications (WPMC), Nov. 2000, Vol. 2, pp. 609-614.

[41]   F. J. LÒPEZ-HERNÀNDEZ, R. PÈREZ-JIMÈNEZ, and A. SANTAMARÌA: "Monte Carlo calculation of impulse response on diffuse in wireless indoor channels", IEE Electronics Letters, June 1998, Vol. 34, No. 12, pp. 1260-1262.

[42]   F. J. LÒPEZ-HERNÀNDEZ and M. J. BETANCOR: "DUSTIN: Algorithm for calculation of impulse response on IR wireless indoor channels", IEE Electronics Letters, October 1997, Vol. 33, No. 21, pp. 1804-1806.

[43]   F. J. LÒPEZ-HERNÀNDEZ, R. PÈREZ-JIMÈNEZ and A. SANTAMARÌA: "Modified Monte Carlo scheme for high-efficiency simulation of the impulse response on diffuse IR wireless indoor channels," IEE Electronics Letters, September 1998, Vol. 34, No. 19, pp. 1819-1820.

[44]   C. R. A. T. LOMBA, R. T. VALADAS, and A. M. de OLIVEIRA DUARTE: "Efficient simulation of the impulse response of the indoor wireless optical channel", International-Journal-of-Communication-Systems. Vol.13, No.7-8, Nov.-Dec. 2000, p.537-549.

[45]   C. R. A. T. LOMBA, R. T. VALADAS, and A. M. de OLIVEIRA DUARTE: "Propagation losses and impulse response of the indoor optical channel: A simulation package", International Zurich Seminar on Digital Communications, 1994., pp. 285-297,

[46]   R. PÉREZ JIMÉNEZ, J. BERGES and M. J. BETANCOR: "Statistical model for the impulse response on infrared indoor diffuse channels", IEE Electronics Letters, 1997, Vol. 33, No. 15, pp. 1298-1301.

[47]   F. J. LÓPEZ-HERNÁNDEZ, R. PÉREZ-JIMÉNEZ and A. SANTAMARIA: "Novel ray-tracing approach for fast calculation of the impulse response in diffuse IR-wireless indoor channels", Proceedings of SPIE - Optical Wireless Communications II, September 1999, Vol. 3850, pp. 100-107.

[48]   T. H. TSAUR, K. C. CHEN, C. LIEN, M. T. SHIH and C. P. J. TZENG: "A nondirective infrared transceiver for indoor high speed wireless data communication", IEEE Transactions on Consumer Electronics, February 1994, Vol. 40, No. 1, pp. 20-27.

[49]   J. R. BARRY and J. M. KAHN: "Design of non-directed infrared links for high-speed wireless networks", IEEE LEOS Annual Meeting - Proceedings, New York, USA, 1994, Vol. 1, pp. 207.

[50]   G. W. MARSH and J. M. KAHN: "50-Mb/s diffuse infrared free-space link using on-off keying with decision feedback equalisation", IEEE Photonics Technology Letters, October 1994, Vol. 6, No. 10, pp. 1268-1270.

[51]   D. ROVIRAS, M. LESCURE, R. BENSALAH and T. BOSCH: "Wireless infrared factory network for hand-held terminals", European transactions on telecommunications, March-April 1995, Vol. 6, No. 2, pp. 207-217.

[52]   A. M. R. TAVARES, A. J. C. MOREIRA, C. R. A. T. LOMBA, L. M. V. MOREIRA, R. J. M. T. VALADAS and A. M. DE OLIVEIRA DUARTE: "Experimental results of a 1Mbps IR transceiver for indoor wireless local area networks", 5th International conference on advances in communication & control, Crete, Greece, June, 1995.

[53]   G. W. MARSH and J. M. KAHN: "Performance evaluation of experimental 50-Mb/s diffuse infrared wireless link using on-off keying with decision-feedback

equalisation", IEEE Transactions on Communications, November 1996, Vol. 44, No. 11, pp. 1496-1504.

[54]   R. VALADAS, A. MOREIRA, C. OLIVEIRA, L. MOREIRA, C. LOMBA, A. TAVARES and A. M. DE OLIVEIRA DUARTE: "Experimental results of a pulse position modulation infrared transceiver", 7th IEEE International symposium on personal, indoor and mobile radio communications, Taipei, Taiwan, October 1996, pp. 252-256.

[55]   P. NICHOLLS, R. T. UNWIN and K. T. DALTON: "10 MB/s optical wireless ethernet: practical results", Proc. SPIE, Vol. 2601, pp. 294-304.

[56]   D. C. M. LEE and J. M. KAHN: "Experimental 25-Mb/s Wireless Infrared Link Using 4-PPM with Scalar Decision-Feedback Equalization", Proceedings of IEEE International Conference on Communications, Atlanta, GA, June 7-11, 1998, Vol. 1, pp. 26-30.

[57]   J.M. KAHN, W.J. KRAUSE and J.B. CARRUTHERS: "Experimental Characterization of Non-Directed Indoor Infrared Channels", IEEE Trans. on Commun., February/March/April, 1995, Vol. 43, No. 2/3/4, pp. 1613-1623.

[58]   IEEE 802.11 standard for wireless LANs.

[59]   Spectrix Corportation, (www.spectrixcorp.com).

[60]   J.M. KAHN, P. DJAHANI, A.G. WEISBIN, K.T. BEH, A.P. TANG and R. YOU: "Imaging Diversity Receivers for High-Speed Infrared Wireless Communication", IEEE Commun. Mag., December 1998, Vol. 36, No. 12, pp. 88-94.

[61]   J. B. CARRUTHERS and J. M. KAHN: "Angle Diversity for Nondirected Wireless Infrared Communication", IEEE Trans. on Commun., June 2000, Vol. 48, No. 6, pp. 960-969.

[62] G. YUN and M. KAVEHRAD: "Spot Diffusing and Fly-Eye Receivers for Indoor Infrared Wireless Communications", Proc. of IEEE Conf. on Sel. Topics in Wireless Commun., Vancouver, B.C., Canada, June 1992, pp. 286-292.

[63] R. T. VALADAS and A. M. de OLIVEIRA DUARTE: "Sectored Receivers for Indoor Wireless Optical Communication Systems", Proc. of 5th IEEE Intl. Symp. on Personal, Indoor, and Mobile Radio Communications, The Hague, Netherlands, September 21-23, 1994.pp. 1090-1095.

[64] C. R. A. T. LOMBA, R. T. VALADAS and A. M. de OIVEIRA DUARTE: "Sectored Receivers to Combat the Multipath Dispersion of the Indoor Optical Channel", Proc. of the Sixth IEEE Intl. Symp. on Personal, Indoor and Mobile Radio Commun., Toronto, Canada, September 1995, pp. 321-325.

[65] A. M. R. TAVARES, R. J. M. T. VALADAS and A. M. de OLVEIRA DUARTE: "Performance of an Optical Sectored Receiver for Indoor Wireless Communication Systems in Presence of Artificial and Natural Noise Sources", Proc. of SPIE Conf. on Wireless Data Transmission, Philadelphia, PA, October 1995, Vol. 2601, pp. 264-273.

[66] R. T. VALADAS, A. R. TAVARES and A. M. de OLVEIRA DUARTE: "Angle diversity to combat the ambient noise in indoor optical wireless communication systems", International journal of wireless information networks, 1997, Vol. 4, No. 4, pp. 275-288.

[67] K. L. STERCKX, J. M. H. ELMIRGHANI and R. A. CRYAN: "Pyramidal fly-eye detection antenna for optical wireless systems", IEE Colloquium on optical wireless communications, London, 1999, pp. 5/1 - 5/6.

[68] K. L. STERCKX, J. M. H. ELMIRGHANI and R. A. CRYAN: "Sensitivity assessment of a three-segment pyramidal fly-eye detector in a semidisperse optical

wireless communication link", IEE Proceedings Optoelectronics, August 2000, Vol. 147, No. 4, pp. 286 - 294.

[69]   K. L. STERCKX, J. M. H. ELMIRGHANI and R. A. CRYAN: "Three-segment pyramidal fly-eye detection antenna for optical wireless communication systems under the constraint of ambient noise introduced by highly directive spotlights", International journal of communication systems, November - December 2000, Vol. 13, No. 7-8, pp. 577 - 588.

[70]   International Electrotechnical Commission (IEC), CEI/IEC 825-1, Safety of laser products, 1993.

[71]   British standard BS EN 60825-1:1994 (IEC 835-1: 1993), Safety of Laser products, part 1: Equipment classification, requirements and user's guide, December 1994.

[72]   P. L. EARDLEY, D. R. WISELY, D. WOOD and P. McKEE: "Holograms for optical wireless LANs", IEE Proceedings Optoelectronics, December 1996, Vol. 143, No. 6, pp. 365-369.

[73]   V. POHL, V. JUNGNICKEL and C. VON HELMOLT: "Integrating sphere diffuser for wireless infrared communication", IEE Proceedings Optoelectronics, August 2000, Vol. 147, No. 4, pp. 281 - 285.

[74]   V. POHL, V. JUNGNICKEL, R. HENTGES and C. VON HELMOLT: "Integrating sphere diffuser for wireless infrared communication", IEE colloquium on optical wireless communications, London, 22 June 1999, pp. 4/1 - 4/6.

[75]   IrDA URL: http://www.irda.org.

[76]   http://www.lightreading.com.

[77]   G. P. AGRAWAL: "Fiber-optic communication systems", John Wiley & Sons. Inc., 1997.

[78] K. PHANG and D.A. JOHNS: "A CMOS optical preamplifier for wireless infrared communications", IEEE Transactions on Circuits and Systems II: Analog and Digital Signal Processing, 1999, Vol. 46, No. 7, pp. 852-859.

[79] A. M. STREET, P. N. STAVRINOU, D. J. EDWARDS and G. PARRY: "Optical preamplifier designs for IR-LAN applications", IEE Colloquium (Digest), 1996, No. 32, pp. 8/1-8/6.

[80] A. J. C. MOREIRA, A. M. R. TAVARES, R. T. VALADAS and A.M. DE OLIVEIRA DUARTE: "Modulation methods for wireless infrared transmission systems: performance under ambient light noise and interference", Proc. SPIE, USA, Oct. 1995, Vol. 2601, pp. 226-237.

[81] R. NARASIMHAN, M. D. AUDEH, J. M. KAHN: "Effect of electronic-ballast fluorescent lighting on wireless infrared links", IEE Proceedings Optoelectronics, Dec 1996, Vol. 143, No. 6, pp. 347-354.

[82] A. R HAYES, Z. GHASSEMLOOY, N. L. SEED and R. McLAUGHLIN: "Baseline-wander effects on systems employing digital pulse-interval modulation", IEE Proceedings Optoelectronics, Aug. 2000, Vol. 147, No.4, pp. 295-300.

[83] IrDA Serial Infrared Physical Layer Specification, Version 1.4, February 2001.

[84] H. H. CHAN, K. L. STERCKX and J. M. H. ELMIRGHANI, R. A. CRYAN: "Performance of optical wireless OOK and PPM systems under the constraints of ambient noise and multipath dispersion", IEEE Communications Magazine, Dec 1998, Vol. 36, No. 12, pp. 83-87.

[85] K. SAMARAS, D. C. O'BRIEN, A. M. STREET, D. J. EDWARDS: "BER performance of NRZ-OOK and Manchester modulation in indoor wireless infrared links", International Journal of Wireless Information Networks, Jul 1998, Vol. 5, No. 3, pp. 219-233.

[86]   A. GARCIA-ZAMBRANA, A. PUERTA-NOTARIO: "Feasibility of OOK modulation with RZ pulses of variable duty cycle in indoor unguided optical links at high bit rates", IEEE International Conference on Communications, 1998, Vol. 2, pp. 821-825.

[87]   T. T. HA, G. E. KEISER and R. L. BORCHARDT: "Bit error probabilities of OOK lightwave systems with optical amplifiers", Journal of Optical Communications, Aug 1997, Vol. 18, No. 4, pp. 151-155.

[88]   B. WILSON, Z. GHASSEMLOOY and I. DARWAZEH: "Analogue Optical Fibre Communications", IEE Telecommunication series, No. 32, 1995.

[89]   B. WILSON and Z. GHASSEMLOOY: "Pulse Time Modulation techniques for optical communication: a review", IEE Proceeding - J, 1993, Vol. 140, No 6, pp. 346-357.

[90]   B. WILSON, Z. GHASSEMLOOY and D. J. T. HEATLEY: "Properties and applications of Pulse Time Modulation techniques for fibre broadband communication networks", International conference on information Engineering (ICIE'91), 1991, pp. 693-702.

[91]   J. PROAKIS and M. SALEHI: "Communication Systems Engineering", Prentice-Hall International, New Jersey, 1994.

[92]   IEEE 802.11 standard for local area networks, IEEE, 1997.

[93]   M. D. AUDEH and J. M. KAHN: "Performance evaluation of L-pulse-position modulation on non-directed indoor infrared channels", International Conference on Communications, May 1994, New Orleans, LA, USA,1994, Vol. 2, pp. 660-664.

[94]   M. D. AUDEH, J. M. KAHN and J. R. BARRY: "Performance of PPM with maximum-likelihood sequence detection on measured non-directed indoor infrared

channels", IEEE International Conference on Communications, Seattle, WA, USA, June 1995, Vol. 2 , pp. 1177-1181.

[95]   M. D. AUDEH, J. M. KAHN and J. R. BARRY: "Performance of pulse-position modulation on measured non-directed indoor infrared channels", IEEE Transactions on Communications, Jun 1996, Vol. 44, No. 6, pp. 654-659.

[96]   M. D. AUDEH, J. M. KAHN and J. R. BARRY: "Decision-feedback equalization of pulse-position modulation on measured nondirected indoor infrared channels", IEEE Transactions on Communications, April, 1999, Vol. 47, No. 4, pp. 500-503.

[97]   J. R. BARRY: "Sequence Detection and Equalization for Pulse-Position Modulation", International Conference on Communications, New Orleans, LA, May 1994, pp. 1561-1565.

[98]   E. A. LEE and D. G. MESSERSCHMITT: "Digital Communication", Kluwer Academic Publishers, Boston, 1994.

[99]   Z. GHASSEMLOOY, A. R. HAYES, N. L. SEED and E. D. KALUARACHCHI: "Digital pulse interval modulation for optical wireless communications", Proceedings of the 3rd IAA annual conference on Computers and Communications, New York, U.S.A., September 1998, pp. 198-202.

[100] A. R. HAYES, Z. GHASSEMLOOY and N. L. SEED: "Optical wireless communication using digital pulse interval modulation", Proc. SPIE, USA, Nov. 1998, Vol. 3532, pp.61-69.

[101] G. CARIOLARO, T. ERSEGHE, and L. VANGELISTA: "Exact Spectral Evaluation of the Family of Digital Pulse Interval Modulated Signals", IEEE Trans. on Information Theory, (scheduled for November 2001).

[102] A. R. HAYES, Z. GHASSEMLOOY and N. L. SEED: "The effect of baseline wander on the performance of digital pulse interval modulation", IEE Colloquium on Optical Wireless Communications, 22nd June 1999, pp. 13/1-13/5.

[103] G. CARIOLARO, T. ERSEGHE, and L. VANGELISTA: "Stationary model of pulse interval modulation and exact spectral evaluation", ICC 2000, New Orleans, Louisiana, USA, June 2000, pp. 660-664.

[104] A. R. HAYES, Z. GHASSEMLOOY and N. L. SEED: "The performance of digital pulse interval modulation in the presence of multipath propagation", 2nd International Symposium on Communication Systems, Networks, and DSP (CSNDSP-2000), Bournemouth, UK, July 2000, pp. 141-146.

[105] IEEE 802.11 working group (http://grouper.ieee.org/groups/802/11).

[106] ANSI/IEEE Std 802.11, Part 11: Wireless LAN Medium Access Control (MAC) and Physical Layer (PHY) Specifications, IEEE Computer Society, 1999.

[107] http://www.itcom.itd.umich.edu.

[108] http://www.computer-design.com.

[109] G. BAISTER, P. GATENBY, B. LAURENT and J. LEWIS: "Applications for optical free space links in inter-satellite and intra-satellite communications", IEE Colloquium (Digest), 1996, No. 032,), pp. 9/1-9/6.

[110] J. P. DODLEY, D. M. BRITZ, D. J. BOWEN and C. W. LUNDGREN: "Free space optical technology and distribution architecture for broadband metro and local services", Proceedings of SPIE, 2001, Vol. 4214, pp. 72-85.

[111] D. M. BRITZ, J. P. DODLEY, D. J. BARNICKEL: "Broadhand local service offerings using free-space optical links; A network business perspective", Proceedings of SPIE, 2001, Vol. 4214, pp. 63-71.

[112] http://www.laserwireless.com.

[113] http://www.lightpointe.com.

[114] http://www.cablefree.co.uk.

[115] www.quantumbeam.com.

[116] http://www.bluetooth.com.

[117] Specification of the Bluetooth System (Core), Volume 1, Version 1.1, February 2001.

[118] Specification of the Bluetooth System (Profiles), Volume 2, Version 1.1, February 2001.

[119] http://www.nwfusion.com.

[120] http://www.searchnetworking.com.

[121] K. WESTERLUND: "Bluetooth 2001: Enabling the Star Trek Generation", IEEE Computer Society Dallas Chapter, Bluetooth™ Presentation, 15 February 2001.

[122] F. G. STREMLER: "Introduction to Communication Systems", Addison-Wesley, USA, 1990.

[123] M. SATO, M. MURATA and T. NAMEKAWA: "A New Optical Communication System Using the Pulse Interval and Width Modulation Code". IEEE Transactions on Cable Television, 1979, Vol. CATV-4, No. 1, pp. 1-9.

[124] Z. GHASSEMLOOY, R. U. REYHER, E. D. KALUARACHCHI and A. J. SIMMONDS, "Digital pulse interval and width modulation for optical fibre communication", Proceedings of SPIE, Vol. 2614, 1995, pp. 60-68.

[125] D. SHIU and J. M. KAHN: "Differential pulse-position modulation for power-efficient optical communication", IEEE Transactions on Communication, 1999, Vol. 47, No. 8, pp. 1201-1210.

[126] G. JAMES, D. BURLEY, D. CLEMENTS, P. DYKE, J. SEARL and J. WRIGHT: "Modern Engineering Mathematics", Addison-Wesley, USA, 1996.

[127] C. C. CHEN and C. S. GARDNER: "Performance of PLL synchronized optical PPM communication systems", IEEE Transaction on Communications, October 1986, Vol. COM-34, No. 10, pp. 988-994.

[128] F. M. DAVISON and X. SUN: "Slot clock recovery in optical PPM communication systems with avalanche photodiode photodetectors", IEEE Transactions on Communications, November 1989, Vol. COM-37, No. 11, pp. 1164-1172.

[129] A. M. STREET, K. SAMARAS, D. C. O'BRIEN and D. J. EDWARDS, "Closed form expressions for baseline wander effects in wireless IR applications", Electronics Letters, June 1997, Vol. 33, No. 12, pp. 1060-1062.

[130] H. TAUB and D. L. SCHILLING: "Principles of communication systems", McGraw-Hill Book Company, Singapore, 1986.

[131] Z. GHASSEMLOOY, A. R. HAYES and N. L SEED: "The effect of multipath propagation on the performance of DPIM on diffuse optical wireless communications", IASTED proceedings, June 2001, Banff, Canada, pp. 166-172.

Appendix A

DH-PIM SIMULATION FLOW CHARTS

A.1 Transmitter
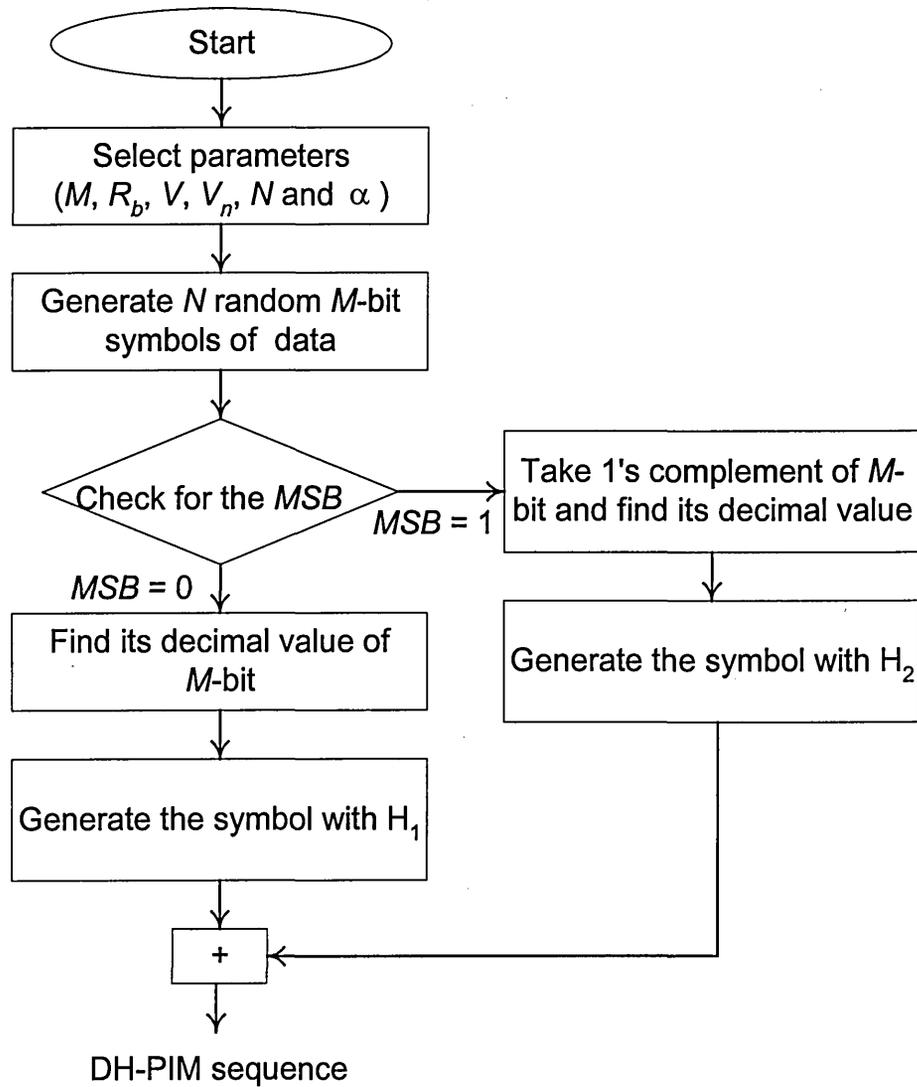
Fig A.1: Flow chart of the simulation of the DH-PIM transmitter.

A.2 Channel and Receiver

DH-PIM sequence

↓

Add filtered WG noise to the DH-PIM pulse train.

↓

Determine the energy (E) at output of the matched filter

↓

Sample E and compare it with the threshold level

↓

Re-generate the DH-PIM

↓

Check for the header

H_1 ↓ H_2 →

Count data slots, convert into a binary sequence and take the 1's complement

Count data slots and convert into a binary sequence

↓

$+$

↓

Output data

↓

All done
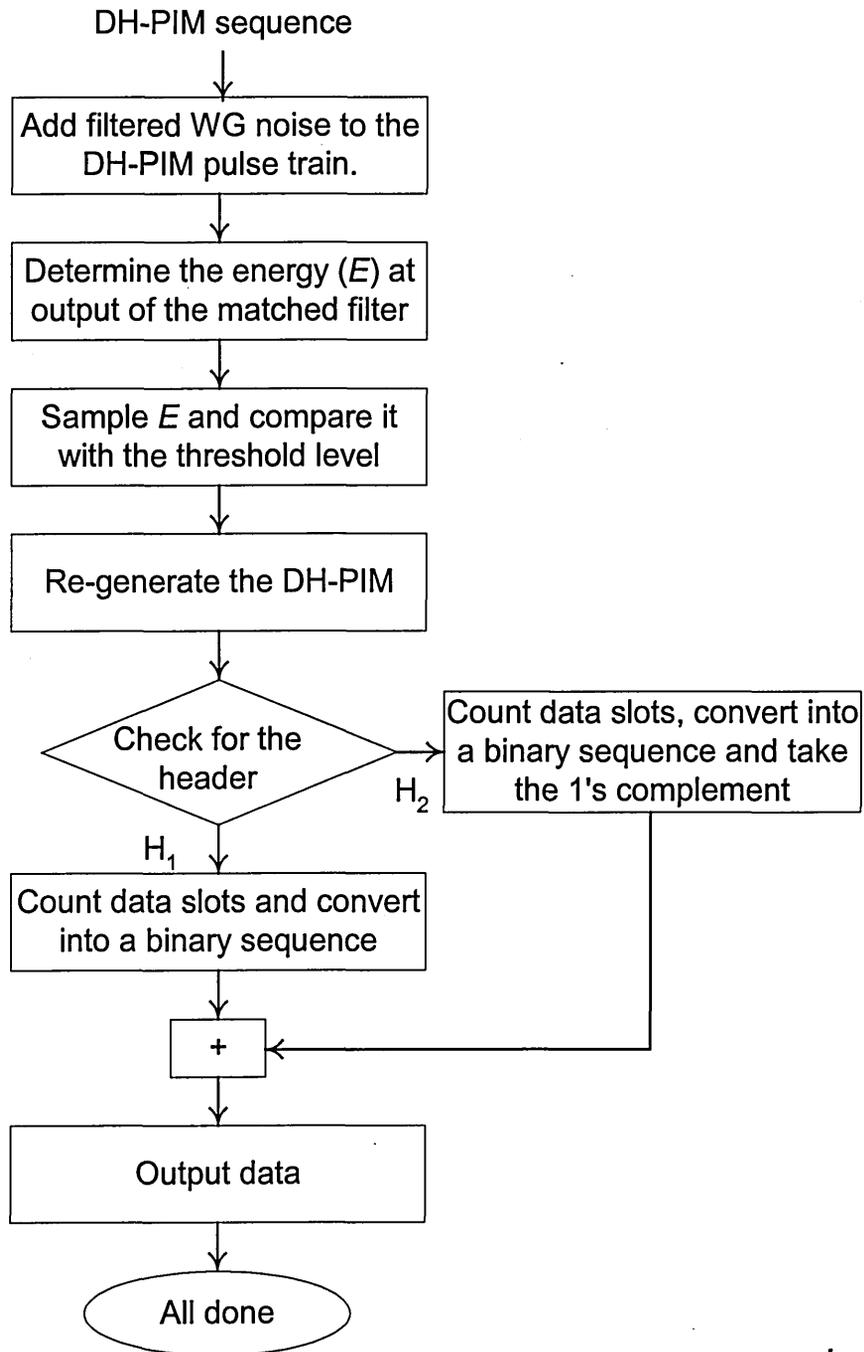
Fig A.2: Flow chart of the simulation of the channel and DH-PIM receiver.

Appendix B

PROBABILITY OF OCCURRENCE

Following the discussion in Section 6.3, Chapter 6, the following is an example of how

to calculate the probability of occurrence in a DH-PIM sequence.

In order to simplify the calculations, it is assumed in this example that $\alpha = 2$, $M = 2$

$(L = 4)$ and $m = 3$. Where, α is the number of pulses in H_2, M is the bit resolution, and

m is the number of taps in the discrete-time impulse response c_k.

The input data can be encoded into one of four possible 4-DH-PIM$_2$ codes as follows:

Input data ($M = 2$)	4-DH-PIM$_2$
0 0	1 0 0
0 1	1 0 0 0
1 0	1 1 0 0
1 1	1 1 0

Table B.1: Encoding input data into 4-DH-PIM$_2$ codes.

We take all the possible slot combinations of a sequence of $m = 3$ slots, therefore there are 8 different sequences as follows:

0 0 0, 0 0 1, 0 1 0, 0 1 1, 1 0 0, 1 0 1, 1 1 0 and **1 1 1.**

However, the last sequence "1 1 1" is not a valid DH-PIM$_2$ code because the maximum renumber of consecutive 1's in a DH-PIM$_2$ code is 2.

Therefore, there are only seven valid possible sequences as follows:

0 0 0, 0 0 1, 0 1 0, 0 1 1, 1 0 0, 1 0 1 and 1 1 0.

To calculate the probability of occurrence for each of the valid sequences, we look at each sequence as comprised of two parts. The first part consists of either a full DH-PIM$_2$ code or a concluding part or a preceded DH-PIM code, and the second part consists of the following DH-PIM$_2$ codes or parts of codes if any. Then the probability of occurrence for each of the sequences is calculated as the multiplication of these two parts.

For example, the sequence "0 1 1" consists of two parts: "0" and "1 1".

"0" ends a preceded DH-PIM$_2$ code, which could be any one of the 4 different DH-PIM$_2$ codes, so its probability of occurrence is $\frac{1}{4}\left(\frac{1}{3}+\frac{1}{4}+\frac{1}{4}+\frac{1}{3}\right)$.

And "1 1" is a start part of a DH-PIM$_2$ code, which could be one of two different codes

("1 1 0" or "1 1 0 0"), thus, its probability of occurrence is $\dfrac{2}{4}$.

Therefore, the probability of occurrence for the sequence "0 1 1" is the multiplication

of $\dfrac{1}{4}\left(\dfrac{1}{3}+\dfrac{1}{4}+\dfrac{1}{4}+\dfrac{1}{3}\right)$ and $\dfrac{2}{4}$, which results is $\dfrac{7}{48}$.

Table B.2 shows the probability of occurrence for each of the valid sequences.

Sequence	Probability of occurrence
0 0 0	$P_{occ}(000) = \dfrac{1}{4}\left(0+\dfrac{1}{4}+0+0\right) = \dfrac{1}{16}$
0 0 1	$P_{occ}(001) = \dfrac{1}{4}\left(\dfrac{1}{3}+\dfrac{1}{4}+\dfrac{1}{4}+0\right)\dfrac{4}{4} = \dfrac{5}{24}$
0 1 0	$p_{occ}(010) = \dfrac{1}{4}\left(\dfrac{1}{3}+\dfrac{1}{4}+\dfrac{1}{4}+\dfrac{1}{3}\right)\dfrac{2}{4} = \dfrac{7}{48}$
0 1 1	$P_{occ}(011) = \dfrac{1}{4}\left(\dfrac{1}{3}+\dfrac{1}{4}+\dfrac{1}{4}+\dfrac{1}{3}\right)\dfrac{2}{4} = \dfrac{7}{48}$
1 0 0	$P_{occ}(100) = \dfrac{1}{4}\left(\dfrac{1}{3}+\dfrac{1}{4}+\dfrac{1}{4}+0\right) = \dfrac{5}{24}$
1 0 1	$P_{occ}(101) = \dfrac{1}{4}\left(0+0+0+\dfrac{1}{3}\right)\dfrac{4}{4} = \dfrac{1}{12}$
1 1 0	$P_{occ}(110) = \dfrac{1}{4}\left(0+0+\dfrac{1}{4}+\dfrac{1}{3}\right) = \dfrac{7}{48}$

Table B.2: Probabilities of occurrence for 3-slot sequences of 4-DH-PIM$_2$ codes.

The summation of the probabilities of occurrence for all the valid sequences must result in 1. Therefore,

$$P_{occ} = \frac{1}{16} + \frac{5}{24} + \frac{7}{48} + \frac{7}{48} + \frac{5}{24} + \frac{1}{12} + \frac{7}{48} = 1.$$

Which confirms the accuracy of the calculations.